MICHIGAN STATE UNIVERSITY LIBRARIES
3 1293 00538 7455

21144879

LIBRARY
Michigan State
University

This is to certify that the

dissertation entitled

INELASTIC-BUCKLING BEHAVIOR OF STEEL STRUTS:
HYSTERETIC MODELING AND APPLICATIONS TO NONLINEAR
"POST-FAILURE" ANALYSIS OF SPACE TRUSSES

presented by

Mohamad-Samer Alawa

has been accepted towards fulfillment
of the requirements for

Ph.D. degree in Civil Engineering

Major professor

Date 11-6-1987

MSU is an Affirmative Action/Equal Opportunity Institution

O-12771

MSU
LIBRARIES

RETURNING MATERIALS:
Place in book drop to remove this checkout from your record. FINES will be charged if book is returned after the date stamped below.

INELASTIC-BUCKLING BEHAVIOR OF STEEL STRUTS: HYSTERETIC MODELING AND APPLICATIONS TO NONLINEAR "POST-FAILURE" ANALYSIS OF SPACE TRUSSES

By

Mohamad-Samer Alawa

A DISSERTATION

Submitted to
Michigan State University
in partial fulfillment of the requirements
for the degree of

DOCTOR OF PHILOSPHY

Department of Civil and Environmantal Engineering

1988

5354547

ABSTRACT

INELASTIC-BUCKLING BEHAVIOR OF STEEL STRUTS: HYSTERETIC MODELING AND APPLICATIONS TO NONLINEAR "POST-FAILURE" ANALYSIS OF SPACE TRUSSES

By

Mohamad-Samer Alawa

A computationally efficient element model was developed for accurately predicting the inelastic-buckling behavior of steel struts under generalized axial excitations. The model was based on theoretical concepts and the physics of the steel strut behavior, with limited reliance on experimental data. It is capable of simulating the effects of the element initial imperfection and end eccentricities, gradual plastification, deterioration under cyclic loads, and residual stresses on its response characteristics. The developed model of steel struts was verified against a wide variety of test results, and it was used for numerical studies leading to recommendations for selection of variables in the design of steel struts.

The element model was incorporated into a computer program for nonlinear analysis of space trusses. This computer program is capable of predicting the inelastic force redistributions within the space truss systems following the yielding and buckling of some critical elements, with due consideration to the complex nonlinear behavior of the X-braces and the in-plane redundants. The structural analysis program is shown

to predict the experimental nonlinear behavior, failure mechanism, and "post-failure" residual strength of different space truss systems with a reliable accuracy. The advantages of this program in the design of structures with ductile failure modes and also in nonlinear analysis of the complex multiple-structure systems have been discussed.

ACKNOWLEDGEMENT

I would like to express my sincere gratitude to Dr. Parviz Soroushian under whose guidance this dissertation was written. His suggestions and criticism from the very beginning of the study up to the preparation of the final manuscript were of great value. I want also to thank Dr. R. K. Wen, Dr. J. L. Segerlind, and Dr. W. E. Kuan for their help as members of my guidance committee.

This study was supported by Michigan Energy and Resource Research Association (MERRA) and Michigan Utilities. This support is sincerely appreciated. Financial assistance from the Department of Civil and Environmental Engineering, Michigan State University, is gratefully acknowledged. Finally, thanks are extended to the Albert H. Case Center for Computer Aided Design in the Engineering College for providing the necessary computing and plotting facilities.

TABLE OF CONTENTS

LIST OF TABLES viii

LIST OF FIGURES ix

LIST OF NOTATIONS xiii

1 INTRODUCTION 1

2 A LITERATURE REVIEW ON THE INELASTIC CYCLIC BEHAVIOR OF STEEL STRUTS AND THEIR CONNECTION 4

- 2.1 INTRODUCTION 4
- 2.2 PHYSICAL BEHAVIOR OF STEEL STRUTS UNDER GENERALIZED LOADS 4
- 2.3 EXPERIMENTAL RESULTS ON STEEL STRUTS 8
  - 2.3.1 Formation of Plastic Hinges 8
  - 2.3.2 Effects of Slenderness Ratio 10
  - 2.3.3 Effects of Local Buckling 10
  - 2.3.4 Effects of Initial Imperfection and Residual Stresses 10
  - 2.3.5 Effective Length Concept 13
- 2.4 ANALYTICAL MODELING OF STEEL STRUTS UNDER GENERALIZED LOADING 13
  - 2.4.1 Finite Element Methods 13
  - 2.4.2 Phenomenological Methods 15
  - 2.4.3 Physical Theory Models 17
- 2.5 STATE-OF-THE-ART IN PHYSICAL THEORY MODELING OF STRUTS 17
  - 2.5.1 Gugerli Model 18
  - 2.5.2 Ikeda Model 20
  - 2.5.3 Zayas Model 25
- 2.6 PHYSICAL BEHAVIOR OF STEEL STRUT CONNECTIONS 29
- 2.7 EXPERIMENTAL RESULTS ON STRUT CONNECTIONS 32
- 2.8 CONNECTION MODELING AND DESIGN 34
- 2.9 SUMMARY AND CONCLUSIONS 38

3 THE DEVELOPED ELEMENT MODEL 41
3.1 INTRODUCTION 41
3.2 THE DEVELOPED FORMULATION 42
3.3 REFINEMENTS OF THE BASIC FORMULATION 49
3.4 ADVANTAGES OF THE PROPOSED MODEL 58
3.5 SUMMARY AND CONCLUSIONS 60

4 VERIFICATION OF THE ELEMENT MODEL AND PARAMETRIC STUDIES 61
4.1 INTRODUCTION 61
4.2 EMPIRICAL DERIVATION OF THE MODEL VARIABLES 62
4.3 COMPARISONS WITH MONOTONIC EXPERIMENTAL RESULTS 64
4.4 COMPARISONS WITH CYCLIC EXPERIMENTAL RESULTS 71
4.5 NUMERICAL STUDIES AND DESIGN RECOMMENDATIONS FOR STEEL STRUTS 89
4.5.1 The Influence of Yield Strength 89
4.5.2 The Influence of End Connection Restraints .. 93
4.5.3 The Influence of Cross-Sectional Shape 93
4.5.4 The Influence of Initial Imperfection 95
4.5.5 The Influence of End Eccentricity 98
4.6 SUMMRY AND CONCLUSIONS 100

5 INELASTIC ANALYSIS OF SPACE TRUSSES 103
5.1 INTRODUCTION 103
5.2 X-BRACING AND IN-PLANE REDUNDANTS : A REVIEW OF THE BEHAVIOR 105
5.2.1 X-Bracing 106
5.2.2 In-Plane Redundants 107
5.3 A BACKGROUND ON THE INCREMENTAL NONLIEAR STRUCTURAL ANALYSIS OF SPACE TRUSSES 110
5.4 THE ADOPTED STRUCTURAL MODELING APPROACH 114
5.4.1 X-Bracing Systems 115
5.4.2 In-Plane Redundants 117
5.5 ADOPTED STRUCTURAL ANALYSIS PROCEDURES AND NUMERICAL TECHNIQUES 119
5.6 COMPARISONS WITH STRUCTURAL TEST RESULTS 120
5.6.1 Double Layer Space Truss System 121
5.6.2 Isolated X-Braced System 131
5.6.3 Lattice Transmission Tower 134

5.7 SUMMARY AND CONCLUSIONS 141

6 SUMMARY AND CONCLUSIONS 143

LIST OF REFERENCES 150

LIST OF TABLES

4.1 Cyclically Loaded Steel Struts[3] 63

4.2 The Empirical Values of the Element Model Variables 63

4.3 Material and Geometric Properties of L 3.54in X 3.54in X 0.27in (L 90mm X 90mm X 7mm) Tested in Monotonic Compression[45] 66

4.4 Properties of the Steel Struts Tested Under Monotonic Loads[46,47] 69

4.5 Properties of the Steel Struts Tested Under Cyclic Loads[1,3] 74

5.1 Properties of Tower Elements 136

LIST OF FIGURES

2.1 Steel Struts and Their Connections in Braced Frames and Space Trusses 5
2.2 Cyclic Behavior of Steel Struts 7
2.3 Detailed Behavior of Plastic Hinges (TS 4in x 4in x 1/2 in, kl/r=80)[1] 9
2.4 Effects of Slenderness Ratio on the Strut Hysteretic Performance (W6x20)[3] 11
2.5 Effects of Cross-sectional Shape (partially caused by local buckling) on the Strut Hysteretic Performance[10] 11
2.6 Effects of Initial Imperfection and Residual Stresses on the Initial Buckling load of Steel Struts.[5,6,7] 12
2.7 Inelastic Buckling Shape Compared with the Elastic Curve[3] 12
2.8 Earlier Strut Models[2] 14
2.9 Finite Element Model 14
2.10 Examples of Phenomenological Models 16
2.11 Typical Element Geometry in Physical Theory Models 16
2.12 Definition of the Location of the Instantaneous Neutral Axis y_n[38] 21
2.13 Axial Load-Displacement Curve Used in the Gegerli Model[1] 21
2.14 Comparison Between Experimental and Gugerli Axial Load-Displacement Curves[1] 22
2.15 Empirical Relationships Used in Formulation of the Physical Theory Strut Model in Reference 1 24
2.16 Theoretical and Experimental Hysteresis Loops[1] 26
2.17 The Physical Theory Strut Model of Reference 2 26
2.18 Possible Failure Modes of Bolted Connections[56] 31
2.19 Bending Moment in Connections Caused by Bowing of Steel Struts 31
2.20 Formation of End Plastic Hinges Due to The Flexural Yielding of Connections 31
2.21 Slippage at Bolted Connections 33
2.22 Rotational Restraint of Gusset Plates in In-Plane and Out-Plane Bending 33
2.23 Effects of The Bolted Connection Slippage on The Steel Strut

Behavior Under Load[43] 35
2.24 Idealization of The Steel Struts End Connections by Linear and Rotational Springs 35
2.25 Strut Concentric Axial Force Used in Connection Design .. 35
2.26 Axial-Flexural Forces Usually Induced in The Strut End Connections 37
2.27 Cantilever Beam Simulation of Gusset Plates 37
2.28 Effective Width of Gusset Plates[42] 37

3.1 Pinned-End Physical Theory Model 41
3.2 Geometry and Deformation of Half-Strut 44
3.3 Effects of Partial Plastification on Axial Force-Plastic ηinge Moment Relationship (W8X20, kl/r=120) 51
3.4 Effects of Partial Plastification on the Axial Force-Plasic Hinge Rotation Relationship[1] 51
3.5 Proposed Idealization of Partial Plastification at the Plastic Hinge 52
3.6 Proposed Model of Tangent Modulus of Elasticity 55
3.7 Idealized Axial Load-Displacement Upon Buckling of Straight Struts 58

4.1 Sensitivity of the Developed Hysteretic Model to the Variations of the Empirical Variables (W6X20, kl/r=80) .. 65
4.2 Experimental and Analytical Maximum Compressive Strength of Angular Struts[45] 67
4.3 Experimental and Analytical Axial Load-Deformation Relationships of Concentrically Loaded Angles[46,47] 70
4.4 Experimental and Analytical Axial Load-Deformation Relationships of Eccentrically Loaded Angles[46,47] 72
4.5 Experimental and Analytical Axial Load-Deformation Relationships of Biaxially Loaded Angles[46,47] 73
4.6 Experimental and Analytical Comparisons of Strut 1, Table 4.5[1] 76
4.7 Experimental and Analytical Comparisons of Strut 2, Table 4.5[1] 78
4.8 Experimental and Analytical Comparisons of Strut 3, Table 4.5[1] 80
4.9 Experimental and Analytical Comparisons of Strut 4, Table

4.5[1] 82
4.10 Experimental and Analytical Axial Load-Displacement Relationships of Strut 5 (Table 4.5)[3] 84
4.11 Experimental and Analytical Axial Load-Displacement Relationships of Strut 6 (Table 4.5)[3] 85
4.12 Experimental and Analytical Axial Load-Displacement Relationships of Strut 7 (Table 4.5)[3] 86
4.13 Experimental and Analytical Axial Load-Displacement Relationships of Strut 8 (Table 4.5)[3] 87
4.14 Experimental and Analytical Axial Load-Displacement Relationships of Strut 9 (Table 4.5)[3] 88
4.15 Effects of Different Yield Strengths on the Axial Load-Displacement Relationships 90
4.16 Effects of Variations in Yield Strength on the Axial Load-Displacement Relationships 92
4.17 Effects of Rotational End Fixities on the Axial Load-Displacement Relationships 94
4.18 Effects of Cross-Sectional Shapes on the Axial Load-Displacement Relationships 96
4.19 Effects of Initial Imperfection on the Axial Load-Displacement Relationships 97
4.20 Effects of End Eccentricities on the Axial Load-Displacement Relationships 99

5.1 Analytical vs. Experimental Axial Forces in Truss Elements[44] 104
5.2 X-Bracing and In-Plane Redundants 105
5.3 X-Bracing Test Configaration and Typical Results 106
5.4 Effects of In-Plane Redundants on X-Braced Systems[44] 109
5.5 Stiffness Analysis Simulation in Incremental Nonlinear Analysis 112
5.6 Convergence Criteria in Incremental Nonlinear Analysis .. 112
5.7 Typical X-Braced Panels with Similar or Opposing Senses of Forces in Crossing Diagonal Braces 116
5.8 Partial / Complete Buckling Over the Element Length 118
5.9 The Selected Structural Systems 122
5.10 The Geometry of the Double Layer Space Truss[57] 123
5.11 Overall Analytical and Experimental Comparisons of the Double Layer Space Truss[57] 124

5.12 Picture of the Buckled Structure[57] 124
5.13 Detailed Analytical Performance of the Double Layer Space Truss 126
5.14 Detailed Behavior of an Isolated X-Braced System 132
5.15 Tower Geometry 135
5.16 Tower Perspective 136
5.17 Analytical Behavior of Some Key Members in the Tower 140

LIST OF NOTATION

A - cross-sectional area
dM - incremental midspan moment
dP - incremental axial force
$d\Delta$ - incremental midspan lateral deflection
$d\delta$ - incremental end axial displacement
$d\bar{\delta}_p$ - incremental plastic hinge axial displacement
$d\theta$ - incremental end rotational displacement
$d\bar{\theta}_p$ - incremental plastic hinge rotational displacement
$d\nu$ - incremental end displacement vector
$d\nu_p$ - incremental plastic hinge displacement vector
E - initial elastic modulus
E_t - tangent modulus of elasticity
F_y - yield stress
K_δ - axial tangent stiffness matrix of strut
K_t - 2x2 tangent stiffness matrix of strut
L - strut length
M - midspan moment
P - axial force
P_c - strut buckling load
P_y - axial yield force
Q_s - reduction factor accounts for local buckling as specified by AISC manual[17]
β_t - indicative of the level of the axial-flexural force combination
β_0 - indicative of the "first-yield" interaction diagram
Δ - midspan lateral deflection
Δ_0 - initial imperfection
δ_e - elastic axial displacement
δ_g - geometric shortening
δ_p - plastic hinge displacement
δ_{po} - accumulated plastic hinge displacement
δ_{ty} - tensile yield displacement
ϵ - axial strain, equals to δ/L
ϵ_0 - axial strain when the P-P_c

Φ - fully plastic interaction function

$\Phi,_M$ - partial derivative of Φ with respect to M

$\Phi,_P$ - partial derivative of Φ with respect to P

γ - weighting factor

λ - plastic deformation scalar

θ - end rotational displacement.

Subscripts

e - elastic

p - plastic

CHAPTER 1

INTRODUCTION

Steel struts are the main load carrying elements in space trusses, and also dominate the response of braced structural systems to certain loading conditions. While generally considered as pure axial elements in structural systems, the actual behavior of steel struts might involve substantial bending, caused by factors such as end eccentricities, initial imperfections, and post-buckling bowing of the element. Under cyclic loads, additional factors such as degradation of the strength and tangent modulus at critical regions further complicate the axial-flexural behavior of steel struts. Gradual plastification is another peculiarity of the strut performance, which can have tangible effects on its response to both monotonic and cyclic loads.

Improvements in inelastic-buckling modeling of steel struts are pre-requisites to the development of reliable nonlinear structural analysis programs capable of simulating the inelastic force redistribution in space trusses and braced structural systems under generalized loading conditions. Improved inelastic structural analysis techniques based on the refined element models will be effective tools in predicting the failure mechanism and "post-failure" behavior of structural systems, thereby providing information on the ductility of structural failure leading to efficient design modifications for improving this ductility. The "post-failure" behavior is of special significance in situations like complete transmission line systems, where a specific structure (e.g., a transmission line tower) reacts like a component of a larger system. Such structures will redistribute their forces to the adjacent components, if they reach the failure conditions. This redistribution phenomenon is strongly dependent on the "post-failure" behavior and residual strength of the collapsing components. Development of nonlinear analysis techniques for complete transmission line systems, capable of simulating the inelastic force redistributions following the failure of certain line structures is one of the major concerns of the electric power industry.[44]

The Research project reported herein has been concerned with the development of a reliable and computationally efficient model of steel struts, and the application of this element model for a more accurate prediction of the inelastic behavior of space trusses, without a detailed treatment of the complexities in the connection nonlinear behavior. This investigation has been performed in two phases. Phase one concentrated on the element modeling, while the structural analysis activities were conducted in phase two. Chapters 2,3, and 4 report on different stages of phase one, and Chapter 5 is devoted to the description of phase two.

Chapter 2 presents the physical performance of steel struts observed in tests under monotonic and cyclic loads. This chapter also critically reviews the available element modeling methodologies for predicting the steel strut performance. A brief discussion on the experimental behavior and analytical modeling of the common connections of steel struts is also presented in Chapter 2.

Chapter 3 describes the development of the new strut model which is distinguished from the previous ones by its computational efficiency, accuracy in predicting the test results performed on a wide variety of steel struts, and a heavy reliance on the theoretical concepts governing the steel performance (with minimum dependence on specific test data). The developed element model has been verified in Chapter 4, using numerous test data reported in the literature. The results of an analytical numerical study with the developed element model, aimed at generating some practical recommendations for design of steel struts, are also discussed in Chapter 4.

Chapter 5 presents an illustration of some peculiarities of the space truss nonlinear behavior, and briefly discusses the analytical techniques popularly used in nonlinear analysis of structural systems. The advantages and shortcomings of these techniques in application to space trusses are also stated. The process of incorporating the developed element model into a structural analysis program for nonlinear analysis of the space truss systems is illustrated in Chapter 5. This Chapter makes a comparison between the experimental nonlinear behavior of three typical space trusses and the predictions of the developed analytical techniques. Detailed discussions on the inelastic force redistributions and failure mechanisms of these truss systems, as predicted by the analytical models, are also presented, and comments are made on the advantages of a reliable nonlinear structural analysis program in optimizing the structural design and in securing a ductile mode of failure.

CHAPTER 2

A LITERATURE REVIEW ON THE INELASTIC CYCLIC BEHAVIOR OF STEEL STRUTS AND THEIR CONNECTIONS

2.1 INTRODUCTION

Steel struts are commonly used in braced frames (Figure 2.1a) and truss structural systems (Figure 2.1b). Their inelastic-buckling behavior tends to dominate the nonlinear response characteristics of such structures under static and dynamic loads. The steel strut performance is influenced not only by the material and geometric properties of the element itself, but also by the performance of their end connections. The end connections can modify the steel strut behavior by providing rotational restraint, generating end eccentricities, causing slippage (in the case of bolted connections), and weakening the element in the vicinity of the connections.

This chapter presents a review of the literature on the experimental behavior of steel struts and the modeling techniques adopted for predicting their hysteretic behavior. The chapter also deals briefly with the experimental behavior and analytical modeling of the strut connections.

2.2 PHYSICAL BEHAVIOR OF STEEL STRUTS UNDER GENERALIZED LOADS

The inelastic-buckling behavior of steel struts under cyclic loads, Figure 2.2a, involves several complex physical phenomena including:

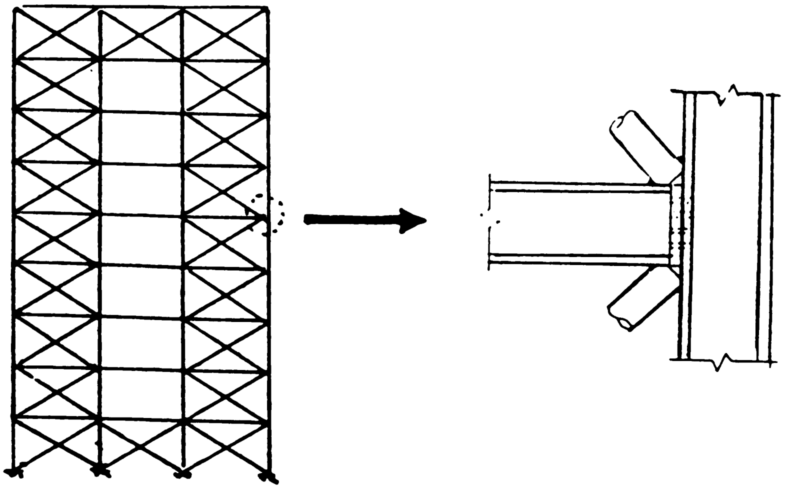

a) Braced Frame

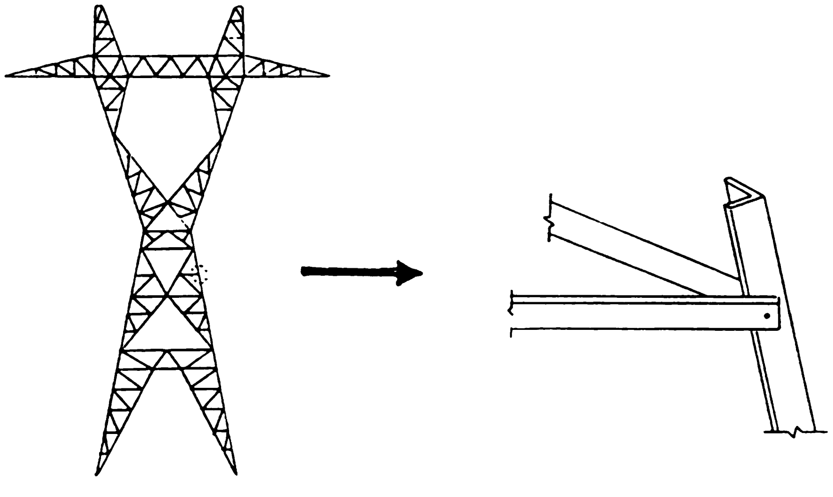

b) Steel Trusses

Figure 2.1 Steel Struts and Their Connections in Braced Frames and Space Trusses

buckling under compression and yielding in tension (Figure 2.2b), nonlinear behavior prior to buckling in compression (Figure 2.2c), post-buckling loss of the compressive resistance (Figure 2.2d), deterioration of the buckling load in the subsequent inelastic cycles (Figure 2.2e), progressive degradation of tangent moduli during cycles in compression (Figure 2.2f) and in tension (Figure 2.2g), and plastic growth in the brace length (Figure 2.2h).

The accuracy of the computed inelastic response of steel trusses and braced frames depends in large part on the accuracy of the strut models.[1,2,4] An ideal strut model is a theoretically-based (and thus generally applicable) one, capable of properly describing the axial force-deformation characteristics of the strut (accounting for the physical phenomena shown in Figure 2.2). Moreover, the model should be computationally efficient for analysis of large structural systems.

A considerable amount of information is now available on the initial buckling load of steel columns.[5,6,7] The understanding of the inelastic behavior of struts under generalized loading conditions is, however, just emerging. A number of proposals have been made for mathematical modeling of the strut inelastic-buckling behavior under cyclic loads,[1,2,3,4,8,9] but the state of the art in this area has not yet developed to the point where all of the influential factors can be accounted for analytically. The key problems in this area seem to be associated with :

a) Development of a computationally efficient and generally applicable model for predicting the strut hysteretic behavior;[1,2]

b) Effect of local plate buckling on the overall hysteretic behavior of struts;[1,3,4,5,10]

c) Degradation of the steel strut capacity and tangent modulus under repeated inelastic load reversals (resulting from the Bauschinger

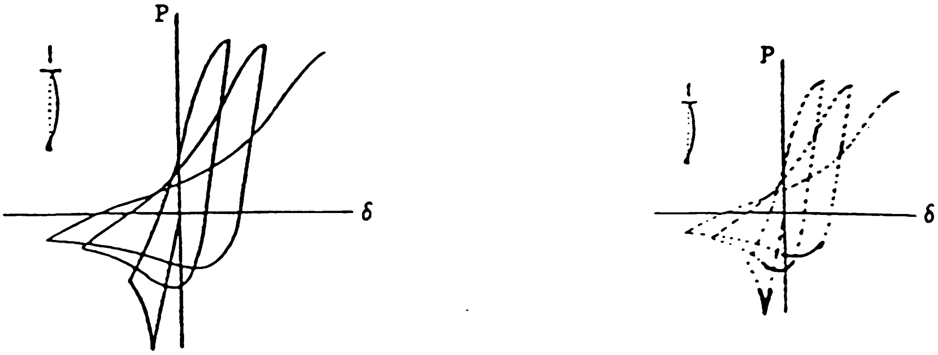

a) General Behavior

b) Yielding and Buckling behavior

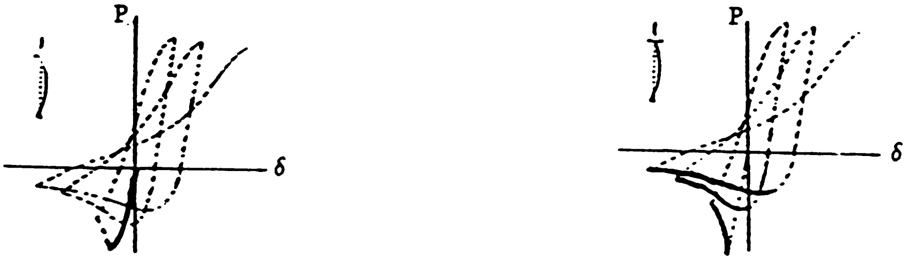

c) Nonlinearity Prior to Initial Buckling

d) Post-Buckling Loss of Resistance

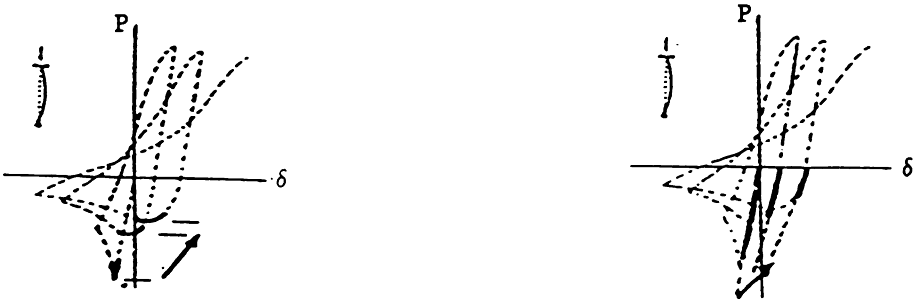

e) Buckling Load deterioration

f) Compressive Tangent Modulus Degradation

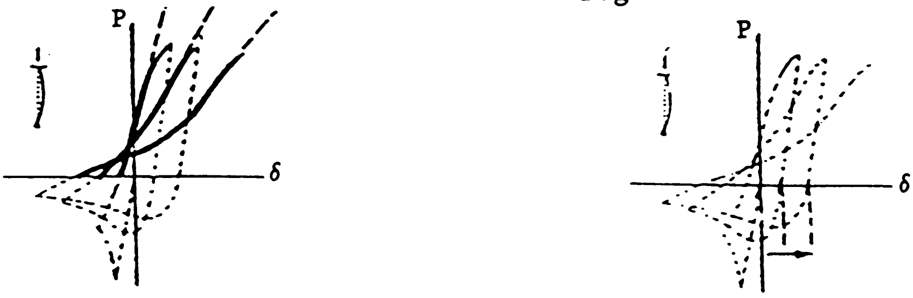

g) Tensile Tangent Modulus Degradation

h) Plastic Growth in Length

Figure 2.2 Cyclic Behavior of Steel Struts

effect and gradual plastification of the highly stressed regions)[3]; and

d) Nonlinearities prior to buckling of the virgin element loaded in compression (due to initial imperfection and residual stresses), and the consequent reduction of the initial buckling load;[2,5,13]

2.3 EXPERIMENTAL RESULTS ON STEEL STRUTS

Experimental studies have helped to identify the following important aspects of the strut behavior under cyclic loads :

2.3.1 Formation of Plastic Hinges : Inelastic deformations concentrate in the critical regions of steel struts (plastic hinges),[2,3,14,15,16] and repeated inelastic load reversals tend to pronounce this concentration.[3] Figure 2.3a shows a typical plastic hinge axial force-moment relationship obtained in cyclic tests on steel struts.[1] The theoretical first-yield and fully-plastic interaction diagrams are also presented. The actual plastic hinge behavior shown in this figure tends to deviate from the commonly assumed elastic-fully plastic type of response. The gradual plastification of the hinge seems to be a major factor influencing the behavior. This is confirmed in Figure 2.3b, while compares an empirical axial force-plastic hinge rotation relationship with a theoretical curve that has been based on an assumed rigid-fully plastic behavior of the hinge.

It should be emphasized that plastic hinges deform both rotationally and axially. The plastic hinge axial deformations have been found to significantly influence the hysteretic performance of steel struts especially those with low and intermediate slenderness ratios.[2]

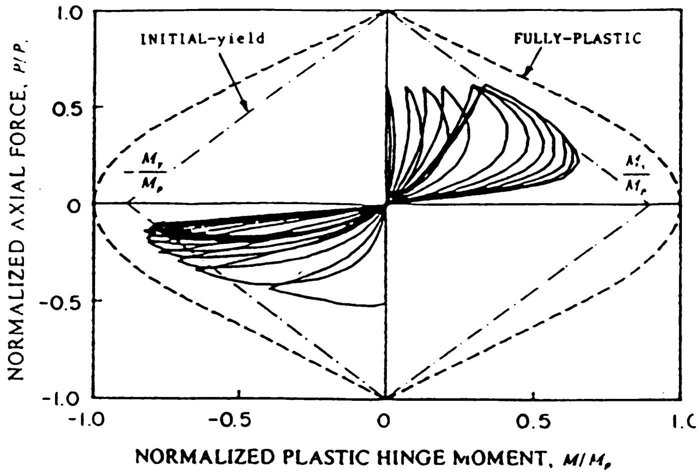

a) Axial Force vs. Plastic
Hinge Momenst

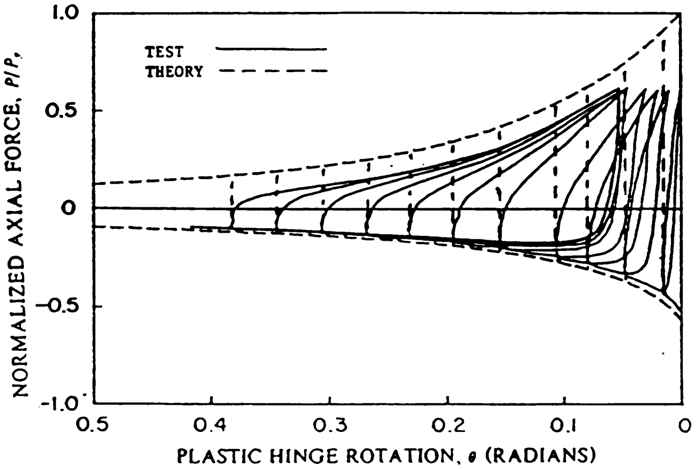

b) Axial Force vs. Plastic
Hinge Rotation

Figure 2.3 Detailed Behavior of Plastic Hinges
(TS 4in x 4in x 1/2in, Kl/r 80)[1]

2.3.2 Effects of Slenderness Ratio : The strut effective slenderness ratio has a dominant effect on its inelastic-buckling behavior.[2,3] Struts with lower slenderness ratios exhibit a more stable hysteretic performance. This is typically shown in Figure 2.4 which compares the experimental hysteretic envelopes of two struts with similar cross sections but with different slenderness ratios (hysteretic envelopes enclose all the hysteretic loops).[3]

2.3.3 Effects of Local Buckling : Local plate buckling is generally recognized as a major factor causing the differences in the inelastic-buckling performance of struts with similar slenderness ratios but with different cross-sectional sizes and shapes.[3,10] A T-section with unstiffened plate elements having relatively large width-to-thickness ratios is shown in Figure 2.5 to have inferior buckling load, post-buckling behavior and energy dissipation capacity, when compared with a pipe made from a relatively thick plate.[10] Test results have also indicated that the local buckling distortions tend to grow with increasing compressive strains, and they generally disappear at tension yielding.[10] Even "compact" sections are observed to suffer local plate buckling at large inelastic compressive strains.[10] The adverse effects of local plate buckling tend to grow under repeated inelastic load reversals (which cause deterioration at the plate buckling locations).

2.3.4 Effects of Initial Imperfection and Residual Stresses : These factors mainly reduce the initial compressive stiffness and strength of the virgin elements. Typical effects of the variations in initial imperfection and residual stresses of struts on their response to monotonic compressive loads are shown in Figures 2.6a and 2.6b, respectively.

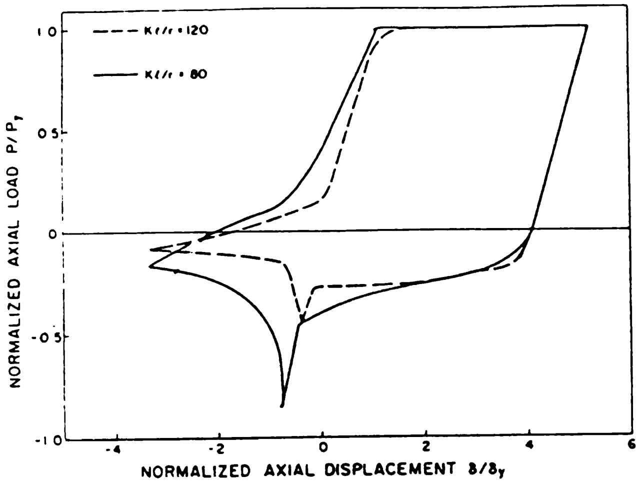

Figur 2.4 Effects of Slenderness Ratio on the Strut Hysteretic Performance (W6x20)[3]

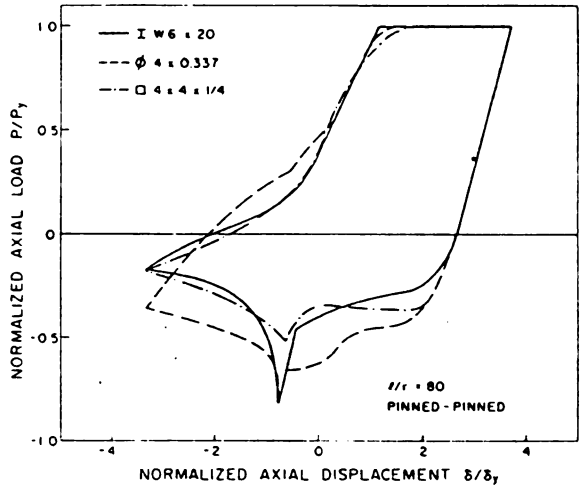

Figure 2.5 Effects of Cross-sectional Shape (partially caused by local buckling) on the Strut Hysteretic Performance[10]

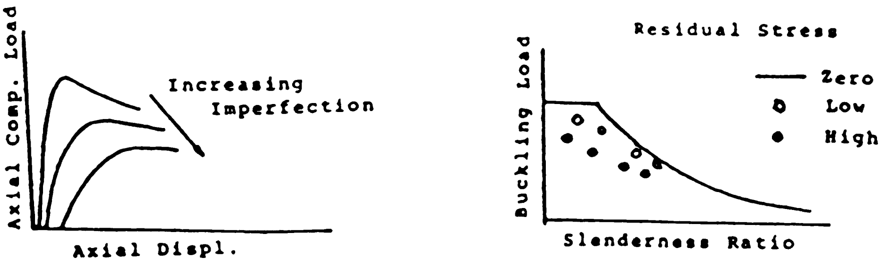

a) Initial Imperfection b) Residual Stersses

Figure 2.6 Effects of Initial Imperfection and Residual Stresses on the Initial Buckling load of Steel Struts.[5,6,7]

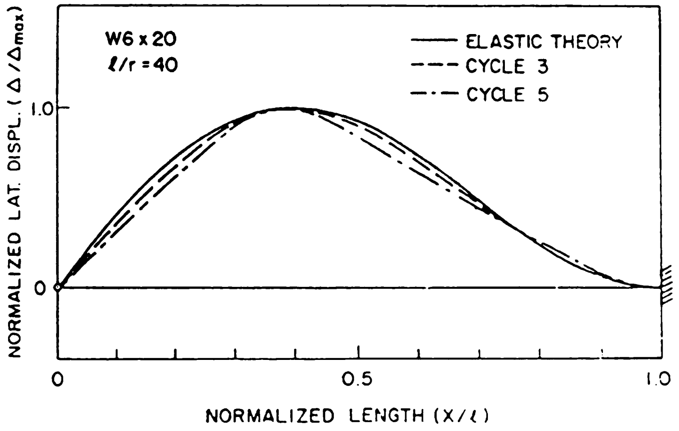

Figure 2.7 Inelastic Buckling Shape Compared with the Elastic Curve[3]

2.3.5 Effective Length Concept : Figure 2.7 compares, at different stages of a cyclic loading history, the buckled shapes of a steel strut fixed at one end and hinged at the other.[3] Although the curvature tends to concentrate more in the plastic hinge region in later cycles, the inflection points coincide with the elastic predictions. The buckled shape is also found in Ref. 3 to be independent of the strut slenderness ratio. Based on these observations, it seems reasonable to adhere to the effective length concept, according to which the portion of strut between the inflection points acts as a hinged-hinged element, even under inelastic load cycles.

2.4 ANALYTICAL MODELING OF STEEL STRUTS UNDER GENERALIZED LOADS

Examples of the earlier steel strut hysteretic models used for nonlinear dynamic analysis of space trusses and braced structures are : "tension-only" without compression resistance, Figure 2.8a, and "yield-elastic buckling", Figure 2.8b.[2] These models can not realistically represent the actual hysteretic performance of struts shown in Figure 2.2a.

More recently, three different modeling techniques have been used to predict the inelastic-buckling behavior of struts : finite element, phenomenological, and physical theory.

2.4.1 Finite Element Models : In this approach,[1,2] the strut is divided longitudinally into a series of segments, Figure 2.9, which are further subdivided into a number of layers, and a large displacement analysis is performed for the complete system. The finite element technique is generally applicable to many types of problems. In this approach, only the member geometry and material properties need to be defined. The finite element technique in application to steel struts is, however,

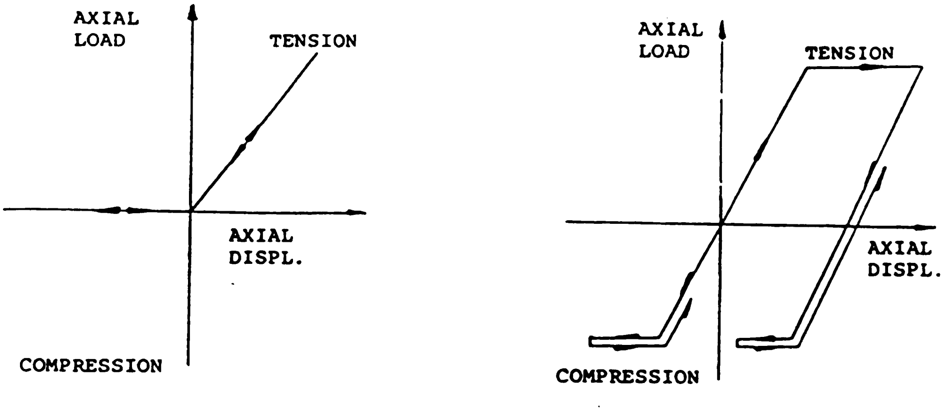

a) Tension-only

b) Yield-Elastic Bukling[2]

Figure 2.8 Earlier Strut Models[2]

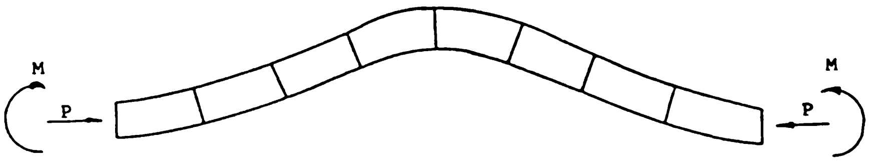

Figure 2.9 Finite Element Model

computationally expensive, and given the large number of degrees of freedom in each member and the large storage requirements for the element property variables, the method is generally considered to be impractical for nonlinear analysis of large structures.[1,2,3] Another disadvantage of the finite element modeling technique in application to some structural systems like lattice transmission towers with bolted connections is the inconsistency in the accuracies achievable at different modeling and analysis steps. Simulation of the behavior of a bolted connection and selection of the element material and geometric characteristics, residual stresses and initial imperfections for input to the finite element model are currently done at degrees of accuracy which are far below that of the finite element modeling technique. Hence, it is questionable if the accuracy of the final analytical results is any where close to the accuracy generally expected from the time- and storage-intensive finite element technique. The finite element models can, however, be useful tools in analytical studies on small subcomponents of structures and their elements. They can substitute experimental techniques commonly used to verify the simpler and more practical element models.

2.4.2 **Phenomenological Models** : The phenomenological models are currently the most common strut models used for nonlinear analysis of steel trusses and braced structures.[1] Phenomenological models are based on simplified rules that only mimic the experimental axial force-displacement relationships, Figure 2.10. These models have only one local degree of freedom, axial deformation, and they are computationally efficient. Their users, however, should usually specify numerous empirical input parameters for each strut. Such parameters can be

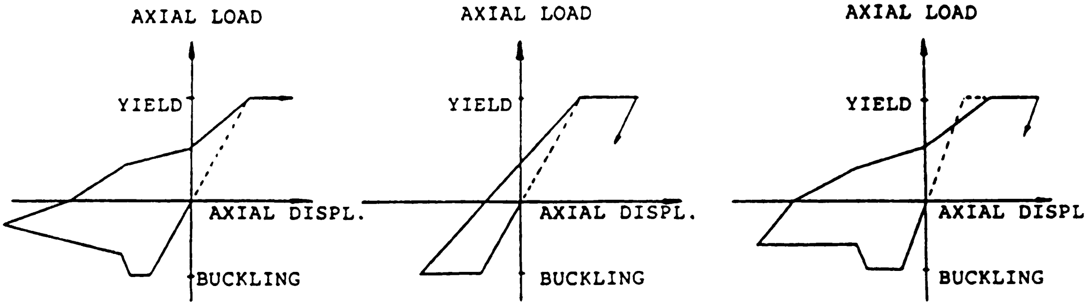

a) Nilforoushan,[19] b) Singh[20] c) Maison[4]

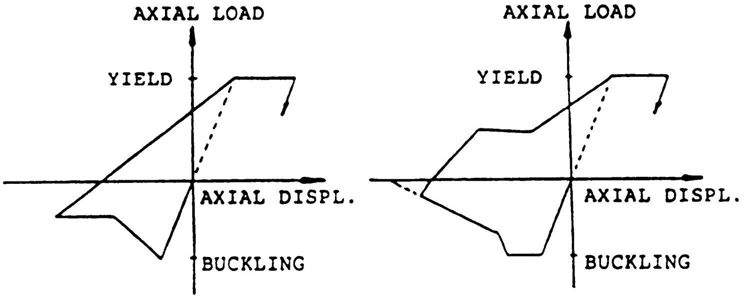

d) Jain[10] e) Ikeda[21]

Figure 2.10 Examples of Phenomenological Models

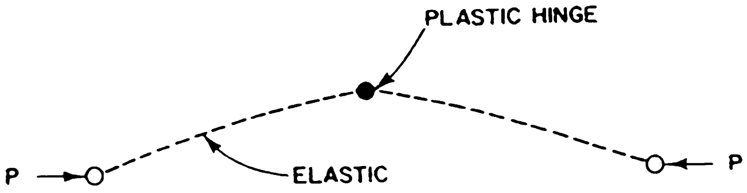
PLASTIC HINGE
P
ELASTIC
P

Figure 2.11 Typical Element Geometry in Physical Theory Models

selected properly only if test results on struts similar to the ones under consideration become available.

2.4.3 Physical Theory Models : These models incorporate simplified theoretical formulations based on some assumptions on the physical behavior of struts. The main assumption of these models is that inelastic deformations are concentrated in dimensionless plastic hinges at critical locations of struts, Figure 2.11. Input parameters for physical theory strut models are simply the member geometric and material properties. They also have a small number of degrees of freedom. Their computational efficiency, however, has been damaged by the fact that the available formulations of physical theory strut models are based on the force method of analysis.[1,2] This deficiency has been overcome ,in this study by successfully applying a formulation based on the displacement method of analysis to these models. With this improvement, the physical theory modeling technique seems to combine the realism of the finite element approach with the computational simplicity of the phenomenological modeling technique, and to provide a promising method for simulating the inelastic-buckling behavior of steel struts in large structures.

2.5 STATE-OF-THE-ART IN PHYSICAL THEORY MODELING OF STRUTS

Several physical theory models have been developed for simulating the inelastic-buckling behavior of steel struts.[1,8,9,10,16,18,22,23,24] These models usually have a plastic hinge at midspan which connects two elastic segments of the element, Figure 2.11.

The axial component of the plastic hinge deformation was neglected in the early physical theory strut models in favor of the rotational component; however, both components have been included in the later models. Most of the available physical theory models have been based on the following set of assumptions :

1) Material properties are elastic-perfectly plastic;
2) The plastic state of the hinge is described by an interaction curve relating the fully plastic values of moment and axial force;
3) Partial plastification within the hinge and along the element length are disregarded;
4) The element bends uniaxially;
5) There is no possibility of local or torsional-flexural buckling;
6) Plane sections remain plane after bending;
7) Shear deformations are negligible; and
8) The effective length concept is valid even under inelastic load cycles.

In the following, first a simple (basic) physical theory model is introduced, and then two recent models that represent the state-of the-art in this area are critically reviewed.

2.5.1 Gugerli Model : The axial displacement δ of the physical theory element model proposed in Reference 38 consists of five components,

$$\delta = \delta_e + \delta_g + \delta_p + \delta_{po} + \delta_{ty} \tag{2.1}$$

where : δ_e = elastic axial displacement;
δ_g = geometric shortening;
δ_p = plastic hinge displacement;
δ_{po} = accumulated plastic hinge displacement; and
δ_{ty} = tensile yield displacement.

The elastic axial displacement δ_e is expressed as

$$\delta_e = \frac{PL}{EA} \tag{2.2}$$

where A is the cross-sectional area.

The expression for δ_g is :

$$\delta_g = - h_1(k)\ \theta_p^2\ L \tag{2.3}$$

where :

$$h_1(k) = \begin{cases} \dfrac{\dfrac{\sin k}{k} + 1}{16\cos^2 \dfrac{k}{2}} & \text{if } P<0 \\ \dfrac{\dfrac{\sinh k}{k} + 1}{16\cosh^2 \dfrac{k}{2}} & \text{if } P>0 \end{cases}$$

$$k^2 = \frac{|P|\ L^2}{EI}$$

θ_p = plastic hinge rotation; and

L = member length.

The axial displacement, δ_p, associated with the plastic hinge deformations takes the form :

$$\delta_p = \int_{Po}^{P} \frac{d\delta_p(P^*)}{dP^*}\, dP^* \tag{2.4}$$

where P_o is the axial force value at which the plastic hinge initially becomes plastic.

Equation 2.4 takes into account the effects of the plastic hinge axial and rotational deformations on the strut length. A plastic rule based on Druker's postulate[39] was also used by Gugerli to arrive at an expression for the incremental axial plastic hinge deformation $d\delta_p$:

$$d\delta_p = - y_n \, d\theta_p \tag{2.5}$$

where y_n denotes the location of instantaneous neutral axis, Figure 2.12

The plastic hinge rotation θ_p can be determined by solving the compatibility and equilibrium equations of the elastic segments of the element model, with due consideration to the boundary conditions :

$$M = g(k) \frac{EI}{L} \theta_p \tag{2.6}$$

where : M = plastic hinge moment;

$$g(k) = \begin{cases} -\frac{k}{2} \tan \frac{k}{2} & \text{if } P<0 \\ \frac{k}{2} \tanh \frac{k}{2} & \text{if } P>0 \end{cases}$$

Five different zones shown in Figure 2.13 are used in formulating cyclic inelastic-buckling behavior of steel struts based on the above equations. The Gugerli model distinguishes between the elastic and plastic states of the plastic hinge behavior, and it accounts for the yielding of the strut when it straightens under tension. A typical comparison of the Gugerli model with test results is presented in Figure 2.14. A major limitation of the Gugerli model is its failure to simulate the drastic deterioration in the buckling load with cycles.

2.5.2 Ikeda Model : In this physical theory element model presented in Reference 1, the axial displacement of the strut is assumed to consist of seven components :

$$\delta = \delta_e + \delta_g + \delta_p + \delta_{po} + \delta_{ty} + \delta_m + \delta_{mo} \tag{2.7}$$

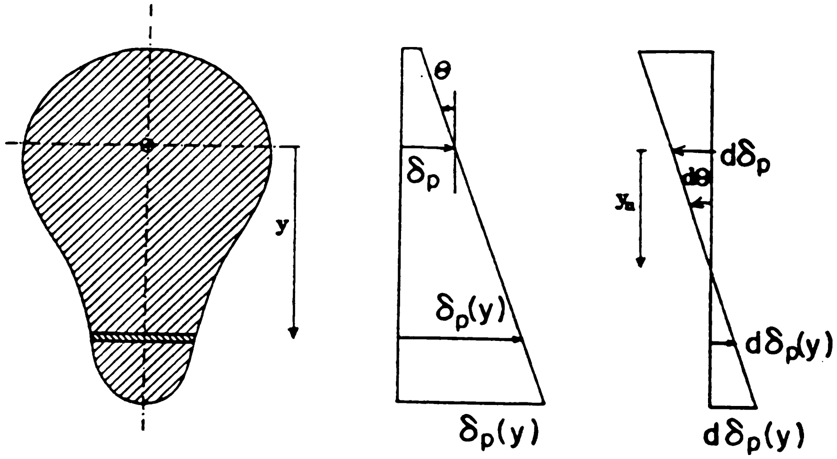
y
θ
δp
δp(y)
δp(y)
dδp
dθ
yn
dδp(y)
dδp(y)

Figure 2.12 Definition of the Location of the Instantaneous Neutral Axis y_n[38]

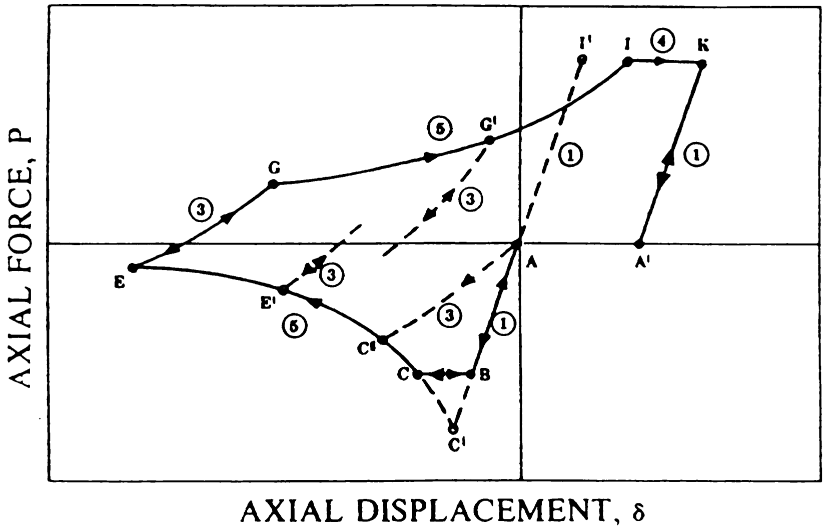

Figure 2.13 Axial load-Displacement Curve Used in the Gugerli Model[1]

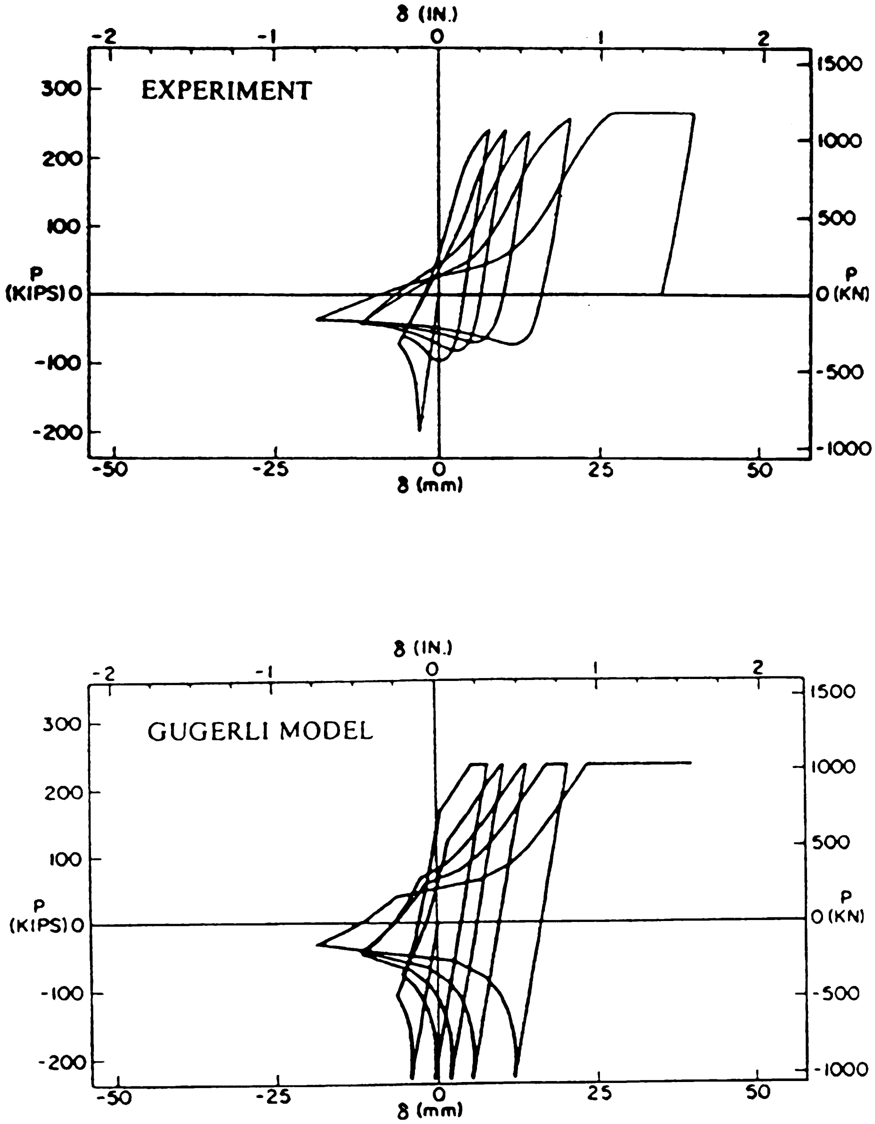

Figure 2.14 Comparison Between Experimental and Gugerli Axial Load-Displacement Curves[1]

where : δ_e, δ_g, δ_p, δ_{po} and δ_{ty} were defined in the previous section (see Equation 2.1)

δ_m = corrective displacement to remove errors resulting from sudden change of tangent modulus upon load reversal; and

δ_{mo} = residual corrective displacement.

The elastic axial and geometric displacements, δ_e and δ_g are derived in Reference 1 using the equilibrium and compatibility equations, with due consideration to the boundary conditions. The plastic hinge contributions to the element axial displacement, δ_p and δ_{po}, are derived in terms of axial load using the fully-plastic interaction diagram concept together with the outward normal plastic flow rule. The physical theory strut model developed in Reference 1 also incorporates a number of empirical refinements illustrated below :

a) Corrective factors are applied to the theoretical fully-plastic interaction diagram, Figure 2.15a;

b) The material tangent modulus, used in calculating δ_e and δ_g, is expressed as a function of axial load, Figure 2.15b; and

c) An axial force-plastic hinge rotation relationship is used to account for the gradual plastification of the hinge, Figure 2.15c.

Figure 2.16 presents a typical comparison between an experimental cyclic axial load-displacement relationship and the theoretical prediction of the model of Reference 1. This comparison is made for a 21/2 in X 0.049 in. pipe having a yield strength of 27.4 ksi and an effective length of 50 in. The model is observed to overestimate the initial and consequent buckling loads, and the maximum tensile loads and tangent stiffnesses of the strut in later cycles.

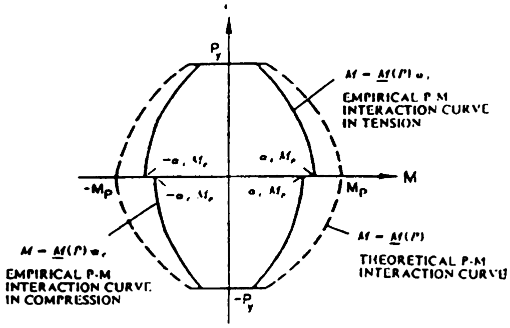
P_y
$M = \underline{M}(P)a_t$
EMPIRICAL P-M INTERACTION CURVE IN TENSION
$-a, M_r$
a, M_r
M
$-M_p$
M_p
$-a, M_r$
a, M_r
$M = \underline{M}(P)a_c$
EMPIRICAL P-M INTERACTION CURVE IN COMPRESSION
$M = \underline{M}(P)$
THEORETICAL P-M INTERACTION CURVE
$-P_y$

a) Fully-Plastic Interaction Diagram

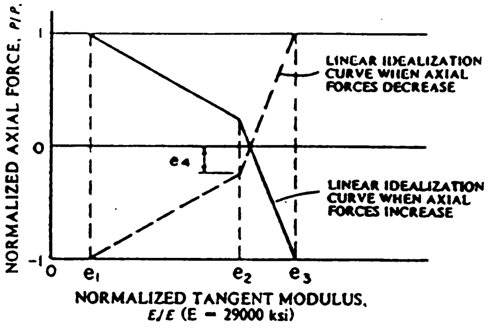

b) Tangent Modulus vs. Axial Load

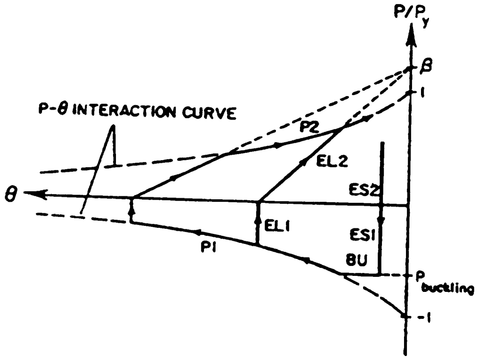
P/P_y
β
1
P-θ INTERACTION CURVE
P2
EL2
θ
ES2
EL1
ES1
PI
BU
$P_{buckling}$
-1

c) Plastic Hinge Rotation vs. Axial Load

Figure 2.15 Empirical Relationships Used in Formulation of the Physical Theory Strut Model in Reference 1

The discrepancies between the experimental results and theoretical predictions observed in Figure 2.16 are possibly caused by the following shortcomings of the model developed in Reference 1 :

a) Effects of the residual stresses and initial imperfection on the behavior of the virgin element in compression are neglected;

b) The incorporated modifications in the fully-plastic interaction diagram and axial force-plastic hinge rotation relationship are purely empirical and based on limited test data. Their general applicability is thus questionable;

c) Modification of the tangent modulus in this model is based on the assumption that the element is under a uniform stress condition along its length, disregarding the concentration of high axial-flexural stresses near the plastic hinge; and

d) The possibility of local plate buckling is disregarded in the model.

There are a relatively large number of empirical parameters that should be input to this model. Moreover, the formulation of Reference 1 expresses the strut axial displacement in terms of axial force and thus it is computationally inefficient for incorporation into the conventional computer programs for nonlinear analysis of large structures, that generally follow the displacement method of analysis.

2.5.3 **Zayas Model** : In order to overcome the computational inefficiency of the physical theory strut models, Reference 2 has introduced, but not fully developed or verified, a theoretical basis for development of an efficient formulation for these models, which is capable of illustrating axial force in terms of axial displacement. In this formulation, one half of the strut, that is assumed to be symmetric, is treated as a two-degree-of-freedom system (Figure 2.17), and the incremental forces , dP

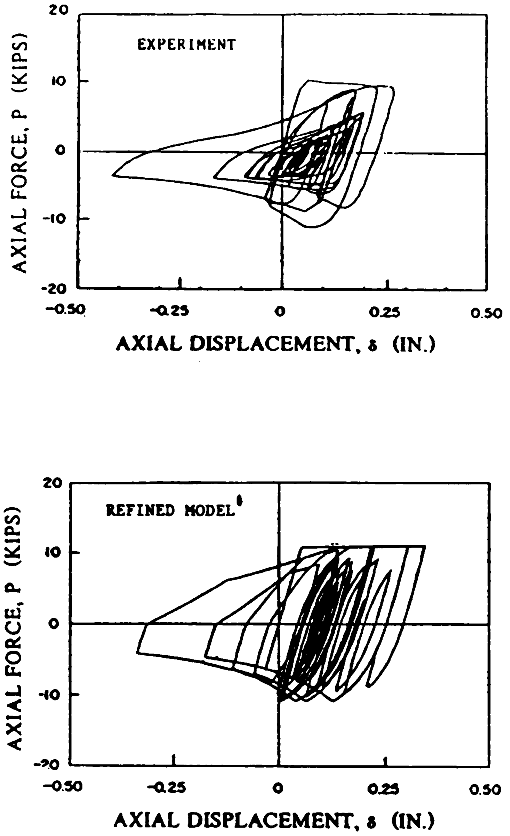

Figure 2.16 Theoretical and Experimental Hysteresis Loops[1]

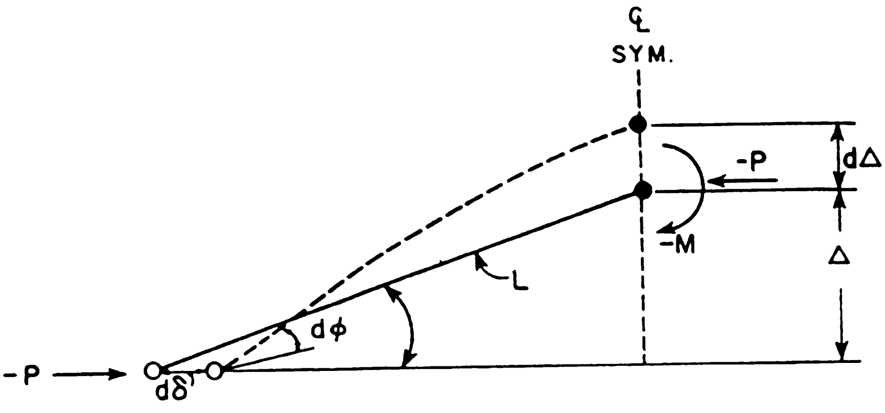
℄
SYM.
-P
dΔ
-M
Δ
L
dϕ
-P
dδ

Figure 2.17 The Physical Theory Strut Model of Reference 2

and dM, are related to the incremental displacements, $d\delta$ and $d\theta$, through a tangent stiffness matrix, k_t :

$$\begin{bmatrix} dP \\ dM \end{bmatrix} = k_t \begin{bmatrix} d\delta \\ d\theta \end{bmatrix} \tag{2.8}$$

The total incremental strut end deformations are assumed to be the sum of the elastic and plastic parts.

$$\begin{bmatrix} d\delta \\ d\theta \end{bmatrix} = \begin{bmatrix} d\delta_e \\ d\theta_e \end{bmatrix} + \begin{bmatrix} d\delta_p \\ d\theta_p \end{bmatrix} \tag{2.9}$$

where the subscripts e and p represent the elastic and plastic contributions, respectively.

Zayas developed the following incremental equation, where the incremental axial force dP and moment dM at the plastic hinge are related to the elastic strut end deformations by means of the elastic force-deformation matrix B.

$$\begin{bmatrix} dP \\ dM \end{bmatrix} = B \begin{bmatrix} d\delta_e \\ d\theta_e \end{bmatrix} \tag{2.10}$$

The plastic portion of end displacements are related to the plastic hinge deformations by means of a geometric transformation matrix.

$$\begin{bmatrix} d\delta_p \\ d\theta_p \end{bmatrix} = \begin{bmatrix} \cos\theta & L\sin\theta \\ 0 & 1 \end{bmatrix} \begin{bmatrix} dL_p \\ d\theta_p \end{bmatrix} \tag{2.11}$$

where L_p is the axial plastic hinge deformation.

The outward normal flow rule[39] can be applied to the plastic hinge deformations.

$$\begin{bmatrix} dL_p \\ d\theta_p \end{bmatrix} = \begin{bmatrix} \Phi,_P \\ \Phi,_M \end{bmatrix} \lambda \qquad (2.12)$$

where : λ = plastic deformation scalar;

Φ = formula for the interaction curve;

$\Phi,_P$ = derivative of Φ with respect to P; and

$\Phi,_M$ = derivative of Φ with respect to M.

Combining Equations 2.11 and 2.12, the flow rule for the strut end deformations can be written as follows :

$$\begin{bmatrix} d\delta_p \\ d\theta_p \end{bmatrix} = \lambda \, J \qquad (2.13)$$

where : $J = \begin{bmatrix} \cos\theta \ \Phi,_P + L\sin\theta \ \Phi,_M \\ \Phi,_M \end{bmatrix}$

Employing the condition that the interaction function Φ remains constant, one can arrive at the following equations

$$\begin{bmatrix} dP \\ dM \end{bmatrix} = B \begin{bmatrix} d\delta \\ d\theta \end{bmatrix} - J\lambda \qquad (2.14)$$

$$\lambda = G \begin{bmatrix} d\delta \\ d\theta \end{bmatrix} \qquad (2.15)$$

where :

$$G = [\Phi,_s^T \, B \, J]^{-1} \, [\Phi,_s^T \, B]$$

$$\Phi,_s = \begin{bmatrix} \Phi,_P \\ \Phi,_M \end{bmatrix}$$

Finally, Equations 2.14 and 2.15 can be combined and solved for the tangent stiffness matrix K_t.

$$K_t = (B - B.J.G) \qquad (2.16)$$

Static condensation is then used to reduce the element into a single-degree-of-freedom system :

$$dP = K_{\delta} \, . \, d\delta \qquad (2.17)$$

where :

$$K_{\delta} = \frac{K_{t11} + K_{t12} \left(\dfrac{P.F_1 - K_{t21}}{K_{t22} - P.F_2} \right)}{1 - \left(\dfrac{K_{t12} . \Delta}{K_{t22} - P.F_2} \right)}$$

The formulation introduced in Reference 22 employs the outward normal plastic flow rule and the fully-plastic interaction diagram concepts to simulate the plastic hinge behavior. This formulation, however, does not incorporate any of the refinements employed in Reference 1 (e.g. variation of tangent modulus as a function of force level and gradual plastification of the hinge). Some corrections and modifications were found to be necessary, and were incorporated in this research, for improving the above formulation. The approach, as introduced in Reference 2 and then modified in this study, provides an alternative implementation strategy for physical theory brace models.

2.6 PHYSICAL BEHAVIOR OF STEEL STRUT CONNECTIONS

Connections in space trusses can have detrimental effects on their overall behavior under load. The ability of connections to transfer moment and shear between elements, the rotational restraint they provide at element ends, their flexural capacity or capacity under different load combinations, slippage of bolted connections, and the weakening of elements at connections are among the factors related to connection behavior that tend to modify the element and structural response characteristics under generalized loads.

Connections of steel trusses are generally designed for monotonic axial forces of elements. Figure 2.18 presents the possible failure modes of a typical bolted connection with gusset plate under this loading condition. The connections of struts in space trusses might also be subjected to large bending moments in addition to axial loads. The bending moments are usually caused by the bowing of elements under axial loads, Figure 2.19, and by the frame action of trusses (which depends on the rotational rigidity of connections).

The connections capable of providing substantial rotational restraints at element ends, which are also the ones developing bending moments, might yield in flexure. The plastic hinges will thus form inside the connections at element ends (Figure 2.20), causing a reduction in the end rotational restraint. The flexural yielding moment of connections depends on the direction of bending, the level of axial load, the history of loading, and also the details of connection design.

Another critical aspect of the bolted connection behavior is the relative movement, slippage, of the connected elements and plates. Slippage occurs initially when the friction between the connected plates is overcome, Figure 2.21a, noticing that the bolts will not in general bear against the hole periphery before some slippage takes place. Eventually, after some slippage, the bolt will come in touch with the hole periphery and will induce stress concentration and yielding at the contact region, leading to the enlargement of the hole, Figure 2.21b, and continuation of slippage at higher loads. Upon the load reversal, a more extensive frictional slippage (with no bearing on the hole) will take place before the contact is made in the other direction (inside the enlarged hole). As a result of this action, the slippage will tend to become more dominant under cyclic load applications.

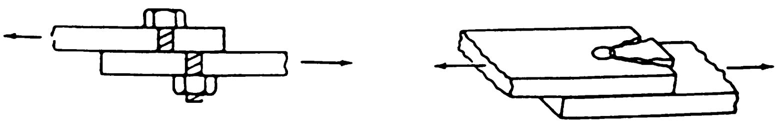

(a) Shear failure of bolt

(b) Shear failure of plate

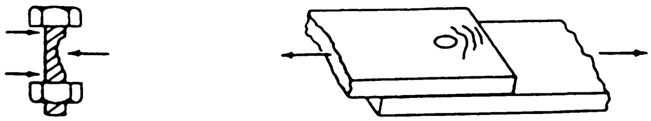

(c) Bearing failure of bolt

(d) Bearing failure of plate

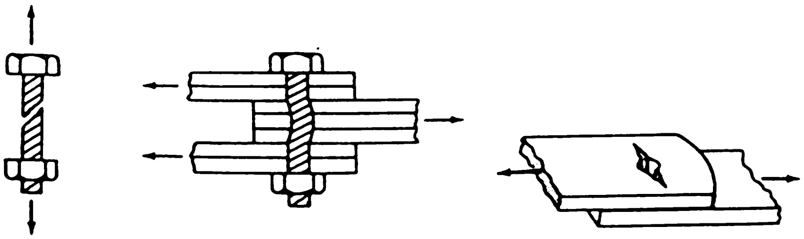

(e) Tensile failure of bolts

(f) Bending failure of bolts

(g) Tensile failure of plate

Figure 2.18 Possible Failure Modes of Bolted Connections[56]

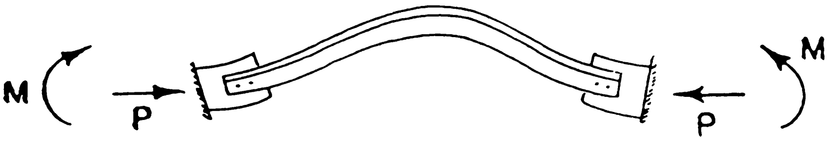

Figure 2.19 Bending Moment in Connections Caused by Bowing of Steel Struts

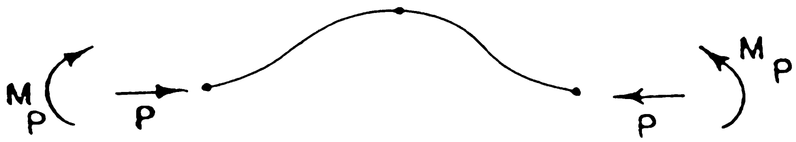

Figure 2.20 Formation of End Plastic Hinges Due to The Flexural Yielding of Connections

The element ends are generally weakened by the connecting action (e.g., drilling holes or welding). Welding might induce large residual stresses and the drilling of holes reduces the net cross sectional area. At both the welded and bolted connections, significant stress concentration might be produced, leading to premature yielding and failure.

2.7 EXPERIMENTAL RESULTS ON STRUT CONNECTIONS

Experimental studies on steel struts have generally been performed on struts having hinged or fixed supports. Test results on steel struts with realistic end connections are scarce, and very few comprehensive tests on truss connections are available in the literature.

References 40,41 and 42 have reported results of monotonic tests performed during 1950's on truss connections with gusset plates. The results indicate that a complex state of stress is induced in the gusset plates, leading to major material and geometric nonlinearities. Test results summarized in Reference 15 indicate that the rotational restraint provided by the gusset plates influences the buckling strength of steel struts under monotonic loading. The restraining effects of the gusset plate connections strongly depend on the direction of element buckling. If the buckling causes bending of the gusset plates in their planes, the plates are capable of providing large rotational restraints (close to fixity), and their large in-plane flexural capacity forces the plastic hinges to form inside the element adjacent to the connections, Figure 2.22a. If the element buckling causes bending of the gusset plates out of their plane, the rotational restraint at the element ends are relatively small, and plastic hinges tend to occur inside the gusset plates, Figure 2.22b. Increasing the thickness (e.g., the rotational stiffness) of gusset plates is found to be especially effective in increasing the element buckling load. The buckling load is not influenced

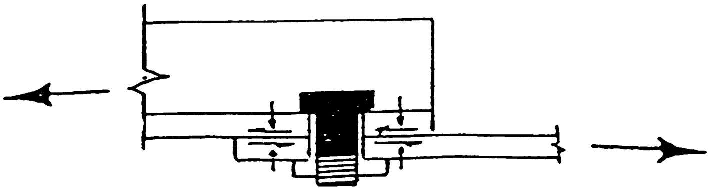

a) With No Bearing Against
Hole Periphery

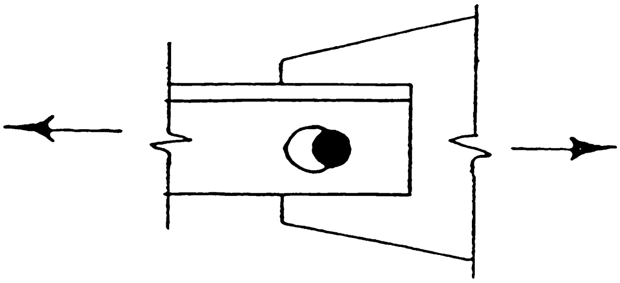

b) Enlarging of Hole by Bearing

Figure 2.21 Slippage at Bolted Connections

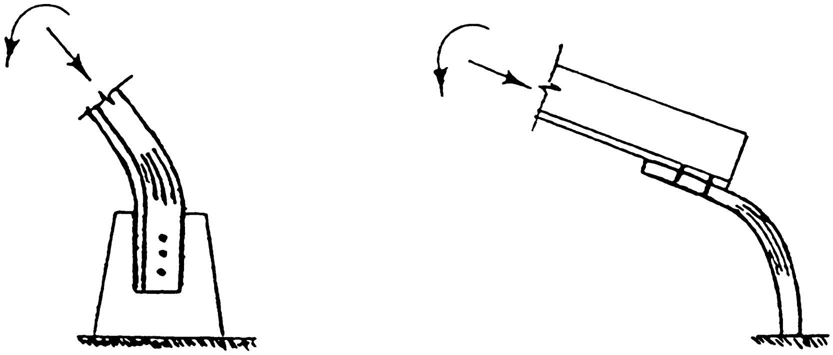

a) In-Plane Bending

b) Out-Plane Bending

Figure 2.22 Rotational Restraint of Gusset Plates in In-Plane and Out-Plane Bending

much by the increase in the gusset plate yield strength, (e.g., moment capacity).

The behavior of steel struts might be adversely influenced by a brittle failure associated with the rotation of the gusset plate connections (as is true for their brittle axial failure modes). The test results presented in Reference 43 have indicated that gusset plates tend to fracture in a brittle manner at relatively small out-of-plane rotations, if sufficient free length is not provided in the plate for the formation of a plastic hinge.

As mentioned earlier, the slippage of bolted connection (Figure 2.21) is an important factor influencing the connection and element behavior under load. Slippage causes a sudden jump in the strut axial deformations at a constant axial load . As can be seen in Figure 2.23, slippage may occur at relatively low axial loads, and can be followed by an almost elastic behavior of the strut. At higher loads, however, the local stress concentration at the bolt contact regions leads to yielding, hole enlargement and major nonlinearities. The increased slippage under load reversal is an indication of the enlargement of the bolt holes during the earlier load applications. This phenomenon would be pronounced as the load cycles are repeated. The considerable "pinching" of the hysteretic loops resulting from the slippage of bolted connections damages the strut behavior by reducing its hysteretic energy absorption capacity and axial stiffness.

2.8 CONNECTION MODELING AND DESIGN

Limited analytical studies have been conducted on the steel strut connections. Some investigators[1] have simply substituted the strut end connections with linear and/or rotational springs, Figure 2.24.

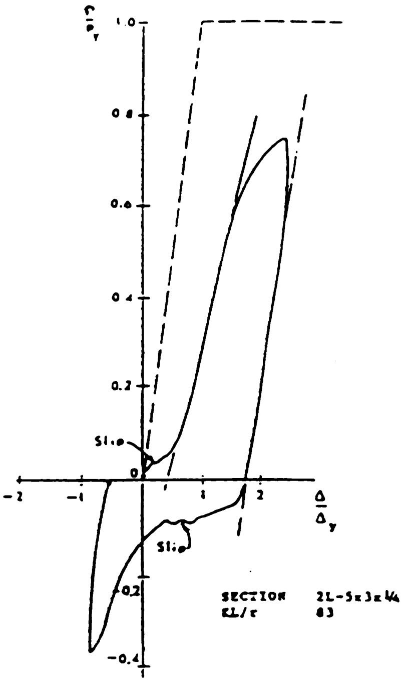

Figure 2.23 Effects of The Bolted Connection Slippage on The Steel Strut Behavior Under Load[43]

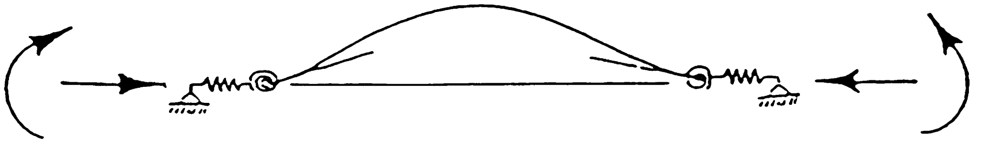

Figure 2.24 Idealization of The Steel Struts End Connections by Linear and Rotational Springs

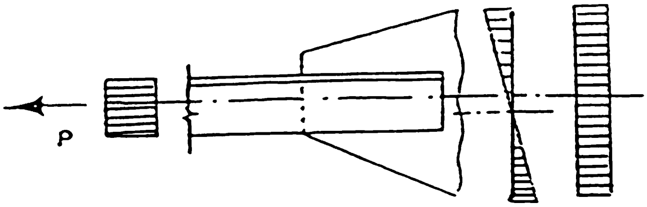

Figure 2.25 Strut Concentric Axial Force Used in Connection Design

However, no refined approaches have been reported for deriving the constitutive models (e.g., characteristic force and deformation values and hysteretic rules) of these idealized springs as functions of the physical properties of typical strut connections. Some simple simulations, like those which treat the connection gusset plate as a cantilever beam,[43] do not seem to realistically reproduce the actual behavior (especially with bolted connections) described above.

Inadequate analytical simulation studies have also led to the adoption of simplistic design approaches for the steel strut connections. The current practice in design of steel strut connections is to proportion the connection to resist a constant tension force acting through the centroid of the member, Figure 2.25. The results of existing tests,[43] however, indicate that the pure axial loading condition seldom exist in reality. The post-buckling behavior of steel struts induces large bending moments in addition to axial forces in connections. Hence, the design of strut end connections for the combined effects of bending moment and axial force, Figure 2.26, seems to be more appropriate. The plasticity condition of the connection under axial-flexural forces may be assumed to define the maximum force limits in designing the connections.

In spite of the complex stress distribution existing in the steel strut connections, the beam theory (Figure 2.27)[40,41,42,44,45] has been found to satisfactorily predict the maximum of stresses in gusset plates under monotonic loading. In addition, Reference 42 proposes that only an effective width of the gusset plate in bolted connections is fully functional in resisting the applied forces. The maximum stresses should be, according to Reference 42, based on this effective width which can be obtained (see Figure 2.28) by drawing 30 degree lines from the outer

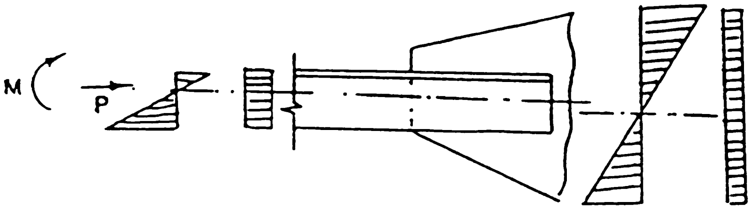

Figure 2.26 Axial-Flexural Forces Usually Induced in The Strut End Connections

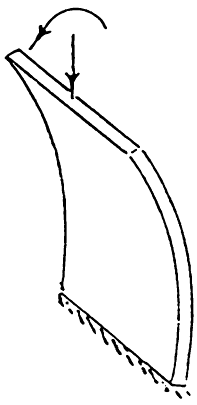

Figure 2.27 Cantilever Beam Simulation of Gusset Plates

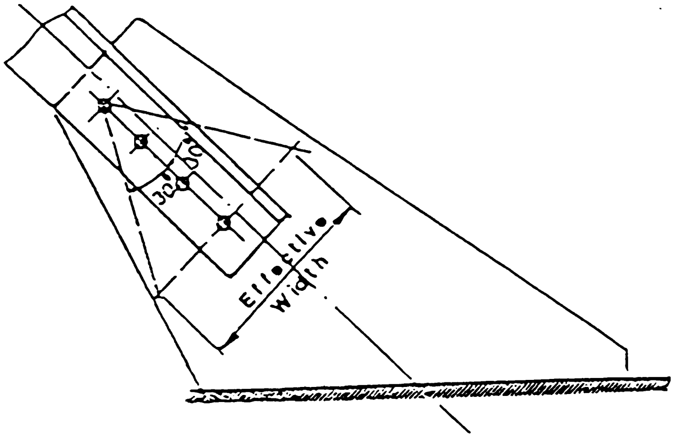
30°
30°
Effective
Width

Figure 2.28 Effective Width of Gusset Plates[42]

fastener in the first row to intersect with a line perpendicular to the line of force action passing through the bottom row of the fasteners. Recent studies, have indicated that some connection details might have detrimental effects on the ductility of failure. Reference 43, for example, suggests that a free length of the gusset plate equal to two times its thickness should be provided beyond the element ends. This free length enables the end plastic hinges, forming in the gusset plates bending out of their plane, to go through large rotations without restraints that cause brittle fracture of the plates in bending.

2.9 SUMMARY AND CONCLUSIONS

The inelastic-buckling behavior of steel struts and their connections plays a detrimental role in the response of steel trusses and braced frames to static and dynamic loads. This chapter has summarized the results of experimental studies on the inelastic, monotonic and cyclic, behavior of steel struts and their connections, and has critically reviewed the suggested analytical techniques for predicting the response characteristics of the strut elements and connections under generalized loading conditions.

The experimental results on steel struts have indicated that the element behavior under cyclic loads is strongly influenced by :
a) concentration of inelastic deformations in the critical regions (plastic hinges); b) slenderness ratio of the struts; c) local plate buckling; and d) initial imperfections and residual stresses. Inelastic cyclic test data have also indicated that the effective length concept, commonly applied to struts under monotonic loads, is also applicable under cyclic loads.

Connections of the steel struts can significantly modify the strut behavior under generalized loads. They influence the element behavior through : a) their ability to transfer moment and shear between adjacent elements; b) rotational restraint of the element ends; c) weakening the element by the fastening action (drilling holes and welding); d) yielding and failure of the connections under axial-flexural forces; and e) slippage at the bolted connections.

The more recently developed analytical models for predicting the steel strut load-deformation behavior under generalized loads can be categorized as the finite element, phenomenological, and physical theory models. Among these, the physical theory simulation techniques seem to combine the realism and generality of the finite element approach with the computational simplicity of the phenomenological modeling technique, and to provide a promising method for simulating the inelastic-buckling behavior of steel struts in large structures. The physical theory models incorporate simplified theoretical formulations based on some assumptions on the physical behavior of struts. From a comprehensive review of the available physical theory models of steel struts, it may be concluded that improvements are needed in : a) their computational efficiency in analysis of large structures; b) consideration of the gradual plastification of the element; c) accounting for the initial imperfections and residual stresses which cause nonlinearities prior to buckling of the virgin element loaded in compression; and d) eccentricities of the axial load at element ends. There are also other aspects of the available physical theory strut models which require improvements, but have been outside the scope of this investigation. These include : a) simulation of local plate buckling, b) the end rotational restraint provided at connections, and c) the possibility of torsional-flexural buckling.

Limited analytical studies have been reported on steel strut connections, especially under cyclic loads. The suggested simplistic simulations of the connection physical performance do not seem to provide realistic means of reproducing the actual behavior, especially in the case of bolted connections. The current practice in design of steel strut connections, based on simple connection models and loading conditions, also fails to account for the combined effects of the transferred axial-flexural forces and the complex stress distribution existing inside connections.

CHAPTER 3

THE DEVELOPED ELEMENT MODEL

3.1 INTRODUCTION

The physical theory models of steel struts incorporate simplified theoretical formulations based on some assumptions on the physical behavior of struts.[2,4,5,9] The main assumption of these models is that the inelastic deformations at axial loads below the yield limit are concentrated in dimensionless plastic hinges at critical locations of struts (Figure 3.1). The theoretical basis of the physical theory strut models improves their reliability and general applicability.

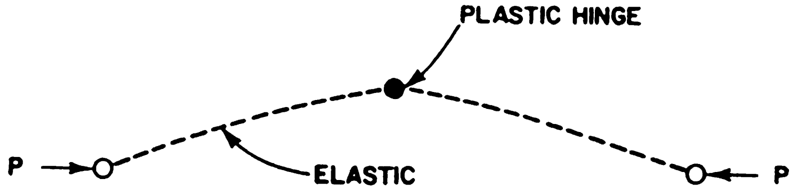

Figure 3.1 Pinned-End Physical Theory Model

The input parameters to physical theory strut models are simply the basic geometric and material properties of the element. These models also involve a small number of degrees of freedom. They are thus convenient to define, and structural analysis employing these models would require relative small amounts of computer time and memory.

The formulations presented in the literature for physical theory strut models, however, are computationally inefficient in the sense that they use the axial force of the element as the input variable defining the external effects and the output is the axial displacement of the element. Hence, in application of these models to nonlinear analysis of structures using the conventional displacement method of analysis, a time-consuming iterative solution is necessary to obtain the axial force when the axial displacement is determined for each element. Other shortcomings of many of the available physical theory strut models result from their assumption of a rigid-perfectly plastic behavior in the plastic hinge and a fully elastic behavior in the element outside the plastic hinge. In the actual behavior, the plastic hinge plastifies partially prior to full yielding, and the partial plastification might also penetrate into the elastic segments outside the plastic region.

The above shortcomings of the available physical theory strut models have been overcome in this study through: a) development of a computationally efficient formulation which defines the strut axial force in terms of axial displacement; and b) refining the conventional physical theory strut model in order to practically simulate the partial plastification and degradation in the plastic hinge region and along the element length.

This chapter describes the proposed efficient formulation of the physical theory strut models and the refinements incorporated for simulating the partial plastification of the element. The accuracy of the developed model in predicting the experimental monotonic and cyclic performance of a variety of steel struts will be demonstrated in the next chapter.

3.2 THE DEVELOPED FORMULATION

The major assumptions on the basis of which the new formulation for physical theory strut model has been developed are :

1) The effective length concept is assumed to be valid even under inelastic cyclic loads. Test results[2,3] support the validity of this concept (which implies that a strut with any support conditions can be simulated as a simply supported element spanning between the strut inflection points).
2) In the basic formulation, the inelastic axial-flexural deformations (except for axial yield in tension) are assumed to be concentrated in a dimensionless plastic hinge at the center of the effective length. It is also assumed that the plastic hinge behaves in a rigid-fully plastic manner. Later refinements of the basic formulation, however, will account approximately for the partial plastification outside the plastic hinge and along the element length, and the gradual plastification prior to full yielding of the plastic hinge.
3) Shear deformations are neglected.
4) Plane sections are assumed to remain plane after bending.
5) The element is assumed to bend and buckle uniaxially.

Based on the above assumptions, an incremental solution procedure is employed where the incremental forces are related to the incremental deformations by means of a tangent stiffness matrix. For the purpose of developing this stiffness matrix, the strut geometry (Figure 3.1) may be simplified as shown in Figure 3.2 using the symmetry about the mid-span of the effective length. This figure also shows the element forces and deformations. In the development of the basic formulation, a key consideration for improving the computational efficiency is to express the element forces in terms of its displacements.

When the plastic hinge is activated (i.e. when the axial-flexural forces at the plastic hinge location reach the fully-plastic interaction

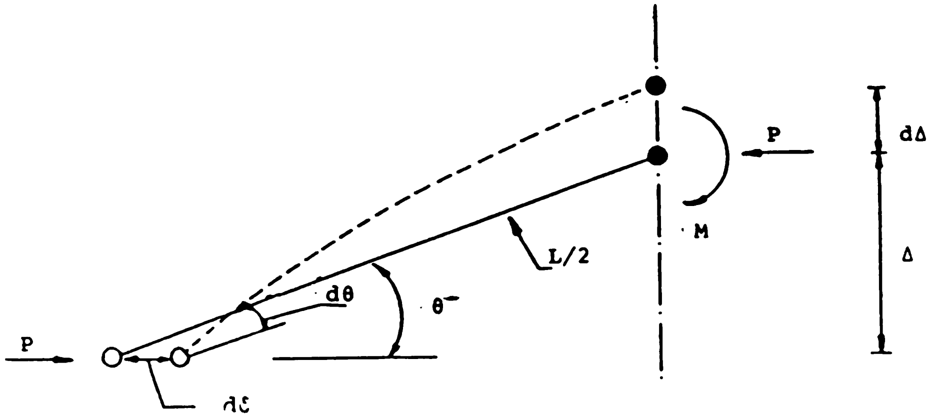

Figure 3.2 Geometry and Deformations of Half-Strut

diagram), the total incremental end deformations of the strut, $d\delta$ and $d\theta$ are the sums of the elastic, $d\delta_e$ and $d\theta_e$, and plastic, $d\delta_p$ and $d\theta_p$.

$$d\nu = d\nu_p \pm d\nu_e \tag{3.1}$$

where : $d\nu = \begin{bmatrix} |d\delta| \\ |d\theta| \end{bmatrix}$; $d\nu_e = \begin{bmatrix} |d\delta_e| \\ |d\theta_e| \end{bmatrix}$; and $d\nu_p = \begin{bmatrix} |d\delta_p| \\ |d\theta_p| \end{bmatrix}$

Note: In this formulation, wherever (±) is used, (+) corresponds to tensile axial force, and the (-) to compressive axial force.

The midspan lateral deflection, $d\Delta$, is also assumed to be the sum total of the elastic and plastic parts.

$$|d\Delta| = |d\Delta_p| \pm |d\Delta_e| \tag{3.2}$$

The elastic midspan lateral deflection can be expressed in terms of the elastic end deformations:

$$d\Delta_e = \pm \, [c_1 \; c_2] \begin{bmatrix} |d\delta_e| \\ |d\theta_e| \end{bmatrix}$$

$$= \pm \, C \, . \, d\nu_e \qquad (3.3)$$

The plastic midspan lateral deflection may be kinematicaly related to the plastic hinge deformations, $d\bar{\delta}_p$ and $d\bar{\theta}_p$:

$$d\Delta_p = \pm \begin{bmatrix} -\frac{\sin\theta}{2} & -\frac{L}{2}\cos\theta \end{bmatrix} d\bar{\nu}_p \qquad (3.4)$$

where : $d\bar{\nu}_p = \begin{bmatrix} |d\bar{\delta}_p| \\ |d\bar{\theta}_p| \end{bmatrix}$

The plastic end deformations are related to the plastic hinge deformations by means of a transformation matrix:

$$\begin{bmatrix} d\delta_p \\ d\theta_p \end{bmatrix} = \begin{bmatrix} \cos\theta & -L\sin\theta \\ 0 & 1 \end{bmatrix} \begin{bmatrix} d\bar{\delta}_p \\ d\bar{\theta}_p \end{bmatrix} \qquad (3.5)$$

Combining Equations 3.4 and 3.5 one can express the plastic lateral deflection of midspan in terms of the plastic end deformations:

$$d\Delta_p = \pm \, [-\frac{\sin\theta}{2} \quad -\frac{L}{2}\cos\theta] \begin{bmatrix} \cos\theta & -L\sin\theta \\ 0 & 1 \end{bmatrix}^{-1} \begin{bmatrix} |d\delta_p| \\ |d\theta_p| \end{bmatrix}$$

$$= \pm \, [-\frac{\tan\theta}{2} \quad -\frac{L}{2\cos\theta}] \begin{bmatrix} |d\delta_p| \\ |d\theta_p| \end{bmatrix}$$

$$= \pm \, D \cdot d\nu_p \qquad (3.6)$$

The incremental axial force and plastic hinge moment, dP and dM, can be related to the elastic end deformations of the strut and the plastic lateral midspan deflection by means of the elastic force-deformation matrix, B:

$$dS = \pm B\ d\nu_e \pm R\ d\Delta_p \tag{3.7}$$

where : $dS = \begin{bmatrix} dP \\ dM \end{bmatrix}$; and $R = \begin{bmatrix} 0 \\ P \end{bmatrix}$

Combining Equations 3.6 and 3.7, one gets:

$$dS = \pm B\ d\nu_e \pm Q\ d\nu_p \tag{3.8}$$

where : $Q = \begin{bmatrix} 0 & 0 \\ Pd_1 & Pd_2 \end{bmatrix}$

The outward normal flow rule can be applied to the plastic hinge deformations;

$$d\bar{\nu}_p = \lambda \cdot \Phi,_s \tag{3.9}$$

where : $\Phi,_s = \begin{bmatrix} \Phi,_P \\ \Phi,_M \end{bmatrix}$;

Φ = fully plastic interaction function;
$\Phi,_P$ = partial derivative of ϕ with respect to P;
$\Phi,_M$ = partial derivative of ϕ with respect to M; and
λ = plastic deformation scalar.

The fully plastic interaction function, Φ, is being derived with due consideration to static equilibrium between the possible forces at the plastic hinge location (P and M) and the resultants of the internal stresses across the plastic hinge (assuming all the fibers in the plastic hinge reached their yield stress in tension or in compression). Combining Equations 3.5 and 3.9, the flow rule for the strut end deformations can be obtained :

$$d\nu_p = \lambda \cdot J \tag{3.10}$$

where : $J = \begin{bmatrix} \Phi,_P \cos\theta - \Phi,_M L \sin\theta \\ \Phi,_M \end{bmatrix}$

The condition that the interaction function remains constant yields that the incremental forces are tangent to the interaction surface:

$$\Phi = 0$$

$$d\Phi = 0$$

$$\Phi,_s^T \cdot dS = 0 \tag{3.11}$$

combining Equations 3.1 and 3.8, one gets:

$$dS = B\ d\nu + (\pm Q - B)\ d\nu_p \tag{3.12}$$

Equations 3.10, 3.11, and 3.12 can now be solved for the plastic scalar, λ :

$$\lambda = G \cdot d\nu \tag{3.13}$$

where : $G = -[\Phi,_s^T (\pm Q - B)\ J]^{-1} [\Phi,_s^T B]$

Equations 3.10, 3.12, and 3.13 can be solved for the tangent stiffness matrix, K_t :

$$dS = \pm K_t\ d\nu \tag{3.14}$$

where : $K_t = [B + (\pm Q - B)\ J\ G]$

Equation 3.14 can be used to solve for the incremental forces when the incremental end displacements are defined. The incremental midspan lateral deflection can also be expressed in terms of the incremental end displacements using **Equations** 3.2, 3.3, **and** 3.6 :

$$d\Delta = \pm F \; d\nu \tag{3.15}$$

where: $F = [C + (D-C) \; J \; G]$

The tangent stiffness matrix, k_t, as well as the matrix relating the midspan lateral deflection to end deformations, F, were derived in the above formulation assuming that the plastic hinge has reached yield conditions, and is loaded inelastically. When the loading is elastic, dv_p and λ are zero and thus matrices k_t and F can be simplified as follows :

$$k_t = B \tag{3.16}$$

$$F = C \tag{3.17}$$

The tangent stiffness matrix, k_t, is a 2x2 matrix. For use in computer structural analysis it is more convenient to represent the brace in terms of the single degree of freedom, $d\delta$. The tangent stiffness, k_t, can be reduced to a scalar by imposing the conditions of equilibrium:

$$M = P \cdot \Delta \tag{3.18}$$

or

$$dM = dP \cdot \Delta + P \cdot d \, \Delta \tag{3.19}$$

Combining Equations 3.14, 3.15, and 3.19, the single degree of freedom stiffness equations can be obtained :

$$dP = K_\delta \cdot d\delta \qquad (3.20)$$

$$d\theta = Z \cdot d\delta \qquad (3.21)$$

where : $$k_\delta = \frac{K_{t11} + K_{t12} \left(\dfrac{P.F_1 - K_{t21}}{K_{t22} - P.F_2} \right)}{1 - \left(\dfrac{K_{t12} \cdot \Delta}{K_{t22} - P.F_2} \right)}$$; and

$$Z = \frac{\Delta}{K_{t22} - P.F_{12}} K_\delta + \frac{P.F_1 - K_{t21}}{K_{t22} - P.F_2}$$

After each incremental step the element geometry is internally updated and the matrices k_δ and F are computed according to the above formulations for use in the next step. In each step, the incremental value of axial displacement ($d\delta$) is the input. The proposed element model is computationally efficient in application to complete structures, because in step by step nonlinear structural analysis, following the conventional displacement method, the input to the element model is the incremental displacement. This is compatible with the proposed element formulation, and thus iterative solutions at the element level can be avoided.

3.3 REFINEMENTS OF THE BASIC FORMULATION

The basic formulation for physical theory modeling of steel struts presented above needs to be modified in order to account for: a) the effects of the partial plastification in the plastic hinge region and along the element length; b) full tensile yielding; and c) the possibility of buckling of straight element (the element might be straight prior to loading or be straightened by tensile yielding during the loading). A general discussion on these refinements and the procedures followed for incorporating them into the basic formulation are described below.

The experimental data on the cyclic behavior of the plastic hinge in steel struts indicate a partial plastification of the hinge before its full yielding. Figure 3.3a presents a typical experimental relationship between the axial load and bending moment at the plastic hinge region of a cyclically loaded steel struts. Figure 3.3b shows the same relationship produced analytically, assuming an elastic-perfectly plastic hinge behavior. The experimental plastic hinge behavior tends to deviate from an elastic performance before the fully plastic condition is reached. The gradual plastification process is indicative of some partial yielding across the critical sections under the axial-flexural loading. Another indication of the partial plastification in plastic hinges is shown in Figure 3.4. This figure compares an experimental axial load-plastic hinge rotation relationship with the corresponding analytical relationship developed assuming an elastic-perfectly plastic behavior. The analytical curve can not predict the gradual transition from an elastic to a perfectly plastic behavior.

In order to simulate the partial plastification of hinges in physical theory modeling of steel struts, it is proposed that the overall performance of the struts beyond a "first-yield" level of the axial-flexural load combinations can be presented as a weighted average of the elastic and fully plastic types of performance, with the fully plastic one becoming dominant as the fully plastic interaction diagram is approached.

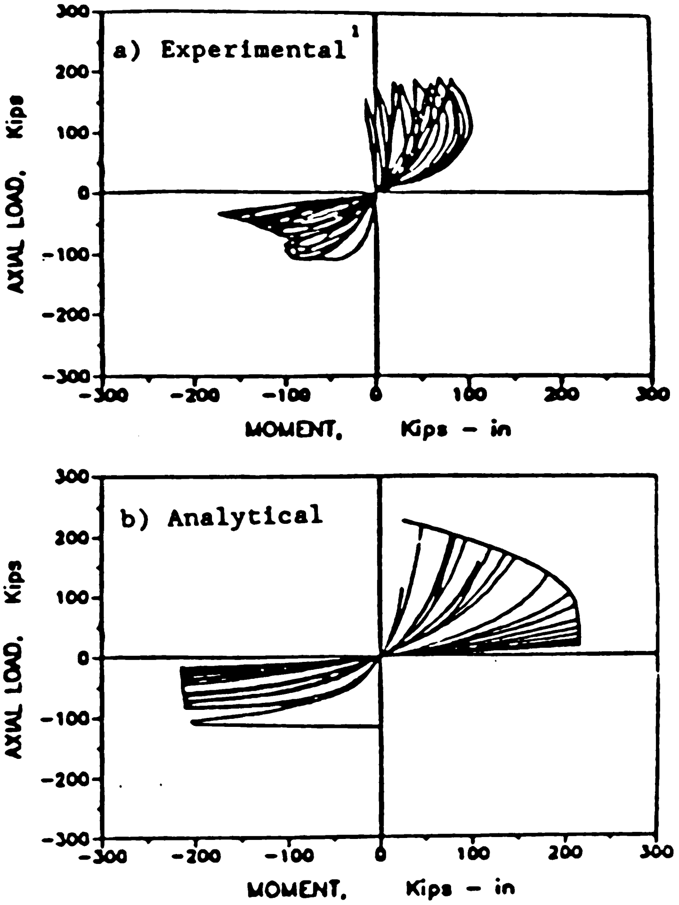

Figure 3.3 Effects of Partial Plastification on Axial Force-Plastic Hinge Moment Relationship (W8X20, Kl/r=120)

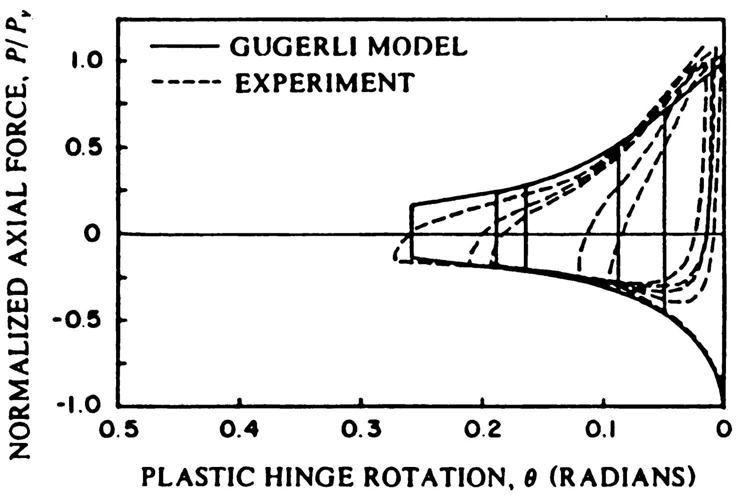

Figure 3.4 Effects of Partial Plastification on Axial Force-Plastic Hinge Rotation Relationship[1]

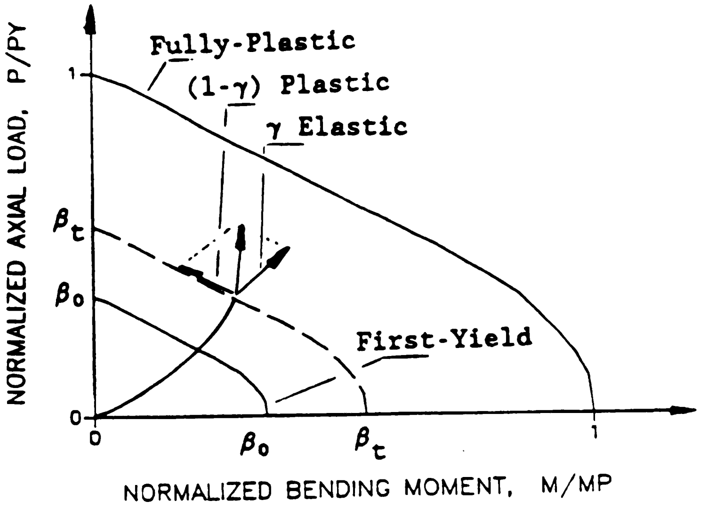

Figure 3.5 Proposed Idealization of Partial Plastification at the Plastic Hinge

A so called "first-yield interaction diagram" was defined as the limit for a pure elastic performance (Figure 3.5). Partial plastification is assumed to be initiated when the load combination at the plastic hinge location exceeds this "first-yield" interaction diagram. In the partial plastification region, the incremental values of the plastic hinge axial force and bending moment (dP & dM, respectively) are calculated as weighted averages of the pure elastic and perfectly plastic ones (Figure 3.5) :

$$\begin{bmatrix} dP \\ dM \end{bmatrix} = \gamma \begin{bmatrix} dP_e \\ dM_e \end{bmatrix} + (1-\gamma) \begin{bmatrix} dP_p \\ dM_p \end{bmatrix} \tag{3.22}$$

where : dP_e, dM_e = The axial load and bending moment increments assuming a pure elastic behavior;

dP_p, dM_p - The axial load and bending moment increments assuming a perfectly plastic behavior of the plastic hinge, with the fully plastic interaction diagram scaled down such that the current load combination is located on it; and

γ - The weighting factor which ranges from 1.0 on the first-yield interaction diagram (pure elastic behavior) to 0.0 on the fully plastic interactive diagram (perfectly plastic behavior of the plastic hinge).

The "first-yield" interaction diagram was assumed in this study to be a scaled down version (by a factor of β_0) of the fully plastic one. When the strut is originally loaded, β_0 is a function of the residual stresses (which decide the initiation of the partial plastification). The value of β_0 is expected to decrease in the subsequent inelastic load cycles due to the Bauschinger effect and plastic hinge degradation. In order to consider this phenomena, β_0 was expressed as a function of the inelastic load history :

$$\beta_0 = \frac{1}{a\,\Sigma|\theta_{pmax}| + b} \tag{3.23}$$

where : $\Sigma|\theta_{pmax}|$ - The sum total of the absolute values of the plastic hinge rotations at the load reversal points;

a, b - Empirical coefficients (a=10.0, b=0.7 derived in Chapter 4 using 18 cyclic strut test results).

The factor γ in Equation 3.22 varies from 1.0 to 0.0 as the axial-flexural load combination moves from the elastic region to the fully plastic condition. The following expression is suggested to be used for deriving γ :

$$\gamma = [\frac{1 - \beta_t}{1 - \beta_0}]^m \tag{3.24}$$

where : β_t = an indicative of the level of the axial-flexural force combination (Figure 3.5);

m = empirical coefficient

$$= \begin{cases} 2.0 & \text{for } P<0 \text{ (compression)} \\ 2.0 \, [\frac{M}{M_p}]^2 & \text{for } P>0 \text{ (tension)} \end{cases}$$

Under tension, m is expressed as a function of M/M_p to account for the fact that as the member straightens (and the plastic hinge bending moment approaches zero), the member tends to yield under pure tension along its length. In this condition, m approaches zero (and γ approaches 1.0), in order to simulate the gradual spread of the inelastic deformations (axial yielding) along the element length and the less concentration of inelasticities at the plastic hinge region.

Another critical aspect of the steel strut hysteretic behavior which is not included in the basic formulation presented earlier, is the partial plastification and full-yielding along the element length. Due to the Bauschinger effect, the steel modulus of elasticity in the subsequent inelastic cycles tends to decrease under increasing levels of axial load. In the first cycle also, due to the presence of residual stresses, there is partial yielding along the element length at axial loads below the yield level. Another factor contributing to partial plastification along the element length is the spread of yielding from

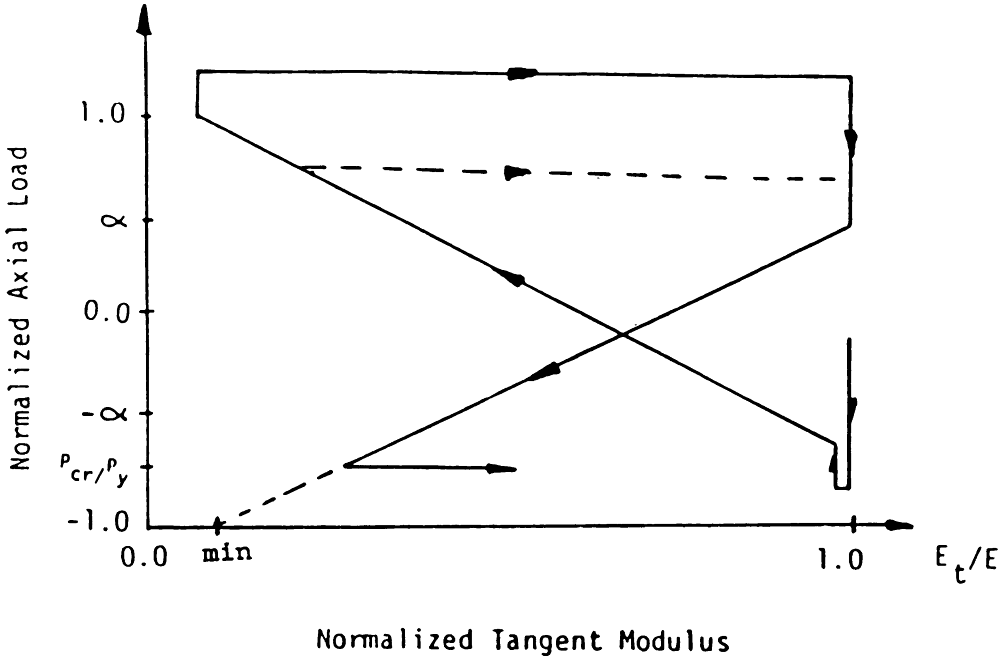

Figure 3.6 Proposed Model of Tangent Modulus of Elasticity

the plastic hinge to the neighboring regions which are generally more critically stressed than locations further away from the plastic hinge.

In order to approximately simulate of the partial plastification along the element length, the modulus of elasticity is expressed as a decreasing function of axial force, varying from a maximum value equal to the elastic modulus to a minimum value of the strain hardening modulus as the axial force increases from zero to the yield force of the element. The general configuration of the model for expressing the tangent modulus of elasticity as a decreasing function of axial force is shown in Figure 3.6. The value of α in this model was derived empirically as a function of the sum total of the absolute values of the plastic hinge rotation at the load reversal points.

$$\alpha = \frac{1}{c\ \Sigma|\theta_{pmax}| + d} \qquad (3.25)$$

where : c, d = Empirical coefficients (c=5.0 d=0.70, derived in Chapter 4 using 18 cyclic steel strut test results)

The proposed formulation makes the partial plastification along the element length a function of the plastic hinge rotations. This reflects the fact that regions near the plastic hinge are more critically stressed and thus are more exposed to partial yielding. An important consequence of using the proposed empirical formulation of the tangent modulus of elasticity (as a decreasing function of the axial load) is the simulation of axial yielding of the strut. As the axial load in tension (or in compression) approaches the element yield strength, the steel modulus of elasticity in the element model gradually lowered to the level of the strain hardening modulus. Beyond the yield load, the modulus of elasticity stays constant at the strain hardening level. This accounts for the axial yielding of the element and the post-yield strain hardening of steel (assuming a bilinear stress-strain relationship).

The possibility of sudden buckling of the straight strut was also considered in the proposed formulation of the physical theory strut models. The element might be straight prior to loading, or it could be straightened during loading by yielding in tension. Buckling of the straight element is assumed to occur when the compressive axial load reaches the buckling load given by the AISC manual[17] (without safety factors) :

$$P_c = \begin{cases} Q_s\left[\, 1 - \dfrac{(kl/r)^2}{2\, C_c^2} \,\right] P_y & \text{for } kl/r<C_c \\[2ex] \dfrac{\Pi^2 EI}{(kl)^2} & \text{for } kl/r>C_c \end{cases} \qquad (3.26)$$

where : $C_c = \left[\dfrac{2\,\Pi^2 E}{Q_s\, F_y}\right]^{1/2}$

P_y = Axial yield strength;

kl/r = Effective slenderness ratio;

E = Tangent modulus of elasticity; and

Q_s = Reduction factor, accounts for local buckling as specified by the AISC manual.[17]

Upon buckling of the straight element, the axial compressive load is assumed to remain constant as the lateral midspan deflection and consequently the end axial deformation increase to a level where the plastic hinge interaction diagram is reached (Figure 3.7). During this process, from the occurrence of the straight element buckling to the formation of the plastic hinge, the relationship between the axial and the midspan lateral displacements is expressed by the empirical function[48] :

$$\Delta = \frac{2\,L}{\pi} \sqrt{\epsilon - \epsilon_0} \qquad (3.27)$$

where : Δ = Lateral midspan strut deflection;

L = Strut length;

ϵ = Axial strain, equals to δ/L; and

ϵ_0 = Axial strain when the load equals P_c.

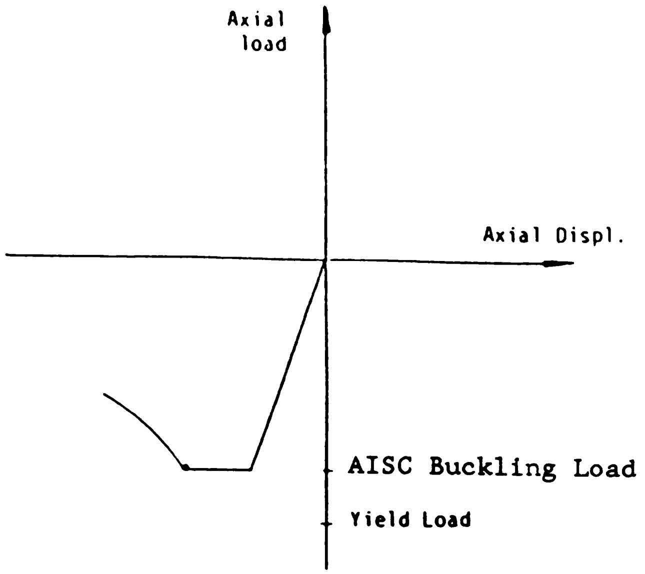

Figure 3.7 Idealized Axial Load-Displacement Upon Buckling of Straight Struts

3.4 ADVANTAGES OF THE PROPOSED MODEL

The suggested formulation for predicting the hysteretic behavior of steel struts is distinguished from the previous strut models by the following advantages :

1) It is practical (economical) for nonlinear analysis of complete structural systems. It involves a limited number of degrees of freedom and limited input information on the material and geometric characteristics of the element, when compared with the finite element and phenomenological models of steel struts. Relatively small computer storage and user times requirements are thus required for work with element model. The developed formulation is also computationally efficient for structural analysis, in the sense that it defines

the element incremental forces in terms of the incremental displacements, and can be efficiently incorporated into the conventional computer programs for nonlinear analysis of complete structures by the incremental stiffness method of analysis.

2) In spite of some limited reliance on empirical refinements, the model is dominantly based on theoretical concepts, and thus, as confirmed in the next chapter, it is generally applicable to steel struts with different geometric and material characteristics.

3) The proposed strut model can be used in structural analysis without requiring a large displacement analysis.

4) The sound theoretical basis of the model makes it possible to incorporate further refinements into the formulations with no conceptual problems.

5) The model approximately accounts for partial plastification within the plastic hinge and along the element length, following semi-empirical procedures which are based on the physics of strut behavior under cyclic loads.

6) The effects of the end eccentricity and initial imperfection of the element on the steel strut inelastic-buckling behavior under generalized excitations have been accounted for in the proposed formulation.

With the above advantages, as shown in the next chapter, the proposed model is capable of accurately predicting the hysteretic behavior of steel struts with relatively small computer time and memory.

3.5 SUMMARY AND CONCLUSIONS

The developed physical theory model of steel struts incorporates simplified theoretical formulations based on some assumptions on the physical behavior of steel struts. This model involves a limited number of degrees of freedom and requires limited computer storage for specifying the geometric and material characteristics of the element.

A computationally efficient formulation has been developed for predicting the inelastic-buckling behavior of steel struts under generalized cyclic loading conditions. This formulation expresses the element incremental forces in terms of the incremental axial displacement. It can thus be efficiently incorporated into a conventional nonlinear structural analysis program which follows the incremental stiffness method of analysis. The basic formulation developed in this investigation is also capable of accounting for the effects of the initial imperfection and end eccentricities.

The basic physical theory strut models assume a rigid-perfectly plastic behavior of the plastic hinge and a pure elastic behavior along the element length outside the hinge. This basic model has been refined to consider, in a practical manner, the effects of partial plastification and degradation of the plastic hinge under cyclic loads and the softening, partial plastification and axial yielding along the element length outside the plastic hinge. These refinements were based on semi-empirical procedures, with due consideration to the physics of the strut inelastic-buckling behavior observed in tests.

CHAPTER 4

VERIFICATION OF THE ELEMENT MODEL AND PARAMETRIC STUDIES

4.1 INTRODUCTION

The constant coefficients of the proposed physical theory brace model are derived empirically in this chapter using the results of tests on a variety of steel struts subjected to generalized axial excitations. The final version of the model is then verified by comparing its predictions with the experimental monotonic and cyclic axial load-deformation relationships of steel struts having different material and geometric properties, subjected to concentric and eccentric loads. Many of the tested struts used in this verification have not been used in deriving the empirical coefficients of the model.

Following the full development and verification of the proposed model of steel struts, it has been used in a parametric study on the effects of different design variables on the monotonic and cyclic axial load-deformation relationships of steel struts. In this parametric study, the effects of the material yield strength, end support rotational fixity (effective length), cross sectional shape, initial imperfection, and end eccentricity on the strut axial load-deformation characteristics have been evaluated. The results can help designers in optimizing their strut designs through the proper selection of design variables.

4.2 EMPIRICAL DERIVATION OF THE MODEL VARIABLES

The basic formulation of the proposed element model has been based on some theoretical concepts and certain assumptions which comply with the physical performance of steel struts observed in tests. The proposed refinements (for simulating the partial plastification and degradation at the plastic hinge and along the element length) were also based on some physically meaningful criteria. Partial plastification, however, is a complex phenomenon, and the proposed simple approach to the modeling of this phenomenon involves some degree of empiricism.

Eighteen cyclic strut test results, reported in Reference 3, were used to empirically derive the variables a & b (used for simulating the plastic hinge partial yielding and degradation in Equation 3.23 of Chapter 3), and c & d (used for idealizing the softening and partial or full yielding along the element length in Equation 3.25 of Chapter 3). Table 4.1 summarizes the material and geometric properties of these hinged-hinged steel struts which were subjected to severe cyclic loading histories. All the struts were concentrically loaded and their material yield strengths were measured using coupon tests.

The variables a,b,c and d were selected to give desirable comparisons between the analytical and experimental hysteretic relationships for the eighteen tested steel struts shown in Table 4.1. The comparison between the experimental and analytical results was performed subjectively (based on the investigator's judgement), with due consideration given to the achievement of analytical buckling load and tangent stiffness deteriorations, hysteretic energy absorptions and post-buckling losses of strength which compare well with the corresponding experimental performances. A subjective approach was employed for this comparison based on the overall hysteretic performance of the

Table 4.1 Cyclically Loaded Steel Struts[a]

Strut No.o	Shape	Slenderness Ratio Kl/r	Yield Strength ksi
1	W 8 X 20	120	40.4
2	W 6 X 25	40	42.4
3	W 6 X 20	80	40.2
4	W 6 X 20	80	40.2
5	W 6 X 20	80	40.2
6	W 6 X 16	120	44.7
7	W 6 X 15.5	40	50.0
8	2L 6 X 3-1/2 X 3/8	80	40.8
9	2L 5 X 3-1/2 X 3/8	40	43.6
10	2L 4 X 3-1/2 X 3/8	120	41.6
11	2C 8 X 11.5	120	35.5
12	WT 5 X 22.5	80	39.5
13	WT 8 X 22.5	80	41.8
14	Pipe 4 Std.	80	47.5
15	Pipe 4 Std.	80	47.5
16	Pipe 4 X-Strong	80	24.0
17	TS 4 X 4 X 1/4	80	59.0
18	TS 4 X 4 X 1/2	80	82.0

Table 4.2 The Empirical Values of the Element Model Variables

Variable	Value
a	10.0
b	0.7
c	5.0
d	0.8

struts, mainly because there are many aspects of the hysteretic performance which of interest, and emphasize on improving the comparison of certain aspect might actually damage some other aspects of comparisons between the experimental and analytical results.

The empirical values, derived for the model variables a,b,c and d, are presented in Table 4.2. It is worth mentioning that the sensitivity of the element hysteretic model to the variations in these variables is relatively small. This is typically shown in Figures 4.1 a,b and c, which compare the analytical hysteretic relationships for strut No.3 (see Table 4.1) derived with the hysteretic variables of Table 4.2 times 1.0, 0.8 and 1.2, respectively. These variations of the hysteretic variables are observed to have relatively small effects on the element hysteresis.

4.3 COMPARISONS WITH MONOTONIC EXPERIMENTAL RESULTS

In order to verify the proposed approach to modeling the steel strut axial load-deformation behavior, the accuracy of the model in predicting several monotonic (and cyclic, in the next section) test data reported in the literature for steel struts with a variety of cross-sectional dimensions and slenderness ratios has been assessed. The monotonic test results used in this section are all for angular cross-sections loaded concentrically or eccentrically. Depending on the experimental data presented for each test, the comparisons have been made either on the maximum compressive strength or the complete axial compression load-deformation relationship.

The first series of comparisons were made on the maximum compressive strength of angular struts subjected to monotonic compressive loading with or without end eccentricities. Table 4.3 presents some details of the tested steel struts.[45] All the struts were L 3.54in x

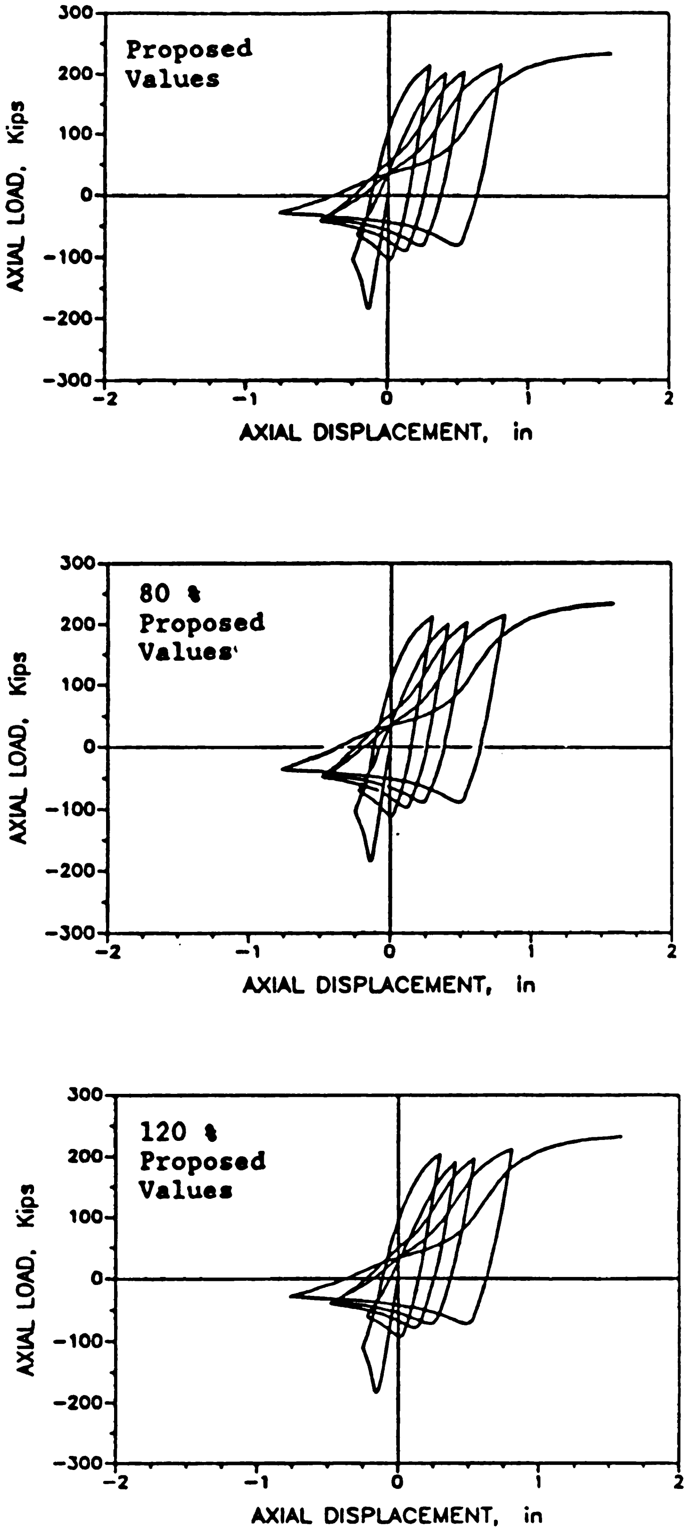

Figure 4.1 Sensitivity of the Developed Hysteretic Model to the Variations of the Epmirical Variables (W6X20, kl/r=80)

Table 4.3 **Material and Geometric Properties of L 3.54in X 3.54in X .27in (L 90mm X 90mm X 7mm) Tested in Monotonic Compression[45]**

Slenderness Ratio Kl/r	Yield Strength ksi	End Eccentricities e_z, in	e_w, in
20,40,60,70,80,90, 100,110,130,150	44.1	0.0	0.0
20,40,60,70,80,90, 100,110,130,150	46.9	0.697	0.0
20,40,60,70,80,90, 100,110,130,150	45.5	0.0	0.685
20,40,60,70,80,90, 100,130,150	45.5	0.697	0.685

3.54in x .27in (L 90mm x 90mm x 7mm), and they were hinged-hinged. Ten tests were performed on elements of different lengths with each of the following loading conditions: concentric, eccentric around the minor axis, eccentric around the major axis, and biaxially eccentric.

Figures 4.2a,b,c and d present the experimental and analytical maximum compressive loads as functions of the minor axis slendness ratio for the angular struts loaded concentrically, eccentrically (about the minor axis), eccentrically (about the major axis), and with biaxial eccentricity, respectively. The comparisons between the experimental and analytical compressive strengths of steel struts subjected to different loading conditions are observed to be satisfactory. In order to analyze the struts loaded with biaxial eccentricity or uniaxial eccentricity around the major axis, which are commonly encountered in bolted space trusses like lattice transmission towers, some modifications were made in the proposed formulation which was originally derived for steel

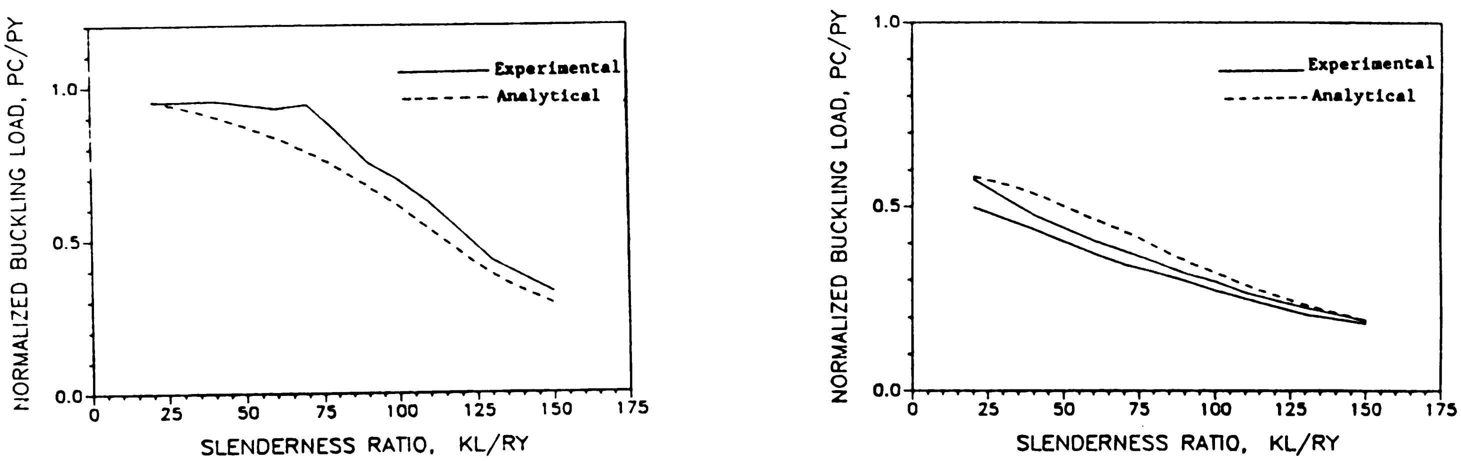

a) Concentric

b) Eccentric around the minor axis

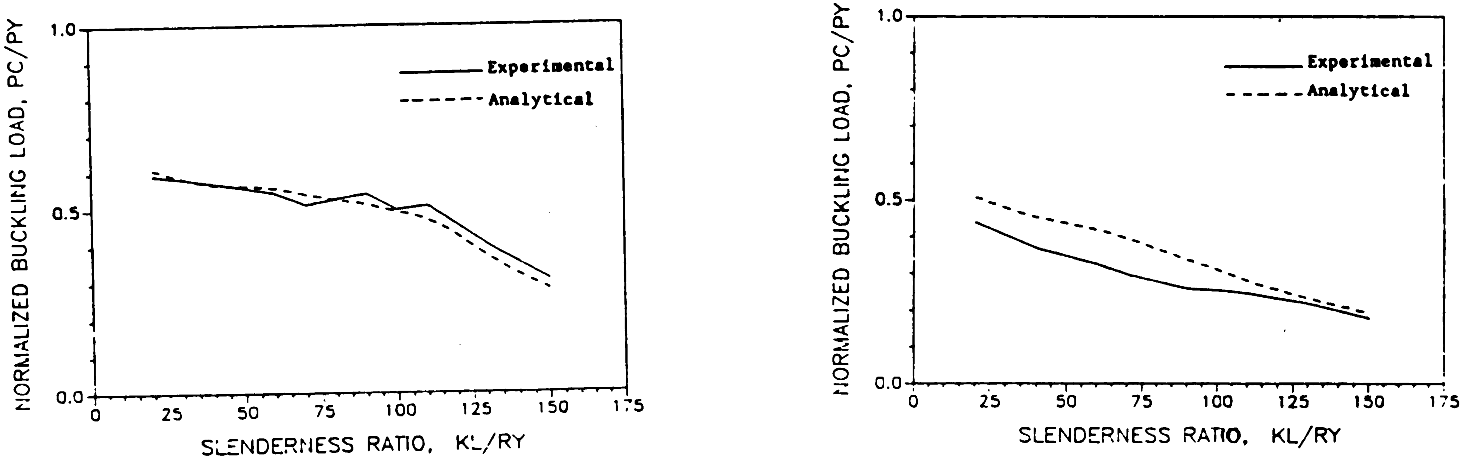

c) Eccentric around the major axis

d) Biaxially eccentric

Figure 4.2 Experimental and Analytical Maximum Compressive Strength of Angular Struts[45]

struts with uniaxial eccentricity around the minor axis. These modifications were based on the physical behavior of steel struts observed in tests. It was assumed that prior to the formation of the plastic hinge, the axial deformations of the strut consist of three components related to axial shortening, bowing around the minor axis, and bowing around the major axis. After formation of the plastic hinge, in the post-peak region, the member is assumed to bow uniaxially around its minor axis. This assumption agrees with the observed behavior of biaxially loaded steel struts in tests. Upon the formation of the plastic hinge, it is assumed that the midspan lateral deformation around the minor axis increases to a value equal to the resultant of the minor and major axis lateral deformations, with the major axis lateral deformations disappearing. The plastic hinge is formed when the axial-flexural force combination (assuming that the resultant lateral deformation occurs around the minor axis) reaches the fully plastic interaction diagram of the element in bending around the minor axis. In the post-peak region, additional bowing of the element is assumed to take place only around the minor axis, and the effects of the major axis eccentricity are neglected. The shift in the direction of bending of the biaxially loaded struts is a phenomenon which has been observed in experiments. It is stimulated by some twisting of the element.

The monotonic experimental axial load-deformation relationships of some angular elements were also compared with the theoretical ones. Table 4.4 presents the geometric and material characteristics as well as the end support conditions and eccentricities of the monotonically loaded angular struts used in these comparisons.[46,47]

Figures 4.3a through 4.3d compare the experimental and analytical axial load-deformation relationships of the concentrically loaded angular elements No.1 through No.4 in Table 4.4. It may be concluded from

Table 4.4 Properties of the Steel Struts Tested Under Monotonic Loads.[46,47]

Strut No.	Cross-Section	Slenderness Ratio, Kl/r	Yiled Strength Ksi	End Eccentricities e_z, in	e_w, in	End Connections Type
1	L 1-3/4 X 1-3/4 X 1/8	301	49.9	0.0	0.0	hinged-hinged
2	L 1-1/2 X 1-1/2 X 1/8	246	52.8	0.0	0.0	hinged-fixed
3	L 1-3/4 X 1-3/4 X 1/8	211	44.4	0.0	0.0	hinged-fixed
4	L 3 X 3 X 1/4	178	52.5	0.0	0.0	hinged-hinged
5	L 3 X 3 X 1/4	193	50.6	0.2	0.0	hinged-hinged
6	L 3 X 3 X 1/4	112	54.8	0.2	0.0	hinged-hinged
7	L 3 X 3 X 1/4	61	54.8	0.2	0.0	hinged-hinged
8	L 2 X 2 X 1/8	263	54.2	0.106	0.0	hinged-hinged
9	L 3 X 3 X 1/4	193	54.8	0.086	1.105	hinged-hinged
10	L 3 X 3 X 1/4	135	54.8	0.086	1.105	hinged-fixed
11	L 3 X 3 X 1/4	61	54.8	0.086	1.105	hinged-hinged

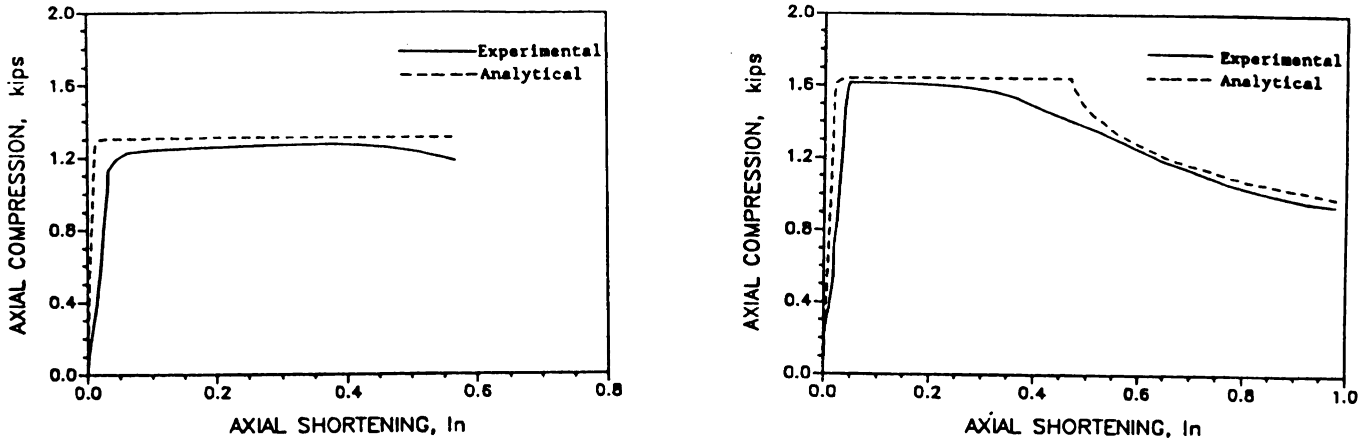

a) Strut 1 (Table 4.4)

b) Strut 2 (Table 4.4)

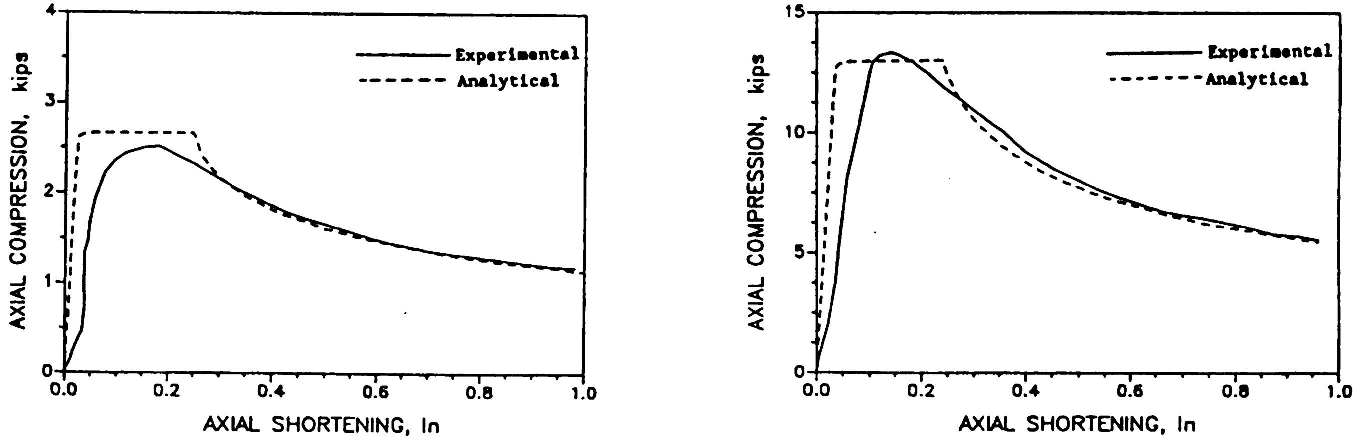

c) Strut 3 (Table 4.4)

d) Strut 4 (Table 4.4)

Figure 4.3 Experimental and Analytical Axial Load-Deformation Relationships of Concentrically Loaded Angles[46, 47]

Figure 4.3 that the proposed formulation is capable of predicting the experimental performance of the struts subjected to monotonic concentric loading with a reasonable accuracy. It is worth mentioning that the end fixtures in tests presented in Figure 4.3 were bolted. Slippage of the bolts might have been a reason for the lower initial stiffness of the struts in tests when compared with the analytical results.

For the steel struts No.5 through No.8 loaded under monotonic compression with uniaxial eccentricity around the minor axis, Figures 4.4a through 4.4d present the experimental and analytical axial load-deformation relationships. From Figure 4.4 it may be concluded that for struts with uniaxial eccentricity, the proposed physical theory formulation is capable of closely simulating the experimental behavior. The discrepancy between the analytical and experimental initial stiffnesses of strut No.8 might have been caused by the slippage at the bolted end fixtures of the element in the experiment.

Figures 4.5a through 4.5c present the experimental axial load-deformation relationships of the biaxially loaded steel struts No.9 through 11 versus the analytical ones. Although the accuracy of analysis for the biaxially loaded struts is less than that for the uniaxial ones (compare Figures 4.4 and 4.5), the proposed analytical approach is still capable of predicting test results with an accuracy which is acceptable for many practical applications.

4.4 COMPARISONS WITH CYCLIC EXPERIMENTAL RESULTS

A verification of the proposed formulation of physical theory strut models was also made using the test data derived from a comprehensive experimental study on steel struts with a variety of geometric and material properties tested under concentric cyclic loading. The proposed formulation was used to derive the axial load-deformation and

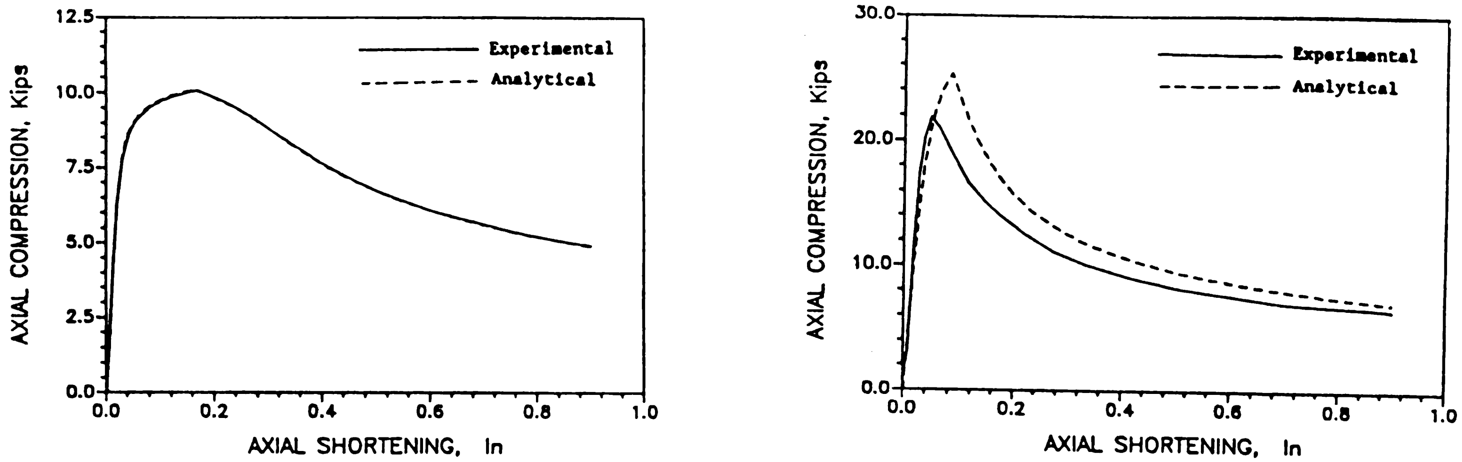

a) Strut 5
(Table 4.4)

b) Strut 6
(Table 4.4)

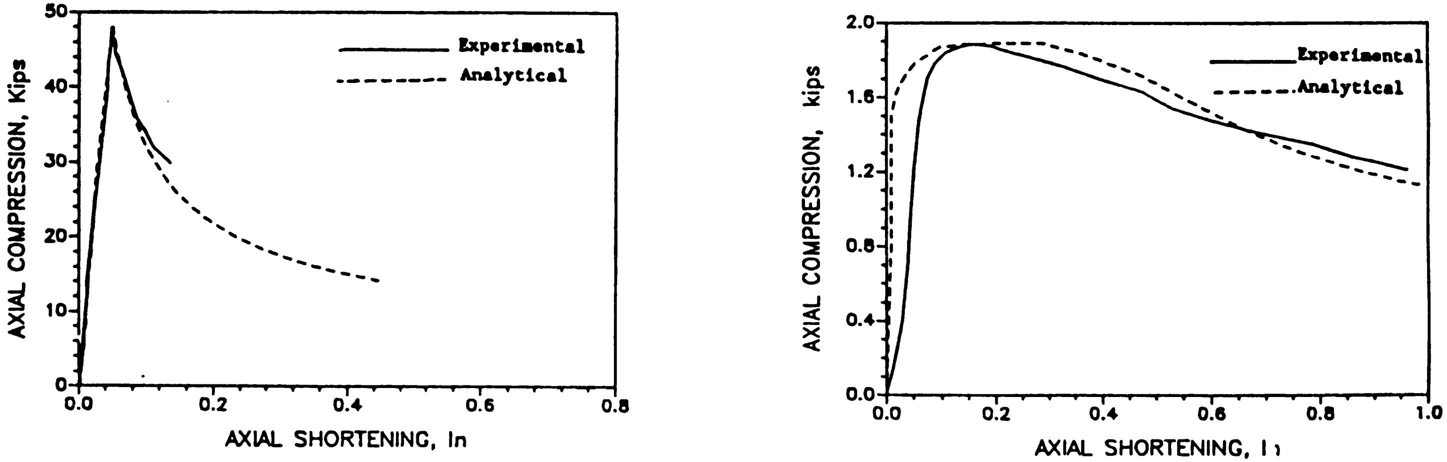

c) Strut 7
(Table 4.4)

d) Strut 8
(Table 4.4)

Figure 4.4 Experimental and Analytical Axial Load-Deformation Relationships of Eccentrically Loaded Angles[46,47]

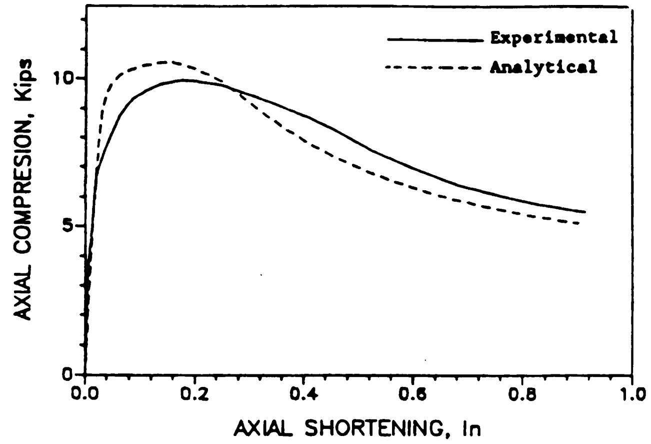

a) Strut 9 (Table 4.4)

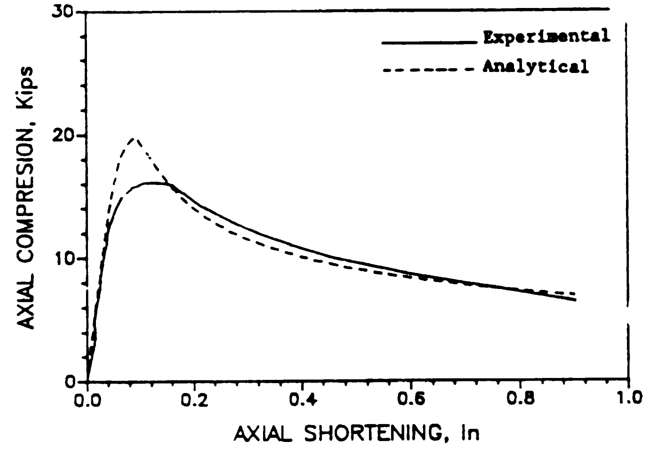

b) Strut 10 (Table 4.4)

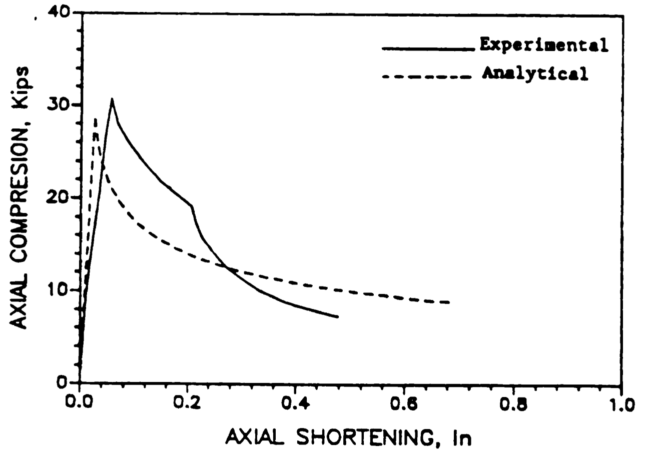

c) Strut 11 (Table 4.4)

Figure 4.5 Experimental and Analytical Axial Load-Deformation Relationships of Biaxially Loaded Angles[46,47]

the plastic hinge axial force-bending moment relationships. these analytical results were compared with the corresponding experimental ones. Some comparative studies were also made between the proposed analytical approach and some other available analytical models, in order to demonstrate the advantages of the proposed formulation in efficiently and reliably predicting the experimental results.

Comparisons were also made between the cyclic experimental and analytical behavior of the steel struts shown in Table 4.5. The wide selection of the steel strut cross-sections, slenderness ratios, and material yield strengths (see Table 4.5) provide data for a comprehensive verification of the proposed physical theory steel strut model.

Figures 4.6a through 4.14a present the experimental axial force-deformation relationships of the steel struts introduced in Table 4.5. The corresponding analytical relationships are presented in Figures 4.6b through 4.14b. The proposed analytical model is found to be capable of accurately predicting the cyclic axial load-deformation relationships for the wide selection of steel struts. Phenomena like the

Table 4.5 Properties of the Steel Struts Tested Under Cyclic Loads[1,3]

Strut No.	Cross-Section	Slenderness Ratio, Kl/r	Yield Strength Ksi	End Connections Type
1	W 8 X 20	120	40.4	hinged-hinged
2	W 6 X 20	80	40.2	hinged-hinged
3	W 6 X 15.5	40	50.0	hinged-hinged
4	W 6 X 20	40	40.2	hinged-fixed
5	W 6 X 20	80	40.2	hinged-hinged
6	W 6 X 16	120	44.7	hinged-hinged
7	WT 8 X 22.5	80	41.8	hinged-hinged
8	Pipe 4 Std.	80	47.5	hinged-hinged
9	TS 4 X 4 X 1/4	80	59.0	hinged-hinged

deteriorations of the buckling load, axial stiffness and energy absorption capacity under repeated inelastic load cycles are closely simulated by the proposed model.

The analytical cyclic axial load-deformation relationships of steel struts No.1 through 4 derived using the refined physical theory strut model of Reference 1 (described in Chapter 2) are also presented in Figures 4.6c through 4.9c. The refined model of Reference 1, which involves a large number of empirical coefficients and is computationally inefficient (i.e., presents axial displacement in terms of axial load), is clearly inferior to the proposed formulation in predicting the deteriorating hysteretic behavior of steel struts under cyclic loads.

The comparisons between the experimental and analytical plastic hinge axial force-bending moment relationships are presented in Figures 4.6(d,e,f) through 4.9(d,e,f). The analytical results have been derived using the proposed physical theory formulation and also the refined model of Reference 1. These comparisons are also indicative of the high degree of accuracy and the realism of the proposed formulation. they also indicate the superiority of the proposed formulation over the complex physical theory model of Reference 1. The proposed model is observed to satisfactorily simulate the partial plastification phenomenon in the plastic hinge, which leads to a gradual transition from the elastic axial force-bending moment relationship to the fully plastic one.

Based on the comparisons between the experimental and analytical performance characteristics of steel struts, it may be concluded that the proposed model provides a practical (economical) tool for accurate prediction of the steel strut inelastic-buckling behavior under generalized loading conditions. The proposed techniques for the simulation of partial plastification also seem to produce a realistic idealization of

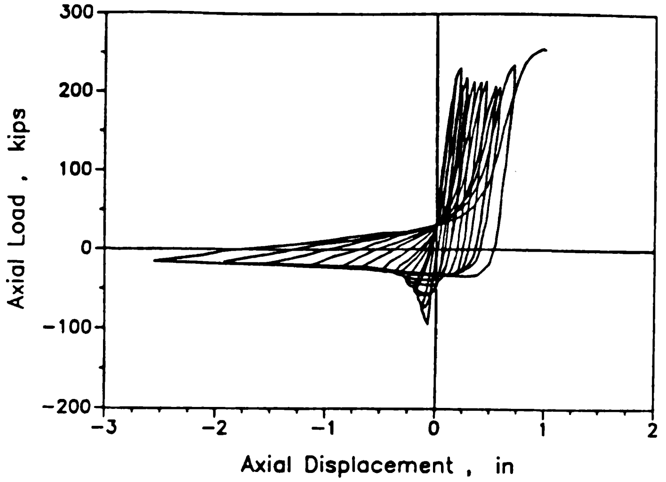

a) P-δ relationship; Experiment

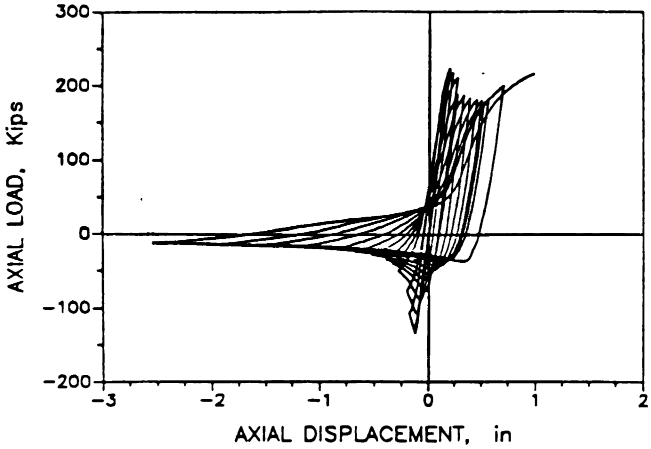

b) P-δ relationship; Developed Model

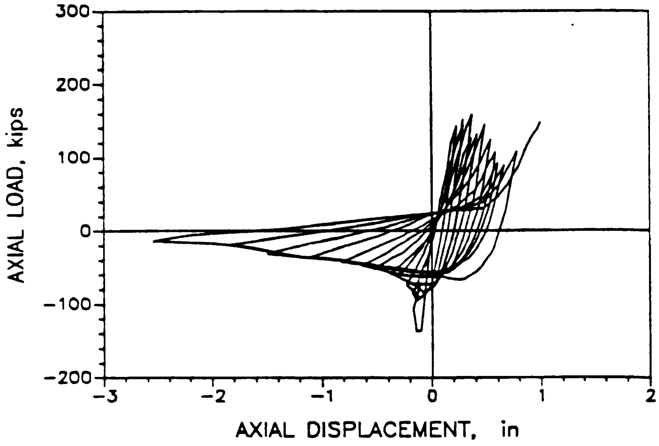

c) P-δ relationship; Ikeda Model

Figure 4.6 Experimental and Analytical Comparisons of Strut 1, Table 4.5[1]

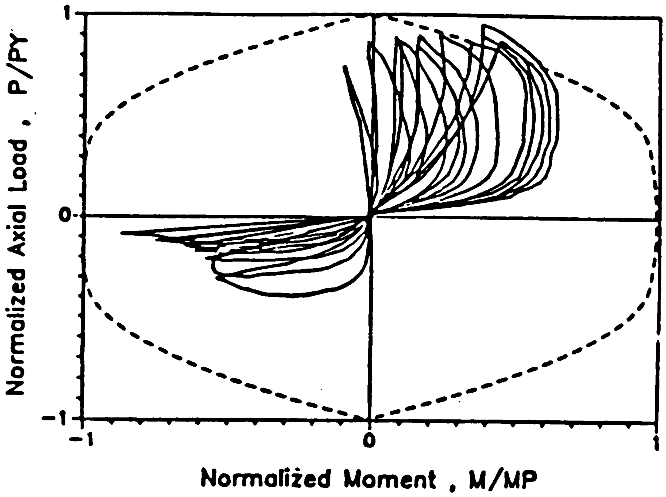

d) M-P relationship; Experiment

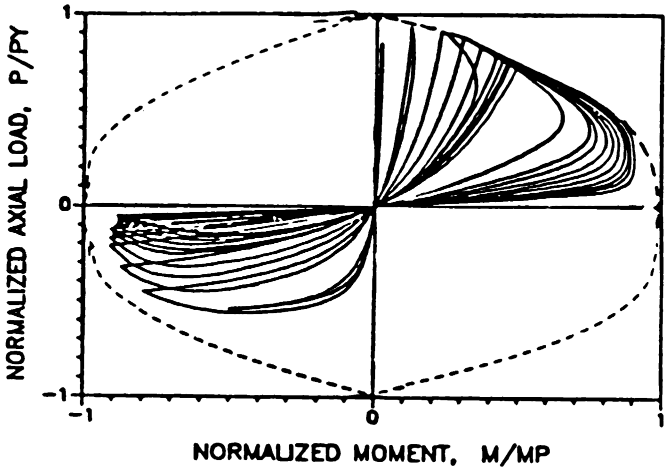

e) M-P relationship; Developed Model

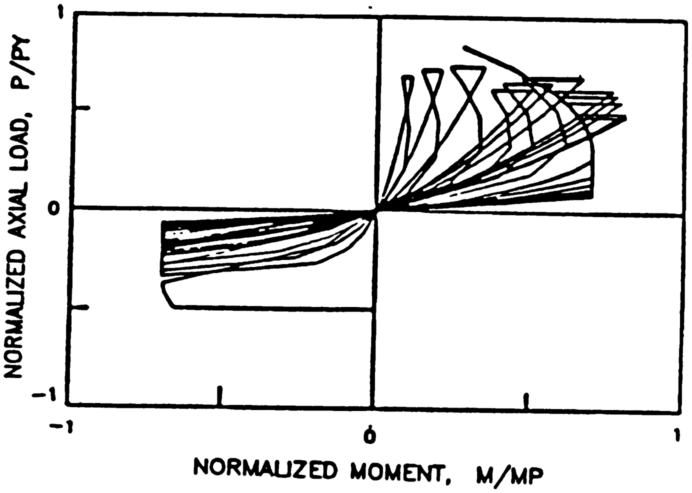

f) M-P relationship; Ikeda Model

Figure 4.6 Experimental and Analytical Comparisons of Strut 1, Table 4.5 (cont' d) ^{1}

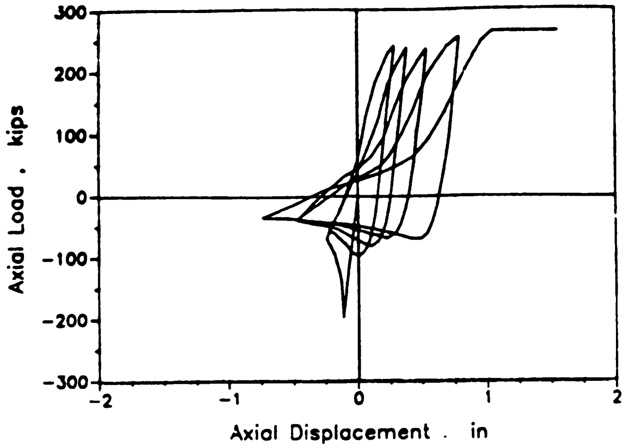

a) P-δ relationship; Experiment

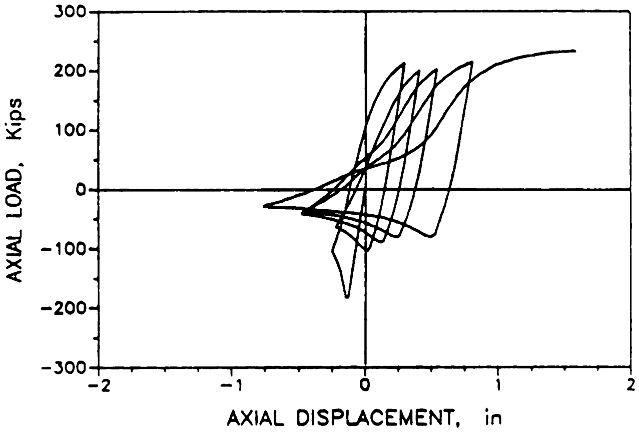

b) P-δ relationship; Developed Model

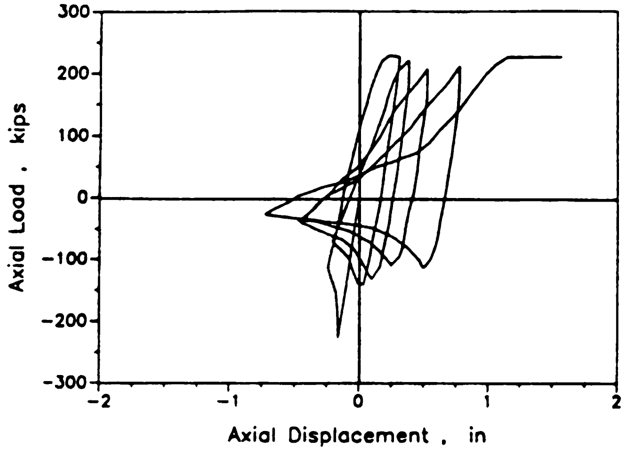

c) P-δ relationship; Ikeda Model

Figure 4.7 Experimental and Analytical Comparisons of Strut 2, Table 4.5[1]

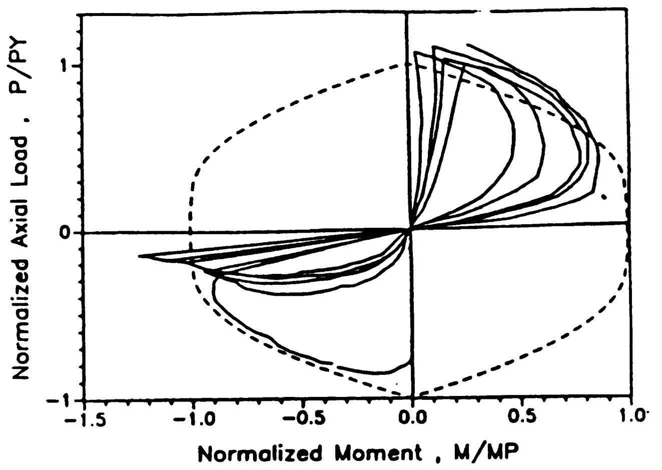

d) M-P relationship; Experiment

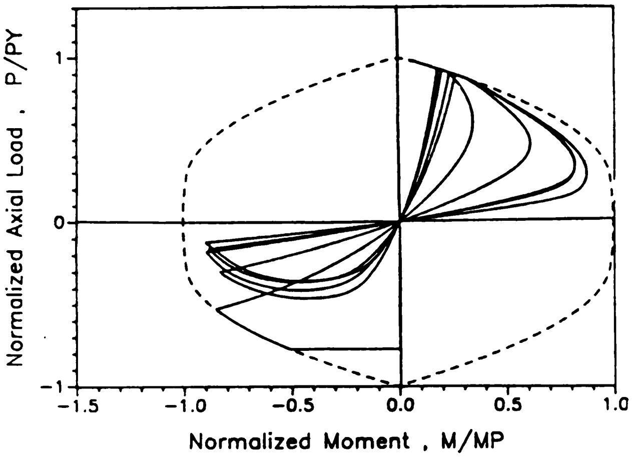

e) M-P relationship; Developed Model

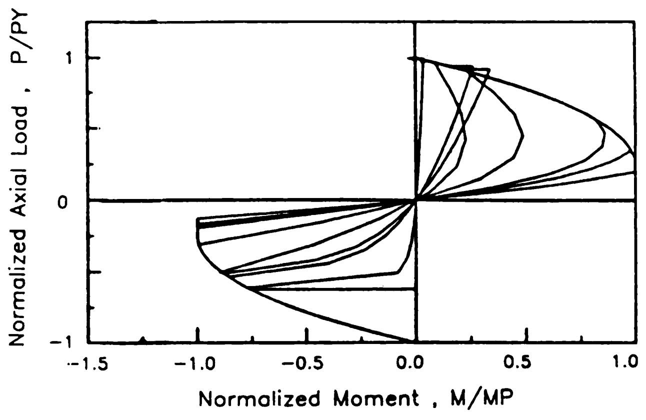

f) M-P relationship; Ikeda Model

Figure 4.7 Experimental and Analytical Comparisons of Strut 2, Table 4.5 (cont' d)[1]

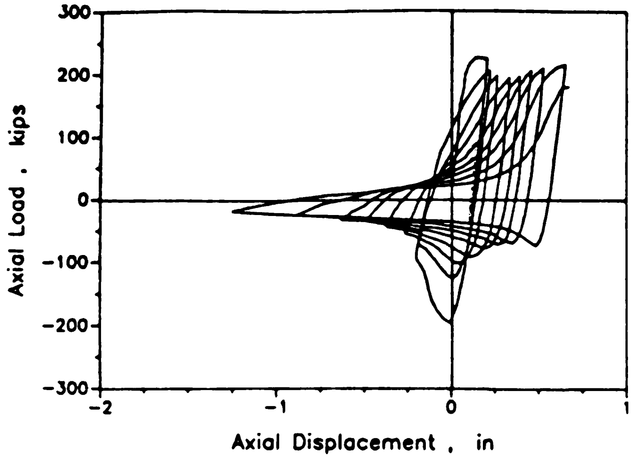

a) P-δ relationship; Experiment

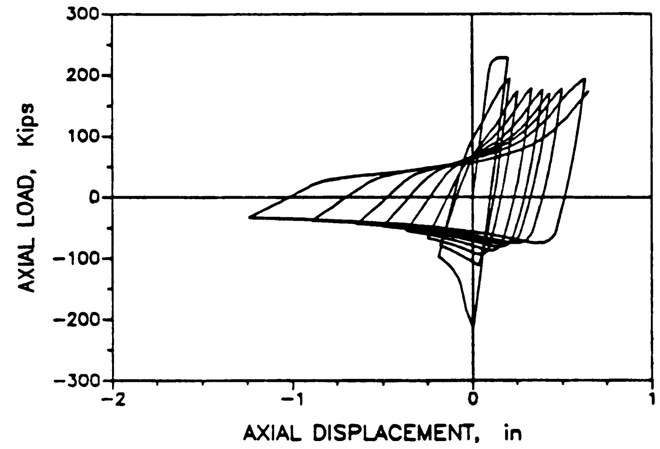

b) P-δ relationship; Developed Model

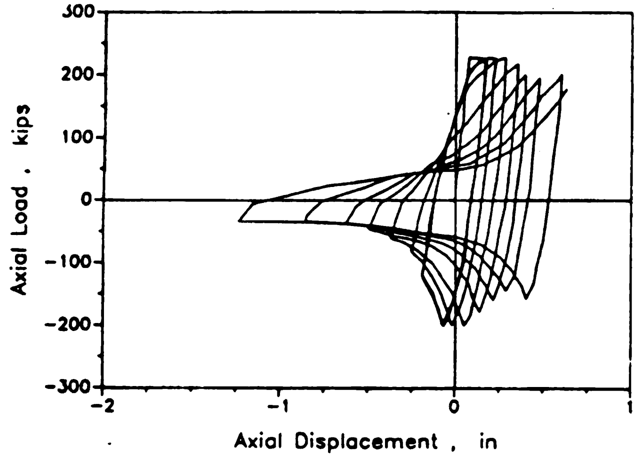

c) P-δ relationship; Ikeda Model

Figure 4.8 Experimental and Analytical Comparisons of Strut 3, Table 4.5 ^{1}

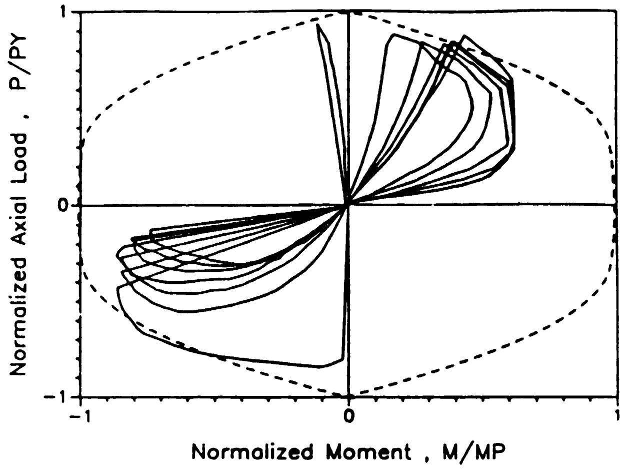

d) M-P relationship; Experiment

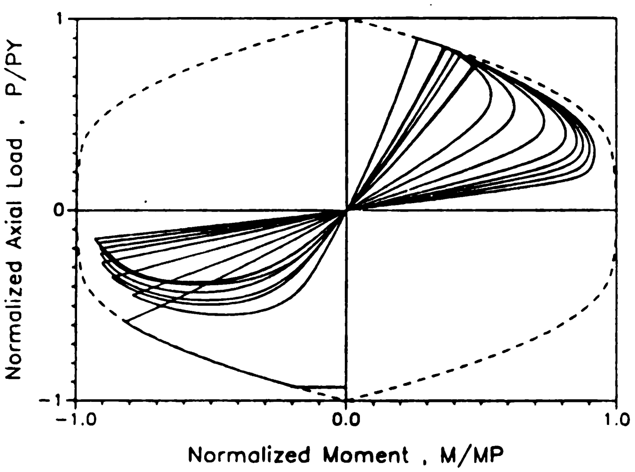

e) M-P relationship; Developed Model

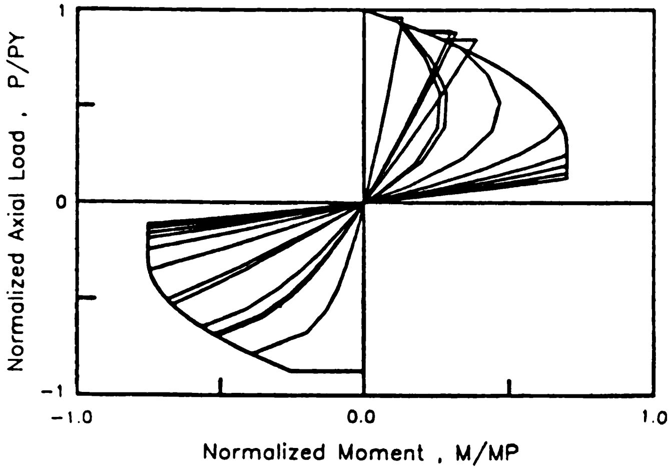

f) M-P relationship; Ikeda Model

Figure 4.8 Experimental and Analytical Comparisons of Strut 3, Table 4.5 (cont' d)[1]

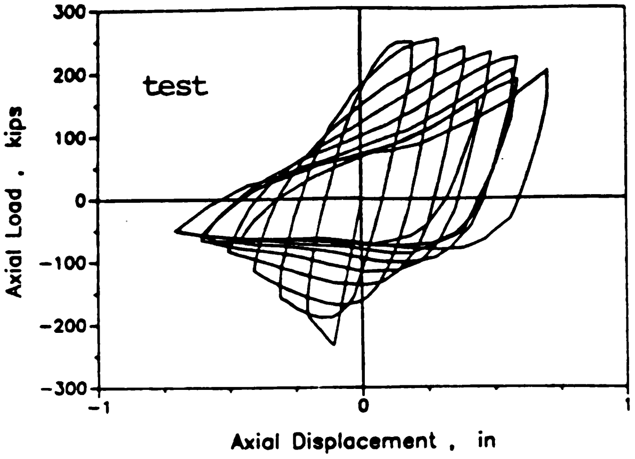

a) P-δ relationship; Experiment

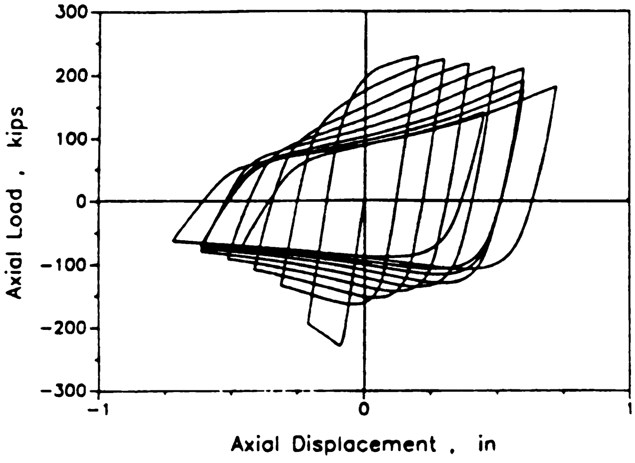

b) P-δ relationship; Developed Model

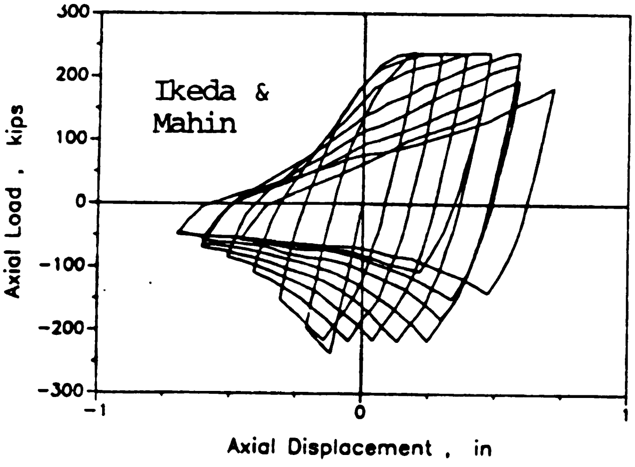

c) P-δ relationship; Ikeda Model

Figure 4.9 Experimental and Analytical Comparisons of Strut 4, Table 4.5[1]

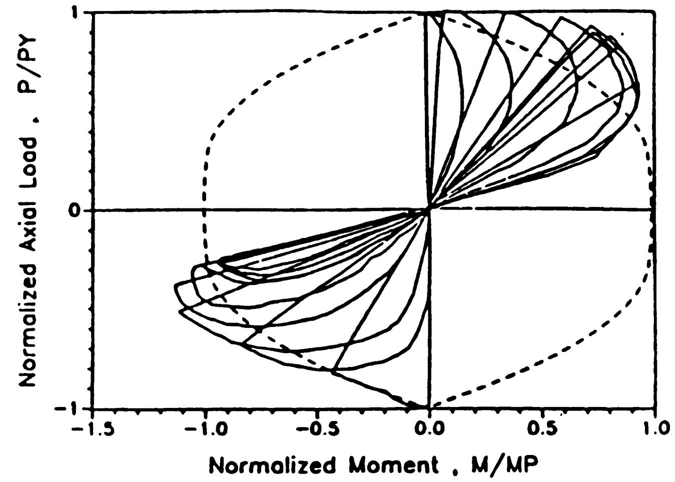

d) M-P relationship; Experiment

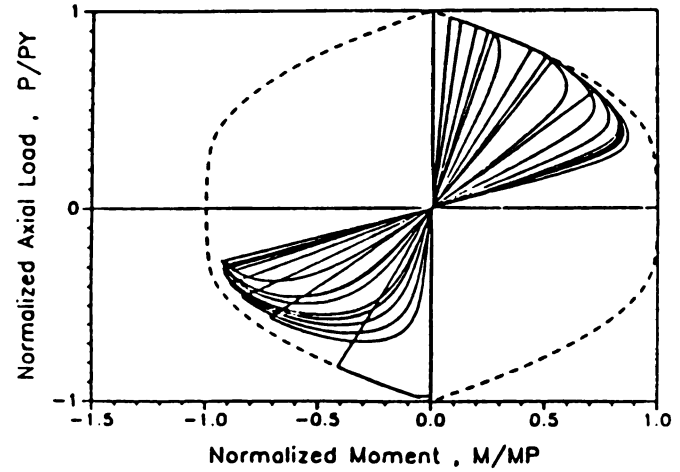

e) M-P relationship; Developed Model

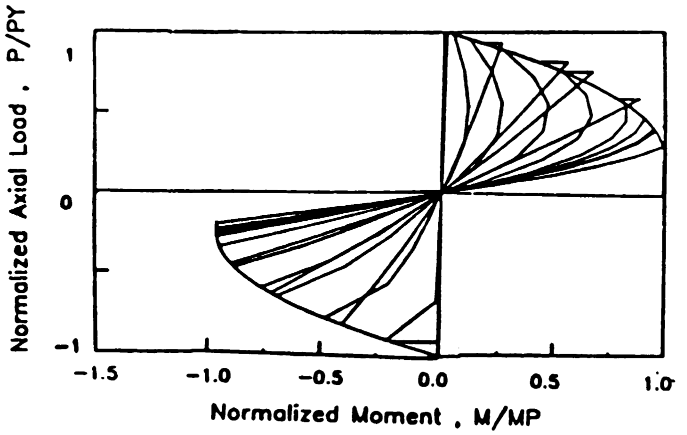

f) M-P relationship; Ikeda Model

Figure 4.9 Experimental and Analytical Comparisons of Strut 4, Table 4.5 (cont' d)[1]

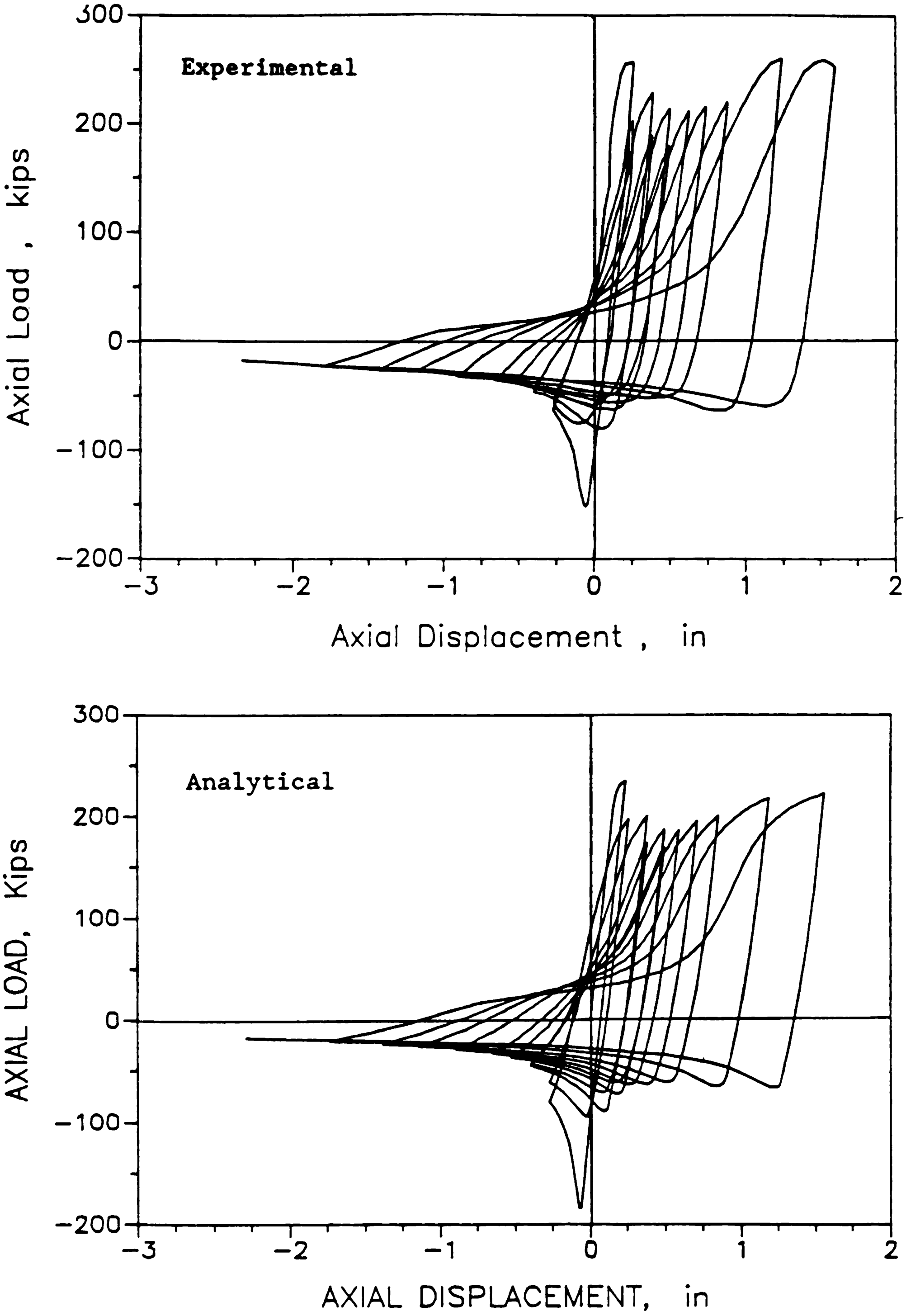

Figure 4.10 Experimental and Analytical Axial Load-displacement Relationships of Strut 5 (Table 4.5)[3]

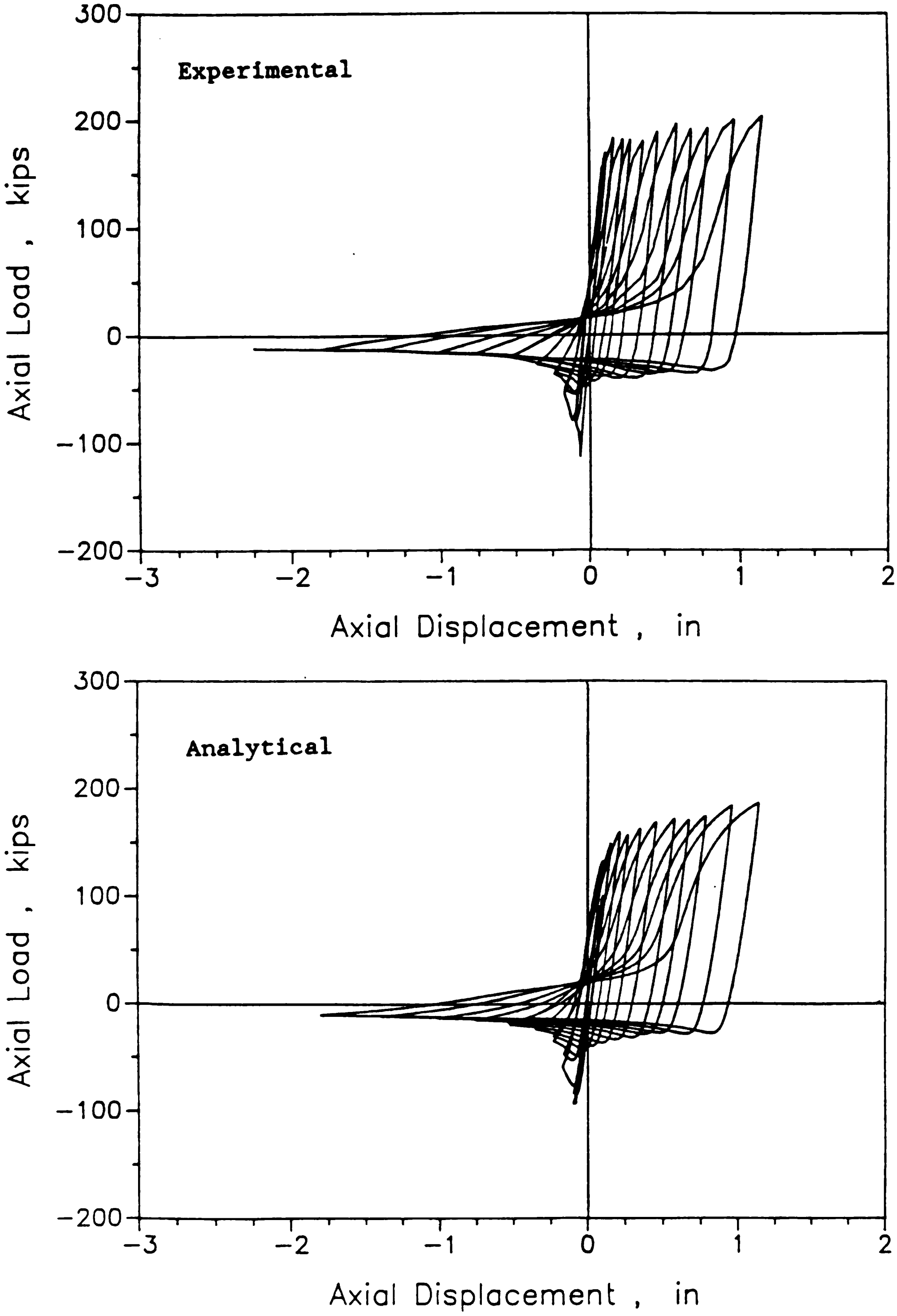

Figure 4.11 Experimental and Analytical Axial Load-displacement Relationships of Strut 6 (Table 4.5)[3]

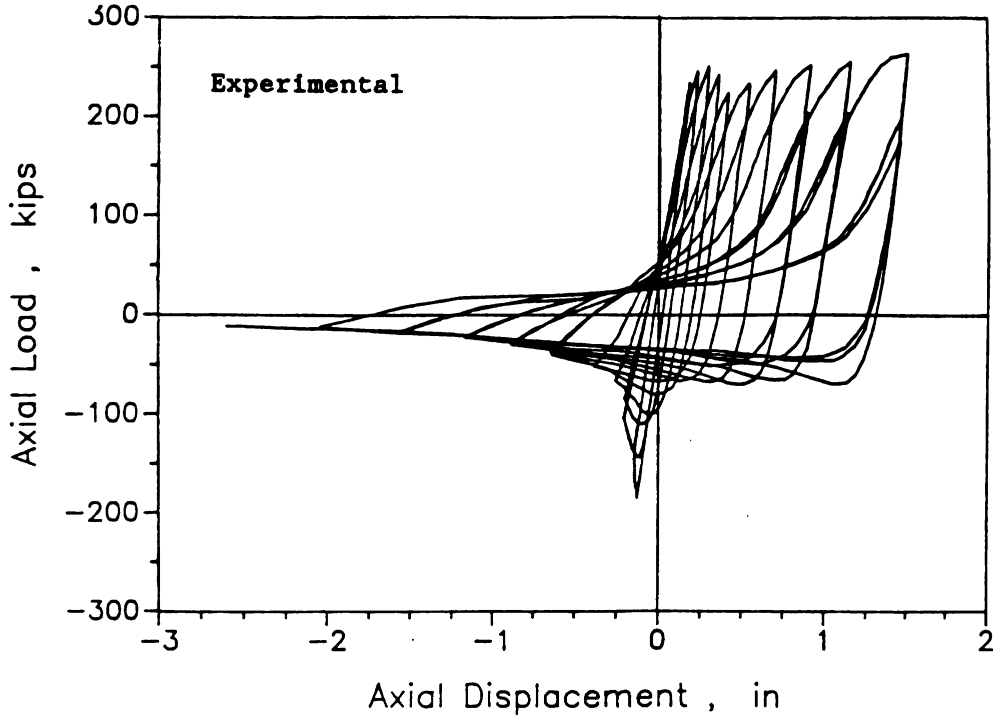

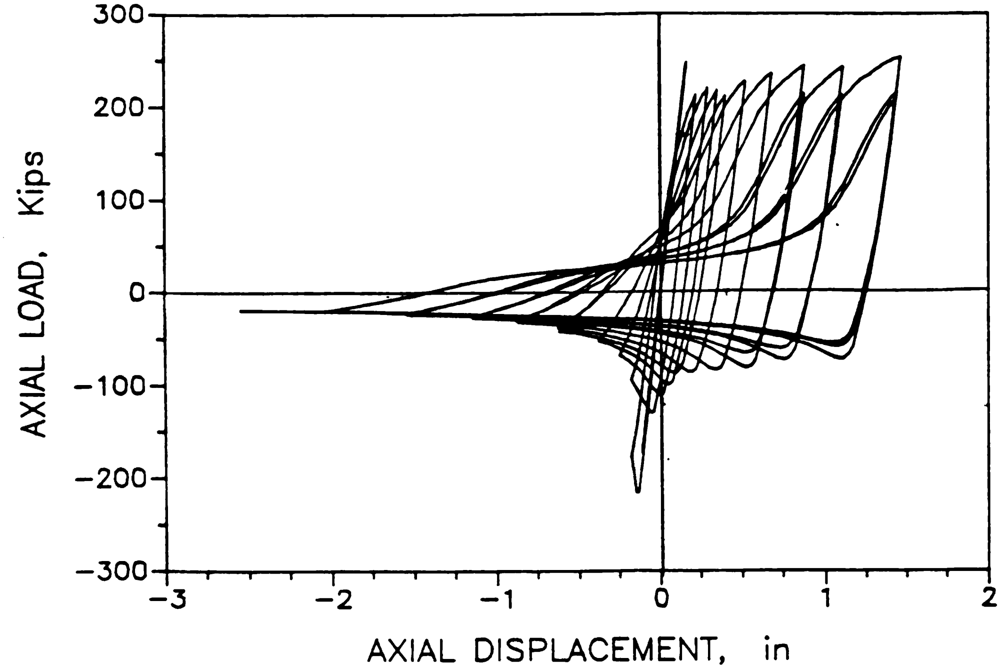

Figure 4.12 Experimental and Analytical Axial Load-displacement Relationships of Strut 7 (Table 4.5)[3]

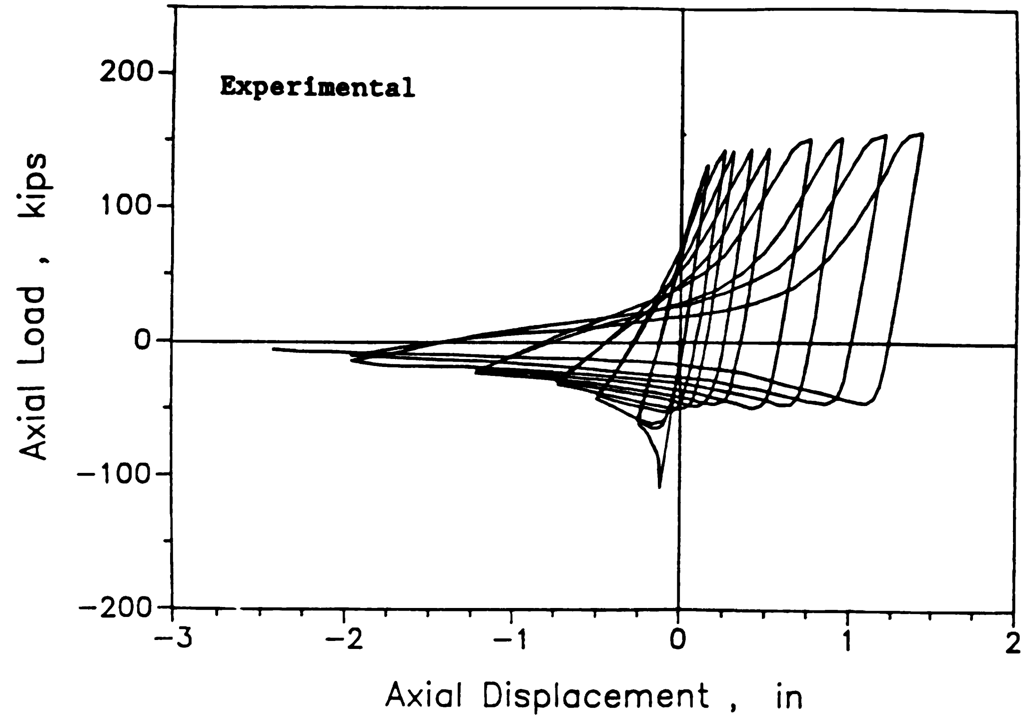

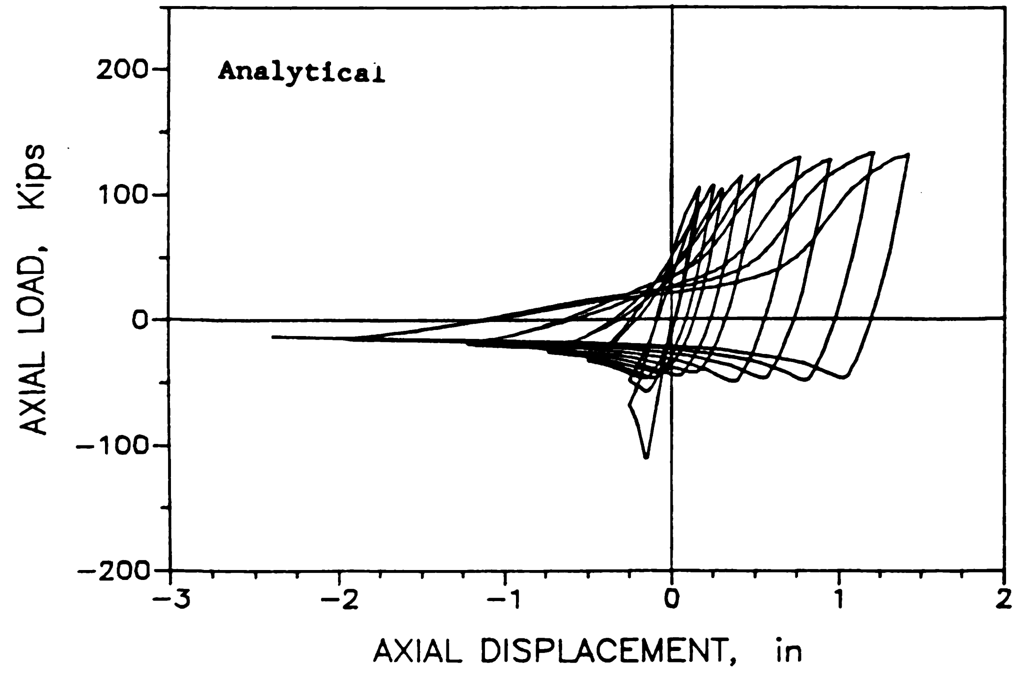

Figure 4.13 Experimental and Analytical Axial Load-displacement Relationships of Strut 8 (Table 4.5)[3]

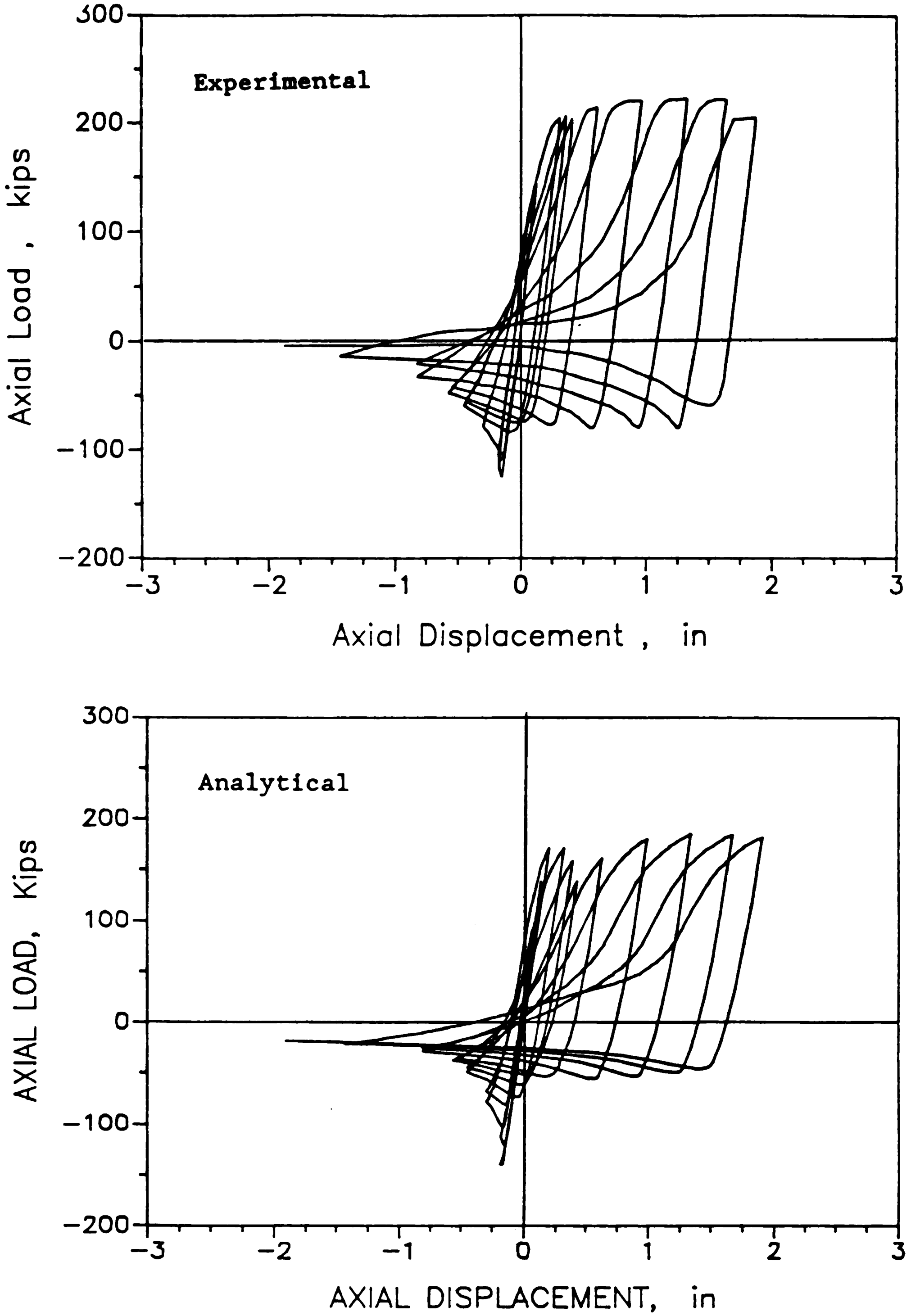

Figure 4.14 Experimental and Analytical Axial Load-displacement Relationships of Strut 9 (Table 4.5)[3]

the actual hinge behavior.

4.5 NUMERICAL STUDIES AND DESIGN RECOMMENDATIONS FOR STEEL STRUTS

Development of reliable models and analysis procedures can reduce the reliance on costly and time-consuming experimental investigations for assessing the effects of different design variables on the performance characteristics of structural systems, and for optimizing the design. The developed analytical model of steel struts can be used for numerical (instead of experimental) parametric studies, leading to the selection of the optimum material and geometric properties of the struts for achieving superior performance characteristics at minimum cost. The model can also be used to numerically evaluate the effects of the variations in the initial imperfection and end eccentricity of steel struts on their performance under load. The results of a numerical study aimed at generating the information needed for optimum design of steel struts are presented below.

4.5.1 Influence Of The Yield Strength : Figures 4.15a and 4.15b present the effects of yield strength on the axial load-deformation relationship of steel struts with effective slenderness ratios of 60 and 200, respectively. Each figure presents the monotonic axial load-deformation diagrams as well as the envelopes of the cyclic diagrams. The envelope curves are chosen to represent the overall hysteretic performance characteristics of the struts. The steel strut under study is a 3in x 3in x 1/4in (76mm x 76mm x 6.3mm) angle, and all the force values in Figure 4.15 have been normalized by the yield force of a strut with 36 Ksi (248 Mpa) yield strength.

The angular section introduced above, and the described axial force

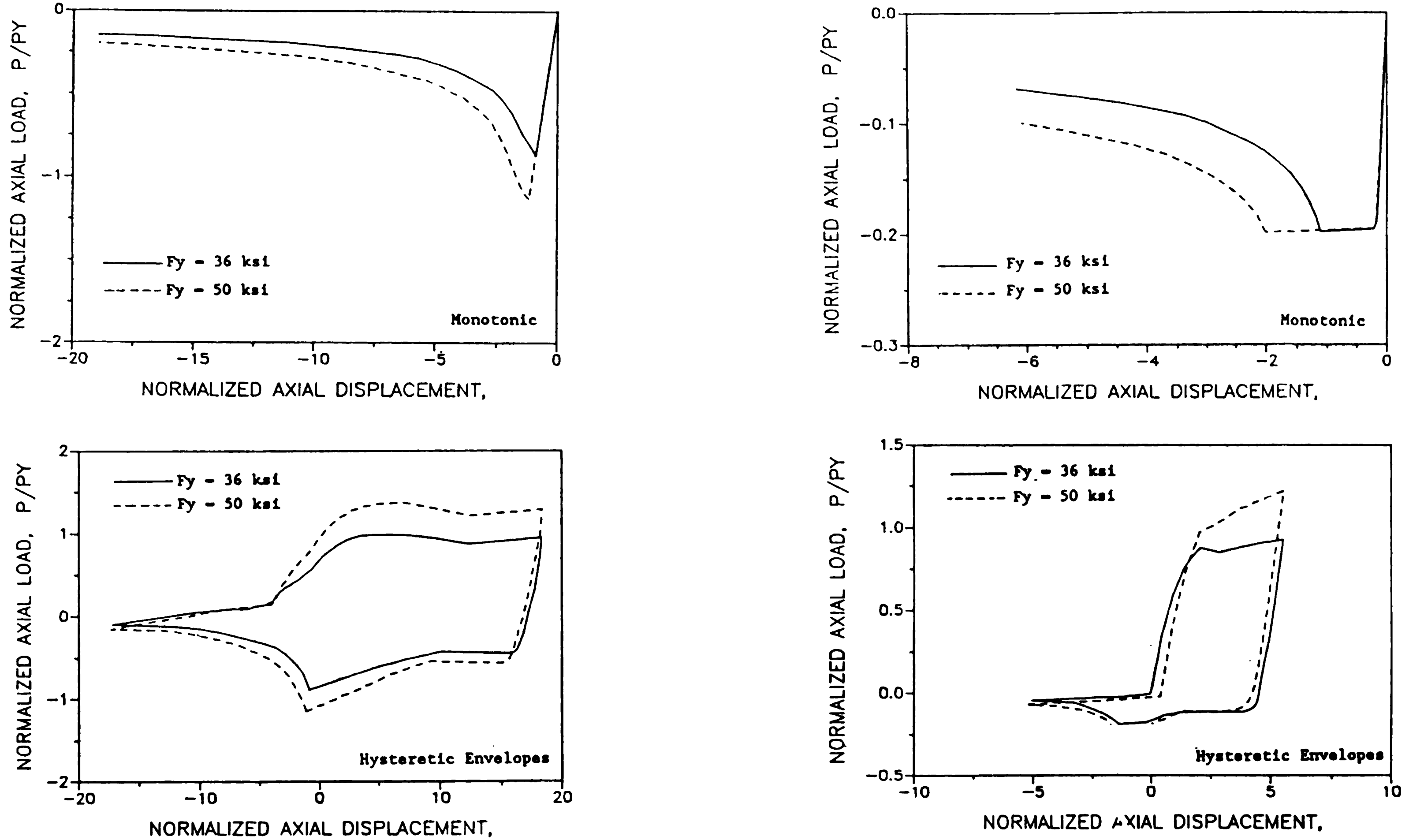

a) kl/r - 60

b) kl/r - 200

Figure 4.15 Effects of Different Yield Strengths on the Axial Load-Displacement Relationships

normalization process are typical of the ones adopted in the other stages of this parametric study.

From Figure 4.15a it may be concluded that an increase in yield strength from 36 Ksi (248 Mpa) to 50 Ksi (345 Mpa) enhances practically all aspects of the monotonic and cyclic axial load-deformation characteristics of the steel strut with an effective slenderness ratio of 60. The ultimate compressive and tensile strengths, the post-buckling resistance and the hysteretic energy absorption capacity of the strut all improve noticeably as the yield strength increases from 36 Ksi (248 Mpa) to 50 Ksi (345 Mpa).

A comparison of Figures 4.15a and 4.15b indicates that the more slender strut of Figure 4.15b is less sensitive to the variations in yield strength, when the loading is in compression. Under tension, however, the variations in yield strength significantly influence the strut performance. It seems that designers should be careful in balancing the cost versus the performance improvements corresponding to the use of higher strength materials for steel struts, especially at higher slenderness ratios.

The variations in the actual material yield strength, compared to the specified one, for steel struts is another important concern in design. Figures 4.16a and 4.16b present the effects of such variations on the axial load-deformation characteristics of steel struts with effective slenderness ratios of 60 and 200, respectively. The steel strut is a 3in x 3in x 1/4in (76mm x 76mm x 6.3mm) angle, and the diagrams in Figure 4.16 are produced for steel struts having the specified yield strength of 36 Ksi (248 Mpa), an increase in yield strength by 20%, and a decrease in yield strength by 10% . The discussion made in the previous paragraph on the effects of yield strength is also valid for the results presented in Figure 4.16. It may be concluded from this figure

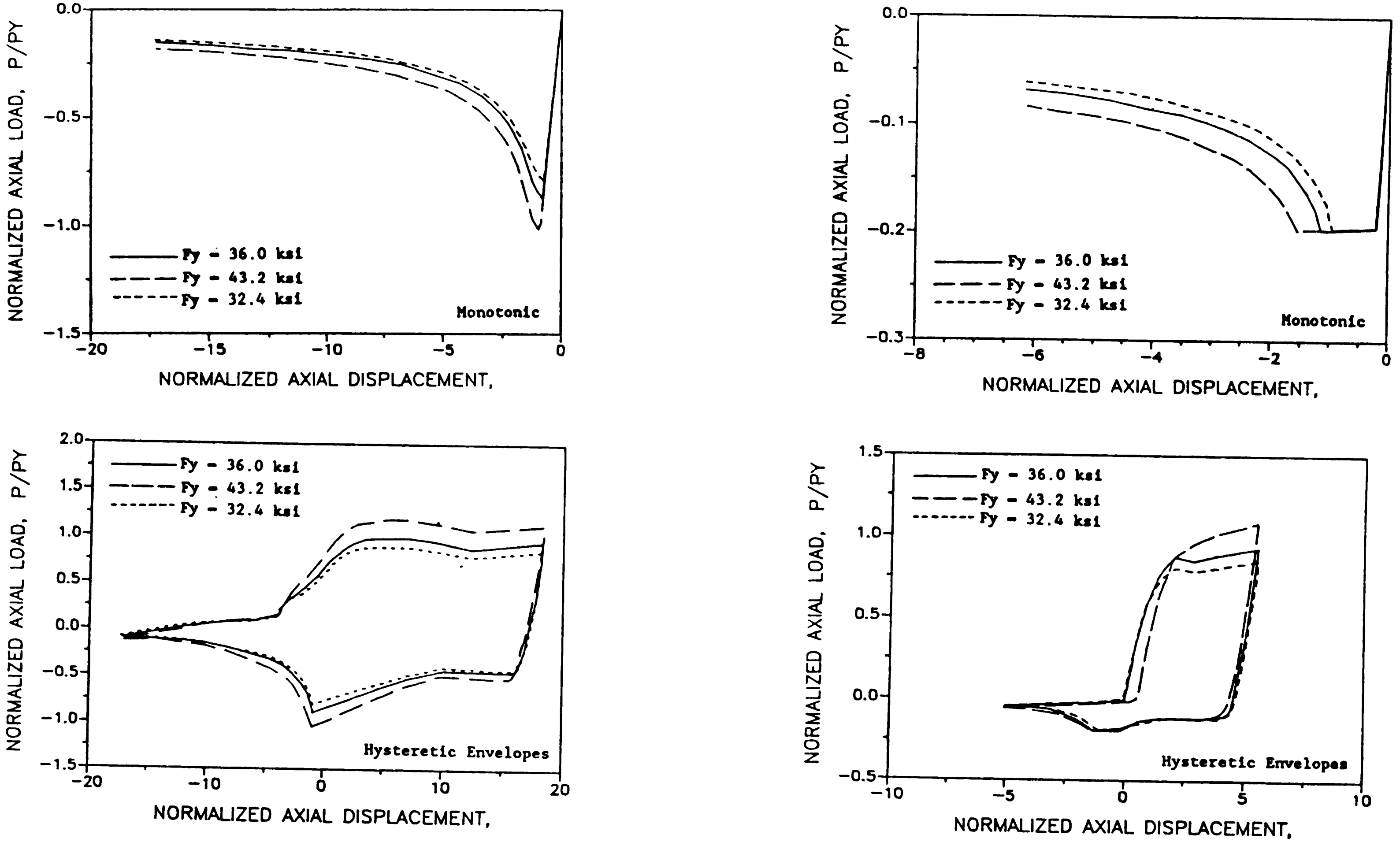

a) kl/r - 60

b) kl/r - 200

Figure 4.16 Effects of Variations in Yield Strengths on the Axial Load-Displacement Relationships

that the effects of a 10% reduction in the material yield strength on the monotonic and cyclic axial load-deformation characteristics of steel struts is relatively small.

4.5.2 The Influence Of The End Connection Restraints : Figures 4.17a and 4.17b present the effects of changing the end rotational fixities of steel struts on axial load-deformation characteristics, for struts with slenderness ratios (calculated as the full length divided by the minimum radius of gyration, disregarding the specified end fixities) of 60 and 200, respectively. The three curves on each diagram of Figure 4.17 correspond to the hinged-hinged, hinged-fixed, and fixed-fixed rotational end conditions. Lateral end deformations were restrained in all cases. The corresponding effective length factors are thus 1.0, 0.7 and 0.5, for the three end conditions.

A comparison of Figures 4.17a and 4.17b indicates that the provision of end rotational restraints is highly effective in enhancing the monotonic and cyclic axial load-defomation characteristics when, loading is in compression, in steel struts with higher slenderness ratios (Figure4.17b). The behavior of the more slender struts under tension and that of the shorter strut under tension and compression (except for the post-buckling resistance of shorter struts) are not much influenced by the changes in the end rotational restraints. This information can be very helpful to designers in making the decision on the details of the end connections.

4.5.3 The Influence Of Cross-Sectional Shape: In order to compare the performance of steel struts with different cross-sectional shapes, typical struts having different shapes but similar lengths and cross-

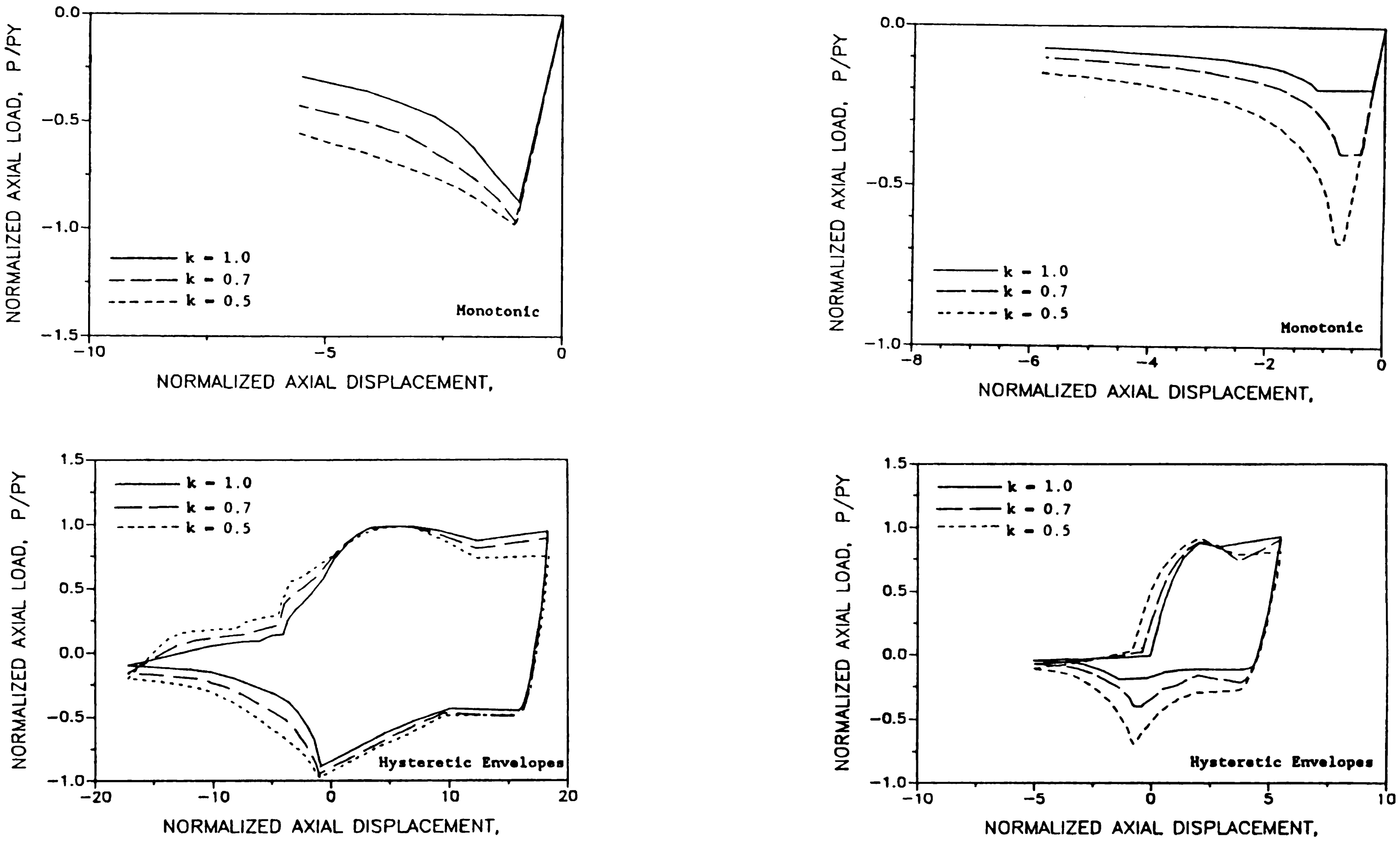

a) 1/r = 60

b) 1/r = 200

Figure 4.17 Effects of Ratational End Fixities on the Axial Load-Displacement Relationships

sectional areas were analyzed under monotonic and cyclic loads. For the 100 in. and 200 in. long steel struts, Figures 4.18a and 4.18b, respectively, show the axial load-deformation relationships (both monotonic and cyclic) of struts with Angle, WT, Pipe, and Square Tube cross-sections. It should be noted that the steel struts in either Figure 4.18a or Figure 4.18b have equal length but not similar slenderness ratios. They were chosen to have comparable cross-sectional areas and consequently material costs. In this approach we will be comparing the performance characteristics of steel struts with comparable prices but different cross-sectional shapes.

From Figure 4.18, it may be concluded that the cross-sectional shape effect on the inelastic-buckling behavior of steel struts is more pronounced for the longer struts when the axial load is in compression. The Square Tube followed closely by Pipe are superior to the other cross-sectional shapes under both monotonic and cyclic loads. It is worth mentioning that in optimizing the cross-sectional shape, attention should also be paid to the cost of connections which are usually used together with certain cross-sectional shapes.

4.5.4 The Influence Of Initial Imperfection : Out-of-straightness is commonly observed in steel struts at the job sites. It is important for the designers and constructors to understand the effects of different levels of initial imperfections on the axial load-deformation relationships of steel struts. Figures 4.19a and 4.19b present the effects of the variations in initial imperfection on compressive axial load-deformation relationship of the 3in x 3in x 1/4in (76mm x 76mm x 6.3mm) angular struts with effective slenderness ratios of 60 and 200, respectively. The three levels of initial imperfection presented in these

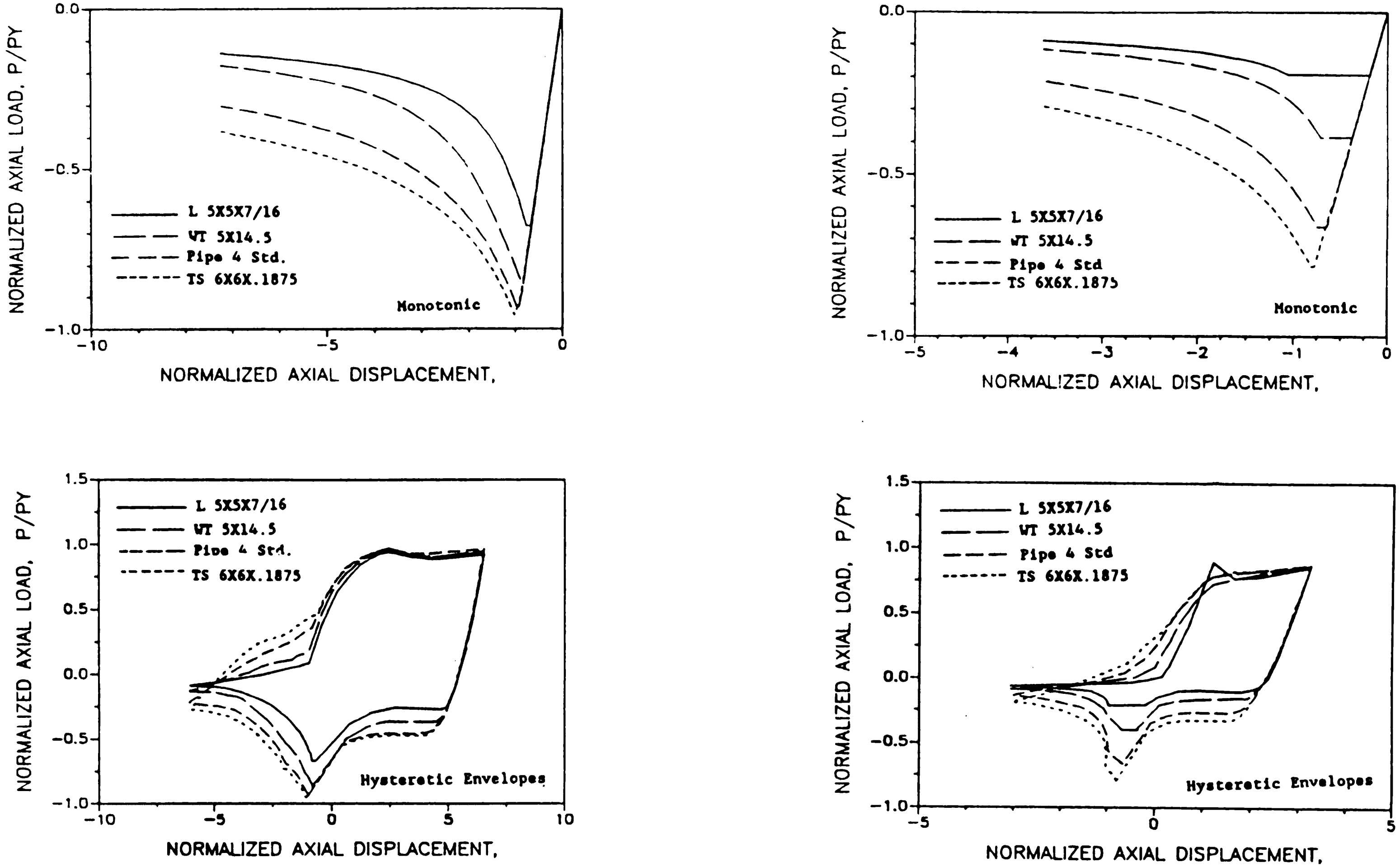

a) L -100 in

b) L - 200 in

Figure 4.18 Effects of Cross-Sectional Shapes on the Axial Load-Displacement Relationships

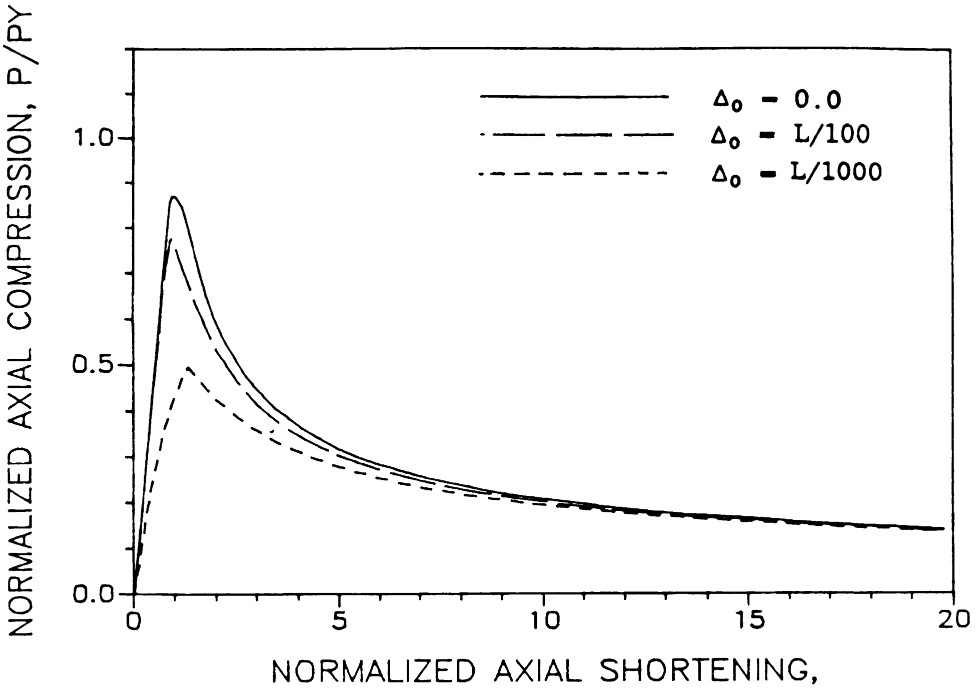

a) $kl/r = 60$

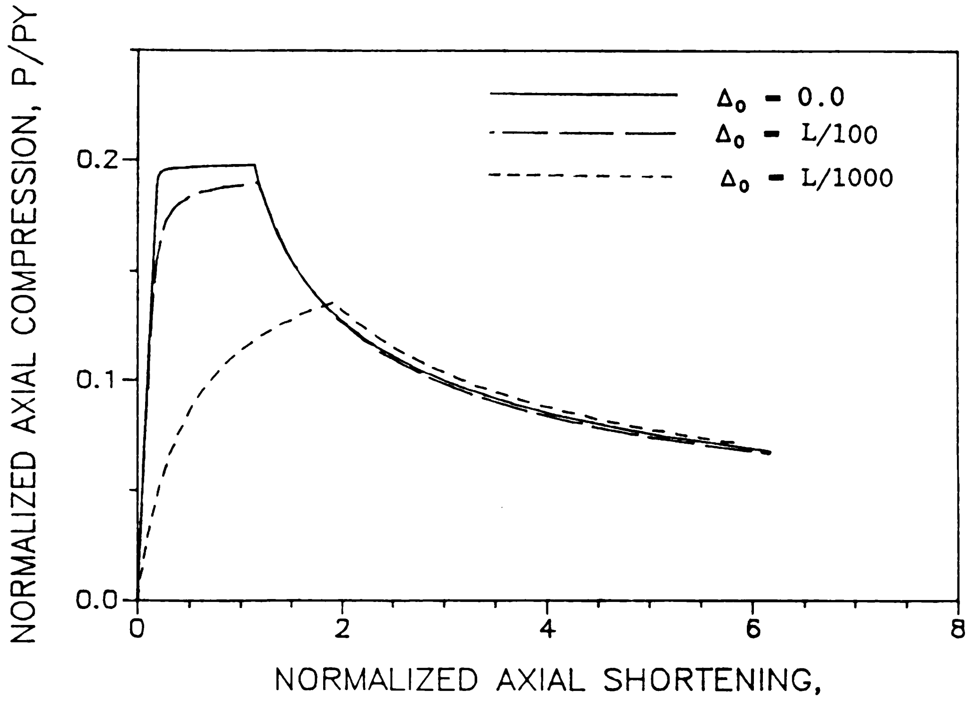

b) $kl/r = 200$

Figure 4.19 Effects of Initial Imperfection on the Axial Load-Displacement Relationships

figures correspond to the maximum out-of-straightnesses of 0.0% , 0.1% , and 1.0% of the length. Figure 4.19 indicates that the increase in initial imperfection, especially from 0.1% to 1.0% of the length, significantly reduces the ultimate compressive strength as well as the strut pre-peak tangent stiffness. The post-buckling behavior of the struts, however, is not much influenced by the presence of the initial imperfection.

4.5.5 The Influence Of End Eccentricity : Figures 4.20a and 4.20b present the effects of the variations in end eccentricities around the minor and major axes, respectively, on the compressive axial load-deformation relationship of a 3in x 3in x 1/4in (76mm x 76mm x 6.3mm) angular struts with an effective slenderness ratio of 60. Figures 4.20c and 4.20d present similar results for the strut with an effective slenderness ratio of 200. The four curves in each figure correspond to end eccentricities of 0.0, 0.3in (7.6 mm), 1in (25.4mm), and 3in (76mm). The increase in end eccentricity around minor axis is observed to significantly reduce the ultimate compressive strength, pre-peak tangent stiffness and post-peak compressive resistance of the struts with an effective slenderness ratio of 200 (Figure 4.20c). Similar effects of the minor axis eccentricity are observed in Figure 4.20a for the strut with an effective slenderness ratio of 60, except that its pre-peak tangent stiffness is not much influenced by the increase in minor axis eccentricity.

In the strut with an effective slenderness ratio of 60, the adverse effects of the major axis eccentricity are comparable to those of the minor axis eccentricity (compare Figures 4.20a and 4.20b). For the more slender struts with an effective slenderness of 200, however, the major

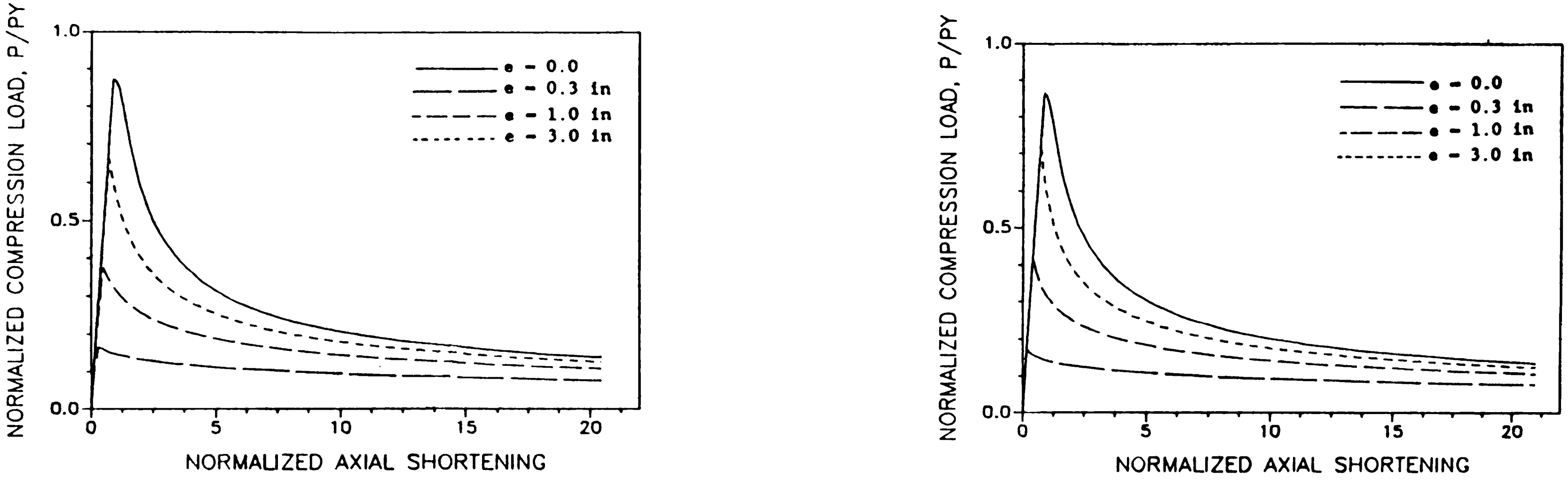

a) Around the minor axis (kl/r - 60)

b) Around the major axis (kl/r - 60)

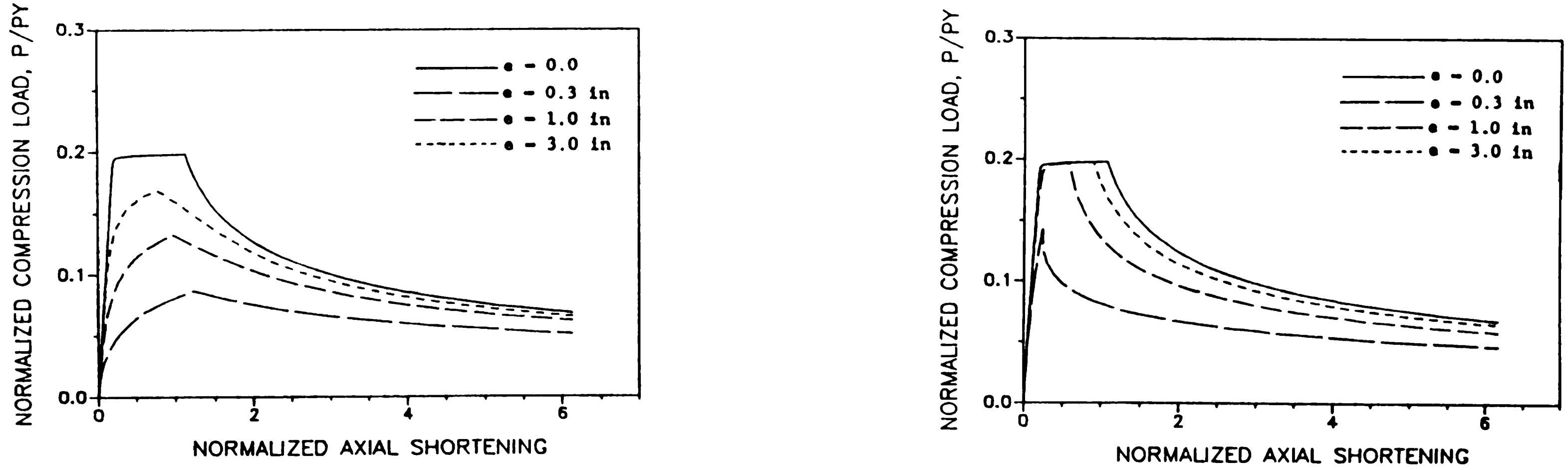

c) Around the minor axis (kl/r - 200)

d) Around the major axis (kl/r - 200)

Figure 4.20 Effects of End Eccentricities on the Axial Load-Displacement Relationships

axis eccentricity reduces the ultimate strength and the pre-peak tangent stiffness of the struts far less than the minor axis eccentricity (compare Figures 4.20c and 4.20d).

4.6 SUMMARY AND CONCLUSION :

The coefficients in the proposed analytical model of steel struts were derived empirically, and the final model was positively verified using monotonic and cyclic test results on steel struts with wide ranges of material and geometric properties and cross-sectional shapes. The fully developed and verified element model was then used for a numerical study on the effects of the material yield strength, end support rotational fixity, cross-sectional shape, initial imperfection, and end eccentricity of steel struts on their monotonic and cyclic axial load-deformation relationships. From the results of the numerical study it may be concluded that :

a) For the less slender steel struts with an effective slenderness ratio of 60, the ultimate compressive and tensile strengths, the post-buckling compressive resistance, and the hysteretic energy absorption capacity of the strut all substantially increase with increasing yield strength. The more slender struts, with an effective slenderness ratio of 200, are less sensitive to the yield strength variations when loaded in compression. Under tension, however, the effects of variations in yield strength on the performance of the more slender strut are still significant.

b) End rotational restraints are highly effective in enhancing the monotonic and cyclic axial load-deformation characteristics of steel struts with higher slenderness ratios under compression. The behavior of the more slender strut under tension and that of the shorter strut under tension or compression (except for its post-buckling resistance) are not much influenced by providing end rotational restraints.

c) The cross-sectional shape effects on the strut performance are more pronounced for the longer struts. At the same cross-sectional areas, among the four cross-sectional shapes considered (Square Tube, Circular Pipe, WT, and Angle), the Square Tube followed closely by the Pipe-section are the more superior ones under monotonic and cyclic loads. The WT comes next followed by the Angle.

d) The increase in initial imperfection significantly reduces the ultimate compressive strength as well as the pre-peak stiffness of the steel struts. The post-buckling behavior, however, is not much influenced by the increase in initial imperfection.

e) The increase in end eccentricity around the minor axis significantly reduces the ultimate compressive strength, the pre-peak tangent stiffness, and the post-peak compressive strength of the more slender struts with effective slenderness ratios of about 200. The effects of minor axis eccentricity on the less slender struts are also similar, except that the pre-peak tangent stiffness is not much sensitive to the minor axis eccentricity. The major axis eccentricity effects on the less slender struts are comparable to those of the minor axis eccentricity. The more slender struts with slenderness ratios of about 200, however, are far less sensitive to the variations in the major axis eccentricity than the minor axis eccentricity. The comparisons between the effects of major and minor axis eccentricities were made for an angular strut which, as observed in test results, eventually buckles around the minor axis, in spite of minor or major axis eccentricities.

The results of the numerical study presented above can be helpful to designers in coming up with balanced designs resulting in steel struts with desirable performance characteristics and minimum material and connection costs.

CHAPTER 5

INELASTIC ANALYSIS OF SPACE TRUSSES

5.1. INTRODUCTION :

The popular approach to the structural analysis of steel trusses treats the connections as ideal hinges and assumes that the elements behave elastically under pure axial loads. This approach disregards some important aspects of the truss behavior observed in tests, including the partial rotational restraint provided by the end connections, and the beam-column (bowing) action of the elements. Comparisons between the analytical and experimental performances of typical steel trusses have indicated some major discrepancies in the results of the analysis.[44] Figure 5.1a presents percentage difference between the analytical and experimental loads in truss elements, versus the number of elements having that percentage error in nine lattice transmission towers (see for example Figure 5.1b) tested in the Transmission Line Mechanical Research Center (TLMRC) of the Electric Power Institute (EPRI).[44] From this comparison between the analytical and experimental results, it may be concluded that only about 25% of the measured member forces could be predicted within an accuracy of ± 10% by the elastic truss analysis approach. The relatively large inaccuracy of the analytical results appears to be inconsistent with the expectations of the design engineers.[44]

The actual behavior of space trusses (especially those with bolted connections) is rather complex. An important consideration for improving the accuracy of structural analysis is the replacement of the

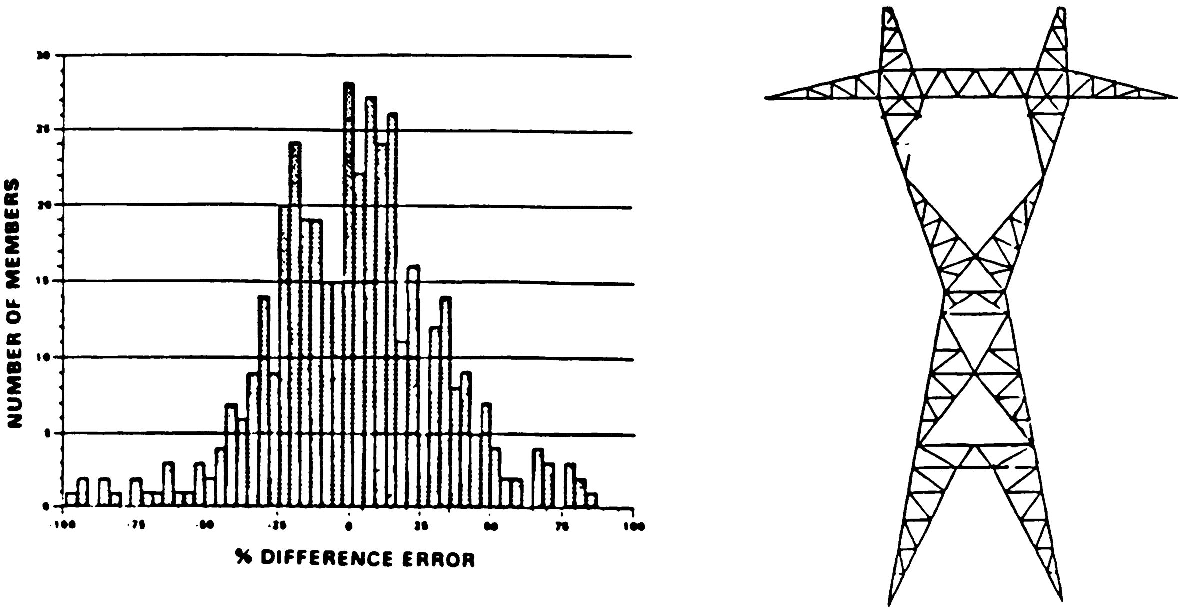

a) Percentage Error Observed

b) Typical Lattice Towere

Figure 5.1 Analytical vs. Experimental Axial Forces in Truss Elements[44]

simplistic linear elastic axial element model with a more realistic one which accounts for the inelastic-buckling beam-column type performance of the element. Simulation of the partial rotational restraint at joints and the slippage at bolted connections can also enhance the accuracy of the truss analysis procedures.

A brief background on some key structural modeling methodologies and numerical procedures used for inelastic analysis of space trusses is presented below. This literature review is followed by a description of a computer program which utilizes the inelastic-buckling element model developed in this study for nonlinear analysis of the space truss systems. Improvements in the structural analysis results were sought through a closer simulation of the actual element behavior and more reliable idealization of some aspects of structural performance like the behavior of X-bracing and in-plane redundants. A detailed treatment of the partial rotational restraint and slippage of the bolted connections is outside the scope of this investigation.

5.2 X-BRACING AND IN-PLANE REDUNDANTS : A REVIEW OF THE BEHAVIOR

Steel truss systems generally include X-bracing (Figure 5.2a) and in-plane reduntants providing intermediate support to main elements only in one plane (Figure 5.2b). The performance characteristics of X-braces and in-plane redundants during the response of structures to applied loads are rather complex, and the simulation of these types of performance by the previous investigators has been based on some simplifing assumptions. Recent test data[49], however, have indicated that some of these assumptions are not realistic. This section describes the performance characteristics and failure modes of the X-braces and in-plane redundants.

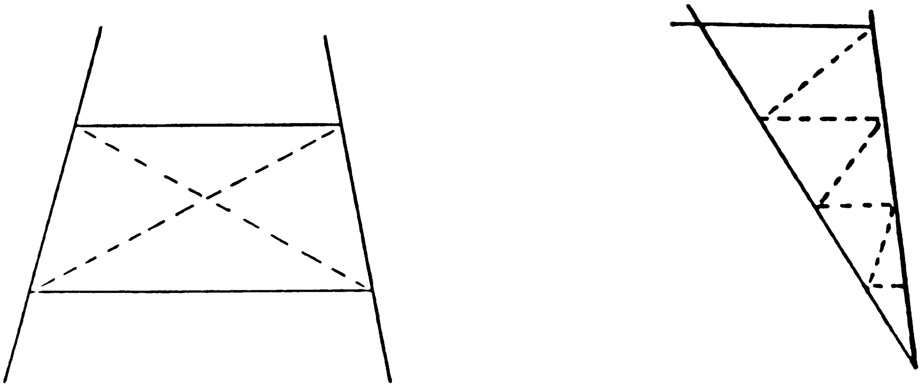

a) X-Bracing

b) In-Plane Redundants

Figure 5.2 X-Bracing and In-Plane Redundants

5.2.1 X-Bracing : X-bracing is economically advantageous over other bracing patterns. It derives its primary benefit from the interconnection of the two diagonals (which cuts down the unsupported buckling length in compression).

In the current practice, the analysis and design of X-bracing members may be performed in one of two ways. The first method completely ignores the strength of the compression member in resisting the imposed loads. The second method, however, recognizes the contribution of the compression diagonal. This method consider the possibilities for an overall out-of-plane buckling of the full diagonal, and the buckling of half-diagonals about their weak principal axes.

In tests performed on X-bracing systems[49,50] (Figure 5.3a), at small deformations under the first loading cycle, the compression diagonal is observed to undergo symmetric out-of-plane buckling over its full length. This buckling is, however, restrained by the tension diagonal which provides lateral and rotational restraints at the point of intersection. The lateral restraint which is dominant, is small in the beginning but increases as the lateral displacement increases, and eventually the lateral restraint from the tension diagonal stops the continuous buckling of the compression diagonal over its full length. At this point, shown as point A in Figure 5.3b, buckling tends to occur about the weak axis over half the element length. Test results on X-braced systems with single angle bracing elements[50] suggest an effective length of 0.85 times half the brace length (reflecting the end rotational restraints) applies to this buckling mode. Yielding of the tension diagonal (point B in Figure 5.3b) may either follow or precede the unrestrained buckling of the compression diagonal. From the experimental results it may be concluded that the compression diagonal has detrimental effects on the response of X-bracing systems to lateral

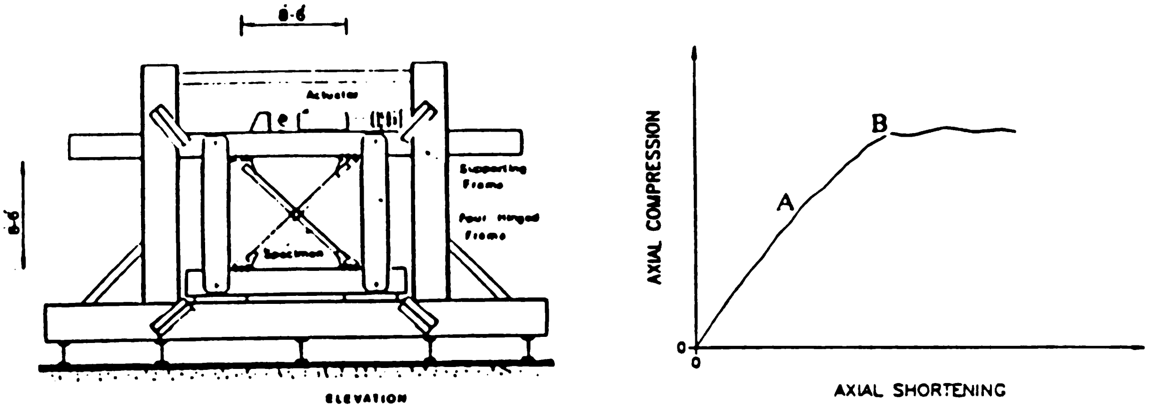

a) Test Set-Up

b) Axial Load-Displacement Relationship

Figure 5.3 X-Bracing Test Configaration and Typical Results

loads, and the buckling of the compression member dominantly takes place over half of the element length. The behavior in subsequent cycles essentially follows the same regime as the first cycle, but with continuous deterioration of the load-carrying capacity and stiffness of the system.

5.2.2 In-plane Redundants : A common method of strengthening the main elements in space trusses is by the use of in-plane redundants to provide intermediate support against buckling of the main elements in a specific plane. The shear forces transferred to the main elements through the in-plane redundants, and the partial restraint provided by these elements against the out-of-plane buckling of the main elements are found in experiments to have important effects on the behavior of the main elements. The transferred shear forces might accelerate the buckling of the main elements, while the resistance of in-plane redundants against out-of-plane movements tends to strengthen the main elements against out-of-plane buckling.

A refined finite element technique has been used in Reference 44 to investigate the effects of the in-plane redundants on the behavior of an X-bracing system under lateral loads. In this study the X-bracing system shown in Figure 5.4a was idealized as shown in Figures 5.4b through 5.4e, in order to assess the effects of different in-plane redundants on the response of the system under lateral loading. These models were different in that the in-plane redundants were partially or completely removed from some of them. Figure 5.4f presents the axial force-deformation relationships of the tension and compression diagonals.

It can ne seen from Figure 5.4f that the compressive strength of the diagonals is significantly influenced by the in-plane redundants. This is due to the partial out-of-plane support provided by the redundants to the compression diagonals. In the complete system of Figure 5.4b and the simplified one shown in Figure 5.4c, the compression diagonal is supported by the redundants and by the tension diagonal (at their bolted intersection). Since these two systems behaved similarely it was deduced that the four redundants excluded from the model shown in Figure 5.4c provide very little out-of-plane support to the compression diagonal. Removal of some other redundants in Figures 5.4d and 5.4e, however, significantly reduces the compression diagonal buckling load. This means that the redundants which are present in Figure 5.4b but not in Figure 5.4d are effective in restraining the compression diagonal against out-of-plane movements. From the results presented in Reference 44 on the buckling modes of different system models it might be concluded that the in-plane redundants strengthen the main elements not only by partially restraining the out-of-plane deformations, but also by providing support against rotation of the compression member and the subsequent weak axis buckling that occurs.

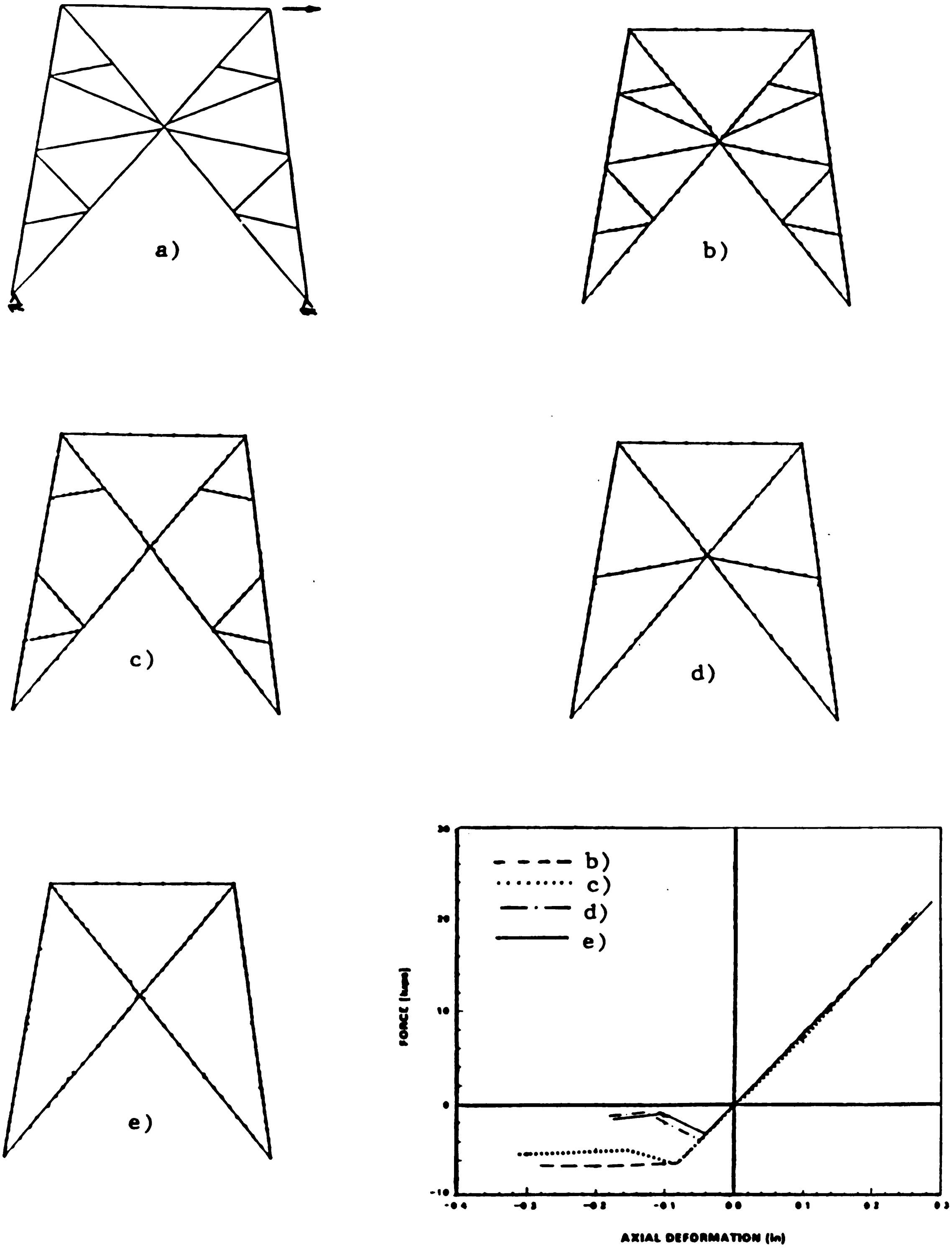
a)
b)
c)
d)
e)
b)
c)
d)
e)
30
20
10
0
-10
FORCE (kips)
-0.4
-0.3
-0.2
-0.1
0.0
0.1
0.2
0.3
AXIAL DEFORMATION (in)

f) Compression and Tension Diagonals Axial Force-Displacement relationships

Figure 5.4 Effects of In-Plane Redundants on X-Braced SYstems[44]

The refined finite element analysis presented above is not economically feasible for everyday use by designers. It requires substantial efforts for defining and inputing the system model, consumes large amount of computer time and memory, and its inaccuracy in considering the complex behavior (involving slippage) of bolted connections and also in predicting the effects of factors like residual stresses and gradual plastification of the element makes it difficult to justify the spending of the excessive computational time and efforts they require. The more practical modeling techniques applied to space trusses generally neglect the out-of-plane and rotational restraints of the main elements by the in-plane redundants.

5.3 A BACKGROUND ON THE INCREMENTAL NONLINEAR STRUCTURAL ANALYSIS OF SPACE TRUSSES :

The nonlinear analysis of space trusses is most effectively performed using an incremental formulation in which the static and kinematic variables are updated incrementally at successive load steps in order to trace the complete solution path. In this solution, the governing equations should be satisfied in each load step to a sufficient accuracy. Otherwise, the solution errors could accumulate and lead to gross and undetectable errors, and often to solution instability.[51]

An accurate solution of the nonlinear structural analysis equations can always be expected if the load increment per step is made sufficiently small, but such a solution can result in many incremental steps that render the analysis of a large structural system prohibitively expensive. In order to solve the nonlinear structural analysis equations efficiently, while maintaining control on the accuracy of the solution, larger load steps may need to be employed with iterations. The convergence process in this approach may be slow requiring a large number of iterations that can again result in a high solution cost. Also, some iterative methods do not converge for certain types of problems or for large load increments.

The purpose of iteration in an incremental nonlinear stiffness analysis of space trusses is to reduce the out-of-balance forces resulting from the nonlinearities within each step to a tolerance limit. The reanalysis in each cycle of iteration might be carried out with a constant stiffness obtained at the end of the previous load step (Figure 5.5a), or it may be performed using an updated stiffness obtained after the previous iteration cycle (Figure 5.5b). Several cycles of iterations may be necessary untill the convergence criterion is satisfied. The advantage in keeping the stiffness at different iterations within one load step constant, is that the computational efforts needed for inverting the updated stiffness matrix in each cycle of iteration can be avoided.

In the incremental solution strategy based on iterative methods, realistic criteria should be used for termination of the iterations. At the end of each iteration the solution should be checked to see whether it has converged within preset tolerance, or whether the iteration is diverged. If the convergence tolerance is too loose, inaccurate results may be obtained, and if the tolerance is too tight, excessive computational efforts might have to be spent in order to obtain a needless accuracy. A divergence check can also help in improving the computational efficiency by terminating the iteration when the solution is not actually converging.

The convergence criteria popularly used in nonlinear analysis (Figure 5.6) generally seek to limit : the out-of-balance forces, or the

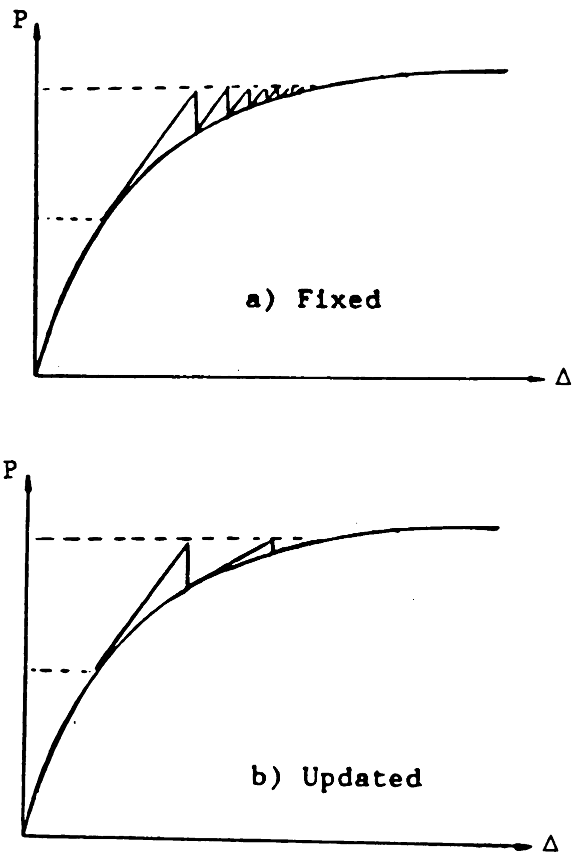
P
Δ
a) Fixed
P
Δ
b) Updated

Figure 5.5 Stiffness Analysis Simulation in Incremental Nonlinear Analysis

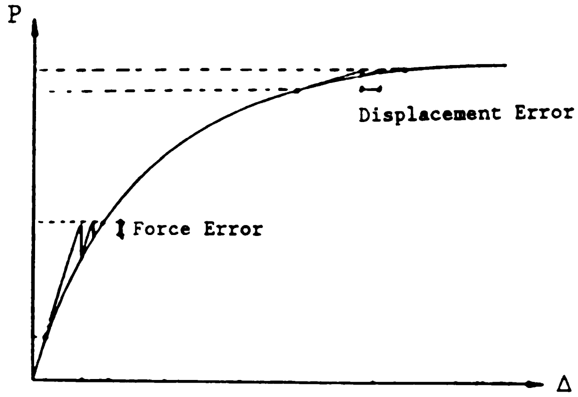
P
Displacement Error
Force Error
Δ

Figure 5.6 Convergence Criteria In Incremental Nonlinear Analysis

increments in displacement and/or internal energy resulting from the application of the out-of-balance forces. The displacement and energy based convergence criteria are advantageous when, due to the softening of the system, small load increments cause large displacement increments. This situation occurs near the peak of the load-deformation relationship. In this condition, the convergence criterion based on the out-of-balance forces is not effective because small out-of-balance loads may produce very large displacement increments.

It is interesting to notice that certain characteristics of the structural performance have decisive influence on the selection of the convergence criteria. Stiffening structures require a tight force convergence, while softening structures (especially near the peak) require a tight displacement or energy tolerance.

Among the iteration schemes, the Newton-Raphson[51] is the one most popularly used in structural analysis. For problems with significant nonlinearities, the linearization of the system in each load step can lead to a very slow convergence in the iterations, or the iterations may even diverge. In order accelerate the convergence and prevent divergence of the solution, it may be effective to use an acceleration scheme. These schemes, in one way or another, approximate the nonlinearities within the load step and the consequent modifications of the stiffness matrix.[51,52] They usually involve only minor additional computational efforts within each iteration step, but can considerably reduce the required number of iterations for satisfying the convergence criteria.

The incremental stiffness analysis of nonlinear structural systems in general and space trusses in particular might run into problem due to the instability of the related formulations in the vicinity and beyond the peak load. This phenomenon is commonly observed in space trusses after the buckling of a number of elements (which makes their axial stiffness negative). In order to overcome this problem, some investigators have adopted the Dynamic Relaxation technique as proposed in References 53,54, and 55. This technique involves a straight forward implementation of a displacement incremental technique, which is based on the fact that the post-peak behavior of a structural system or subassemblage in each load step is comparable to the damped vibration to rest in the displaced position of static equilibrium for the system under the action of applied forces. This approach changes the unstable static problem, with force dropping under increasing deformations, to a dynamic problem in each load step which does not require any provisions for handling the negative diagonal stiffness elements. The formulaion of the Dynamic Relaxation technique, as presented in References 53,54, and 55, solves the governing equations using the force-deformation relationships (tangent stiffness) of individual elements, eliminating the need to form the global tangent stiffness matrix of the complete system. This discrete element approach requires a relatively small amount of computer storage.

5.4 THE ADOPTED STRUCTURAL MODELING APPROACH :

In the overall idealization of the space trusses it is assumed that no moment can be transferred between the elements at joints. This assumption can be justified by the fact that the common space truss elements have relatively low rotational stiffnesses.[44] Hence, the transfer of moments between the elements of space trusses does not significantly influence the distribution of internal forces.

The end rotational restraints provided by some types of joints in space trusses, however, might substantially modify the response characteristics of individual elements. This is considered in structural modeling by assigning an effective length factor to each element, depending on the degree of end rotational restraint provided by the joints. The effective length factor can range from 0.5 for the rotationally rigid joints, to 1.0 for the ideally pinned joints.

In addition to providing end rotational restraints, some connections also tend to transfer the axial loads to the elements eccentrically. The bending actions resulting from those eccentricities will be considered in element modeling, but again the transfer of moments between the adjacent elements will be disregarded.

In short, the structural modeling approach adopted in this investigation considers the bowing and internal moments of the elements, and the end rotational restraint and eccentricities provided by the connections, but disregard any overall frame action of the structure resulting from the transfer of moments between the elements through the joints.

The structural modeling approach adopted in this study also included approximate features for simulating the behavior of the X-bracing systems and the in-plane redundant elements supporting the main elements. These two subassemblages are frequently encountered in some popular space truss systems like the lattice transmission towers. A detailed description of the procedures used in this study for idealizing the X-bracing systems and the in-plane redundants in space trusses is presented below.

5.4.1 X-Bracing Systems : In the case of the X-braced systems with no connection between the bracing elements, buckling of the compression diagonal is assumed to take place, independent of the tension diagonal, about the weakest axis with an effective length factor close to 1.0 (depending on the end rotational restraints).

In the case of the X-bracing systems with their crossing diagonals jointed together at the intersection point, however, the interaction of the crossing diagonals can not be disregarded.[49,50] The nature of this interaction depends on the internal axial forces in the two bracing diagonals being of the same or opposite signs.

If one of the bracing diagonals is in tension and the other in compression, as in planes A and A' of Figure 5.7, the tension diagonal tends to develop a lateral stiffness which works to restrain the lateral movement and buckling of the compression diagonal. In this case, due to the lateral restraint at the intermediate point, buckling of the compression diagonal can not take place over the full-diagonal length. Buckling will dominantly occur over the longest segment of the compression diagonal (on either side of the intermediate joint) around the minor axis of the diagonal, and some partial rotational restraint will be provided at the segment ends. In order to consider this partial restraint, an effective length factor of 0.85 to 1.0 should be applied to the longest segment of the compression diagonal. This range of

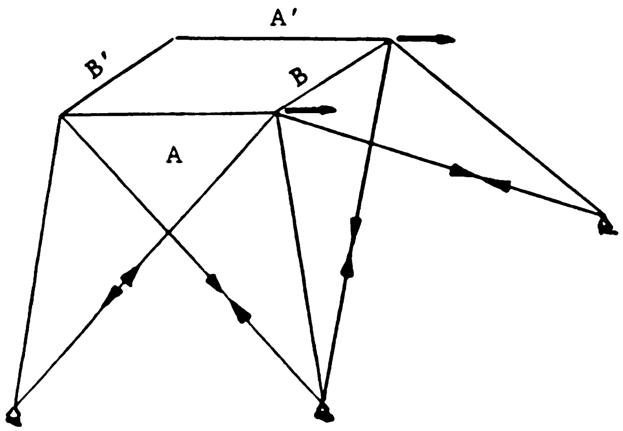

Figure 5.7 Typical X-Braced Panels with Similar or Opposing Senses of Forces in Crossing Diagonal Braces

effective length factor is based on the experimental results on angular diagonal braces bolted together at their intermediate joint.[49,50]

The approach adopted in this study for modeling of the bracing diagonals with opposing senses of axial forces, involves the use of an effective length factor (equal to the ratio of the longest segment length to the full length times an effective length factor ranging from 0.85 to 1.0) on the full length of the compression diagonal. In this approach, there is no need to include the intermediate joint in the structural model.

The other category of braced panels is the one with both diagonals having axial forces in the same sense (both in compression or tension), as in panels B and B′ of Figure 5.7. When the bracing diagonals are both in compression, two modes of buckling might dominate the behavior. In one mode, the diagonals buckle perpendicular to the braced plane. Since the buckling elements provide small resistance against lateral movements, the interaction between the two bracing diagonals in out-of-plane buckling can be assumed to be negligible. In this condition, the effective length factor (usually ranging from 0.85 to 1.0) is applied over the full length of the compression diagonal. The other mode involves the buckling of the compression diagonals over the longest segment on either side of the intermediate joint around the minor axis of the element. If the buckling load corresponding to this case is small enough to dominate the behavior, modeling of the braced system would be comparable to the case illustrated before with the bracing diagonals having axial forces with opposite senses.

5.4.2 In-Plane Redundants : As discussed earlier, the in-plane redundants prevent or restrain the lateral movements of the main elements in this plane, and provide some partial rotational restraint against out-of-plane movements (see Figure 5.2b).

The approach adopted in this study for modeling the in-plane redundants approximates their effects without physically including them in the structural model. In this approximation, the buckling mode and the slenderness ratio of the main elements are influenced by the presence of the in-plane redundants. Buckling of the main elements might take place either along the full length out of the panel plane or along an unrestrained fraction of length about the minor axis, depending on the relative values of the corresponding buckling loads. Any partial restraint at the ends of the buckling length can be considered by applying an appropriate effective length factor.

In the X-bracing diagonals or main elements with in-plane redundants, when the dominant buckling mode takes place over a fraction of the element length, the partial- length buckling might immediately lead to the complete buckling of the element (Figure 5.8a), or the buckling might be restricted to a segment of the element (Figure 5.8b). The modeling approach adopted in this study assumes, based on the experimental observations,[44] that partial-length buckling tends to be followed

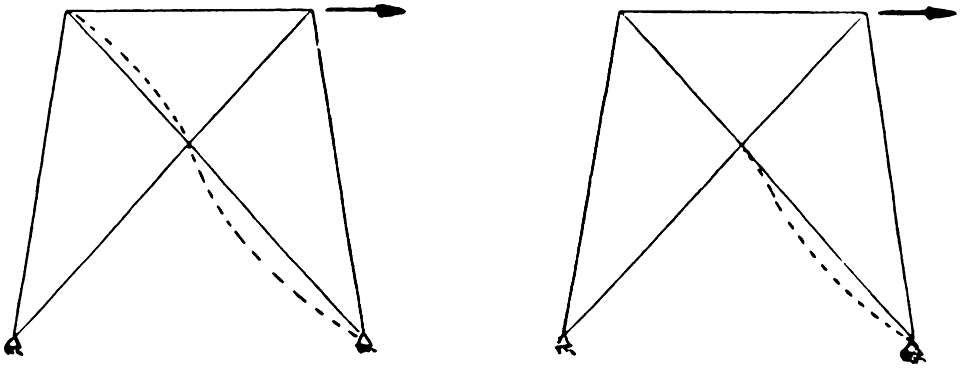

a) Complete

b) Partial

Figure 5.8 Partial / Complete Buckling Over the Element Length

immediately by a complete buckling of the element (Figure 5.8a).

5.5 ADOPTED STRUCTURAL ANALYSIS PROCEDURES AND NUMERICAL TECHNIQUES :

A computationally efficient structural analysis strategy (with appropriate numerical techniques) was chosen for nonlinear-inelastic analysis of space trusses with due consideration to the buckling of compression elements.

At each load step, the global tangent stiffness matrix of the structure is formed using the tangent stiffnesses of the elements (which depend on the level and history of element loading), considering the deformed geometry of the system. In the formation of the tangent stiffness matrix advantage is taken of the symmetry and the variable banded nature of the matrix. The elements of the matrix with the half band width (including the diagonal) are stored in a vectorial (skyline) form after determining the variable band width for each column,[51] thus reducing the amount of computer memory needed for the stiffness matrix.

Following the formation of the global tangent stiffness matrix in the vectorial form, the incremental equilibrium equations are solved by first factorizing the stiffness matrix into lower triangular, diagonal and upper triangular matrices, and then employing the backward and forward substitution techniques. In order to reduce the computer memory required at this stage, the factorized matrices are also stored in a vectorial form, using the same memory spaces as the global tangent stiffness matrix. It is also worth mentioning that the factorized matrices can be used repeatedly for different load increments, as long as the global tangent stiffness is not updated.

Within each load step, an iterative procedure is followed to limit the error in equilibrium of the external and internal forces. Following the satisfaction of the load equilibrium check a second check is made on the nodal displacement increments caused by the application of the error forces. If necessary, further iterations are performed to limit the displacement increments. In this iteration procedure the equilibrium errors are repeatedly applied as incremental loads to the corresponding nodes, and the global tangent stiffness matrix might or might not be updated for each iteration.

The developed program is also capable of accounting for the post-buckling residual strength of the compression elements, thereby considering the inelastic force redistribution within the structural system. For this purpose, in case the overall structure is still resisting increasing loads, the buckled elements would be substituted with their residual forces (obtained from their axial load-deformation relationships). After the structure can not resist any increase in the applied loads (simulation of this range of behavior is of interest because , for example, a failing tower structure could affect and be affected by the neighboring undamaged towers through the connecting wires), the actual tangent stiffnesses of the buckled and unbuckled elements are used in the construction of the global stiffness matrix. The program can decide if the applied load is increasing or decreasing (with due consideration to the sense of the displacement changes) by checking the convergence conditions.

5.6 COMPARISONS WITH STRUCTURAL TEST RESULTS :

In order to verify the element modeling methodology and the structural analysis techniques used in this study, the developed computer program for nonlinear analysis of space trusses was used to predict the experimental response characteristics of three different types of trusses. Comparisons were made between the experimental and analytical overall load-deformation characteristics of the structures and their failure modes. The inelastic redistribution of the internal forces was also assessed analytically. This information is needed for distinguishing the back-up force transfer mechanisms within the structure which get activated following the buckling and yielding of some critical elements in the originally critical force-transfer mechanisms. Strengthening of such back-up systems (which may play minor roles in the elastic range) can have detrimental effects on improving the ductility of the structural failure. Hence, the results of nonlinear structural analysis (especially the data on inelastic redistribution of internal forces) can lead to better designs which ensure (and control) the ductility of the failure mode.

Experimental results on three structural systems were selected to verify the developed analytical models and to demonstrate their applications and advantages. These structures are : a) a double layer space truss (Figure 5.9a), b) an isolated X-bracing system (Figure 5.9b), and c) a complete lattice transmission tower (Figure 5.9c). A discreption of the structural systems, and the experimental and analytical results are presented below.

5.6.1 Double Layer Space Truss System : Reference 57 has presented test results on a 6x6 bay double layer space truss (Figure 5.10). Each bay measures 12 in (305 mm) square by 8.5 in (215.9 mm) deep. The truss was simply supported at each bottom layer perimeter joint and loaded at the corners of the central 2 feet (610 mm) square on the lower layer. All the elements were from 0.5 in (12 mm) OD aluminum tubes with a thickness of 0.06 in (1.5 mm), and all the joints were hinged. The tensile yield strength of the aluminum was approximately 42 ksi (289 Mpa). The elastic moduli of the aluminum tubes were 5966 ksi (41100 Mpa) at the upper

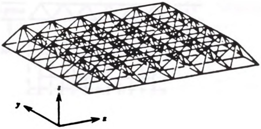

a) Double Layer Space Truss

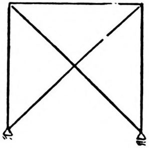

b) Isolated X-Braced System

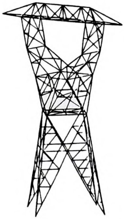

c) Lattice Transmission Tower

Figure 5.9 The Selected Structural Systems

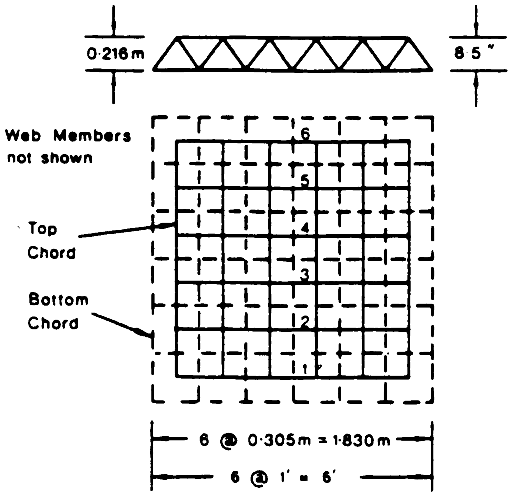

Figure 5.10 The Geometry of the Double Layer Space Truss[57]

layer, 7229 ksi (49800 Mpa) at lower layer, and 6605 ksi (45500 Mpa) for the web members. Experiments on the tubular elements with actual end connections of the truss system indicated an effective length in buckling equal to approximately 0.85 times the center to center spacing of the end joints.

The experimental relationship between the total applied load and the vertical deformation at the center of the bottom layer has been reported in Reference 57. Figure 5.11 compares this experimental relationship with the analytical one produced using the developed element modeling and structural analysis procedures. The analytical approach of this study is observed to predict the experimental inelastic behavior of the structure with a resonable accuracy. The accuracy reached in predicting the structural behavior after major inelasticities is especially important.

Some joint slippage and also a non-symmetric structural behavior were observed in the experiment. These may have been caused by the random variations of the element and especially the joint characteristics.

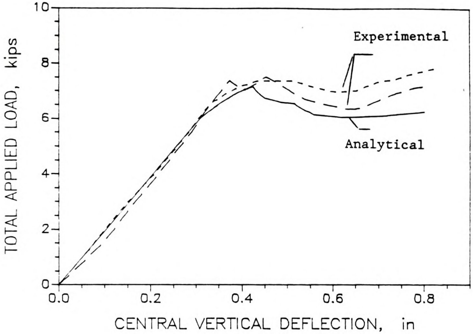

Figure 5.11 Overall Analytical and Experimental Comparisons of the Double Layer Space Truss[57]

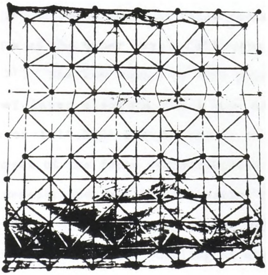

Figure 5.12 Picture of the Buckled Structure[57]

Major inelasticities and collapse of the structural system were initiated by the buckling of some compression members at the upper layer of the truss near the applied load locations (see Figure 5.12).

In the analytical model, major inelasticities were initiated by the buckling of elements 3 and 3′in Figure 5.13a simultaneously with the buckling of the corresponding elements in the other three quarters of the structure. This was followed by the buckling of the elements 7 and 7′and a major force redistribution within the system. In spite of all these, the structure could still preserve major fractions of its ultimate load resistance at large deformations. Figures 5.13b,c, and d show typical relationships between the axial forces of the steel struts in the upper layer, web and lower layer, respectively, of the structural system and the vertical displacement at the center node of the lower layer. From Figure 5.13b through 5.13d, it may be concluded that the peak resistance of the complete structure is reached following the buckling of elements 3 and 3′, when the descending branch of the compressive load-deformation relationship in these elements is initiated. Figure 5.13b is also indicative of major internal force redistributions within the compressive elements of the upper layer following the buckling of elements 3,3′,7 and 7′. The key aspect of this phenomenon is the unloading of those upper layer elements which are connected to the buckling ones (elements 1,1′,2,2′,8,8′,9, and 9′ in Figures 5.13a,b), another significant aspect of the force redistribution within the upper layer elements is the accelerated rate of compressive force increases in elements 4,4′,5,5′,6, and 6′ at the boundary of the upper layer. These phenomena indicate that following the buckling of elements 3,3′,7, and 7, the post-peak load carrying capacity of the structure has been upheld by the transfer of the compression forces to the elements at the exterior of the upper layer.

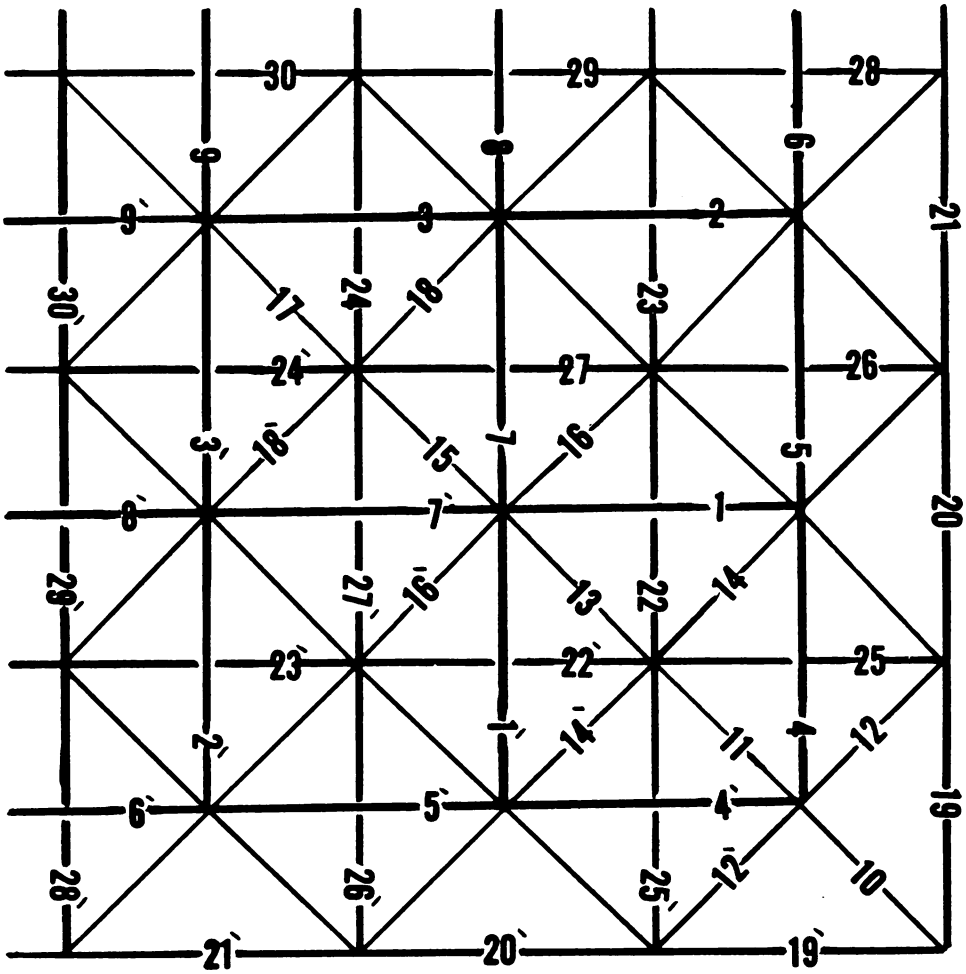
30
29
28
9
8
6
9'
3
2
21
30'
17
24
18
23
24'
27
26
3'
18'
15
7
16
5
8'
7'
1
20
29'
27'
16'
13
22
14
23'
22'
25
2'
1'
14'
11
4
12
19
6'
5'
4'
28'
26'
25'
12'
10
21'
20'
19'

a) One Quarter

Figure 5.13 Detailed Analytical Performance of the Double Layer Space Truss

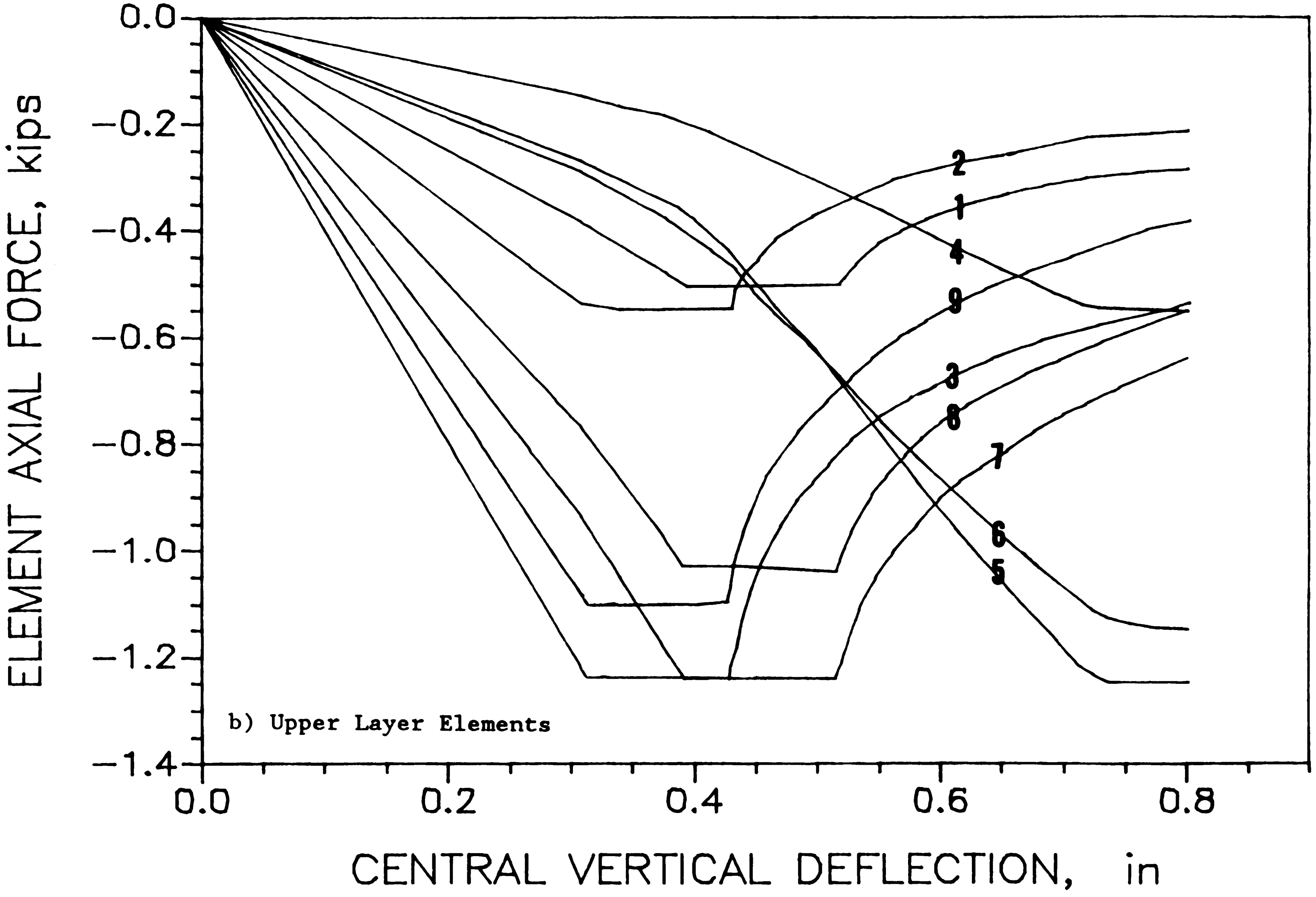

Figure 5.13 Detailed Analytical Performance of the Double Layer Space Truss (cont' d)

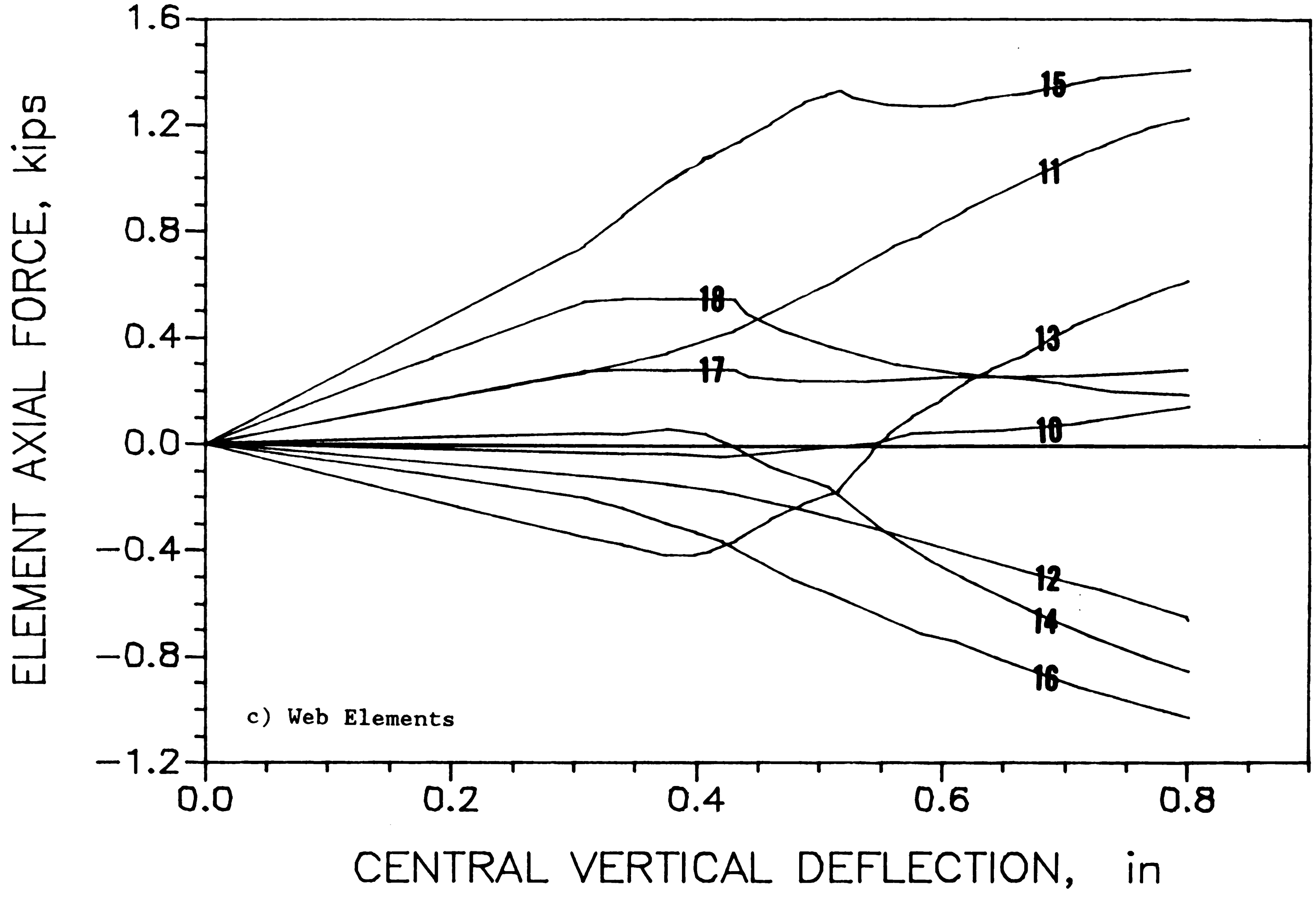

Figure 5.13 Detailed Analytical Performance of the Double Layer Space Truss (cont' d)

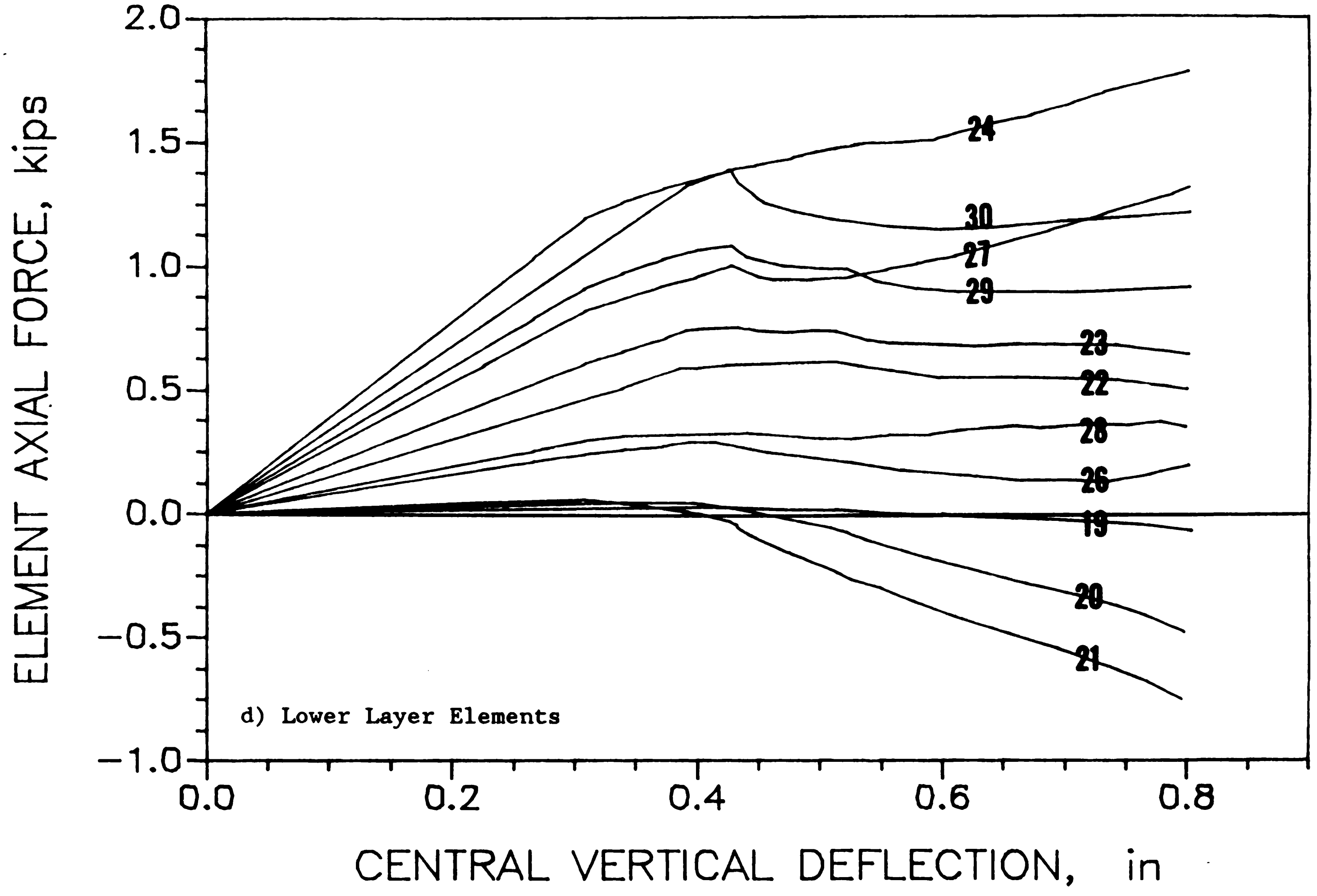

Figure 5.13 Detailed Analytical Performance of the Double Layer Space Truss (cont' d)

As shown in Figure 5.13c, the redistribution of the upper layer internal forces is accompanied with the redistribution of the internal forces within the web elements. The dominating factor here is the loss in the significance of some web elements such as 15,17,18, and 18′ in Figures 5.13a and c which transfer the applied external loads to the buckling upper layer elements, and the increase in the significance of other web elements such as 11,12,12′,13,14,14′,16, and 16′ in Figures 5.13a and c, which transfer the applied forces to the exterior elements of the upper layer. It is important to know that the internal force redistribution within the web elements might actually change the direction of forces in some elements. This is an indication of major modifications in the structural performance following the buckling of some elements (see the behavior of elements 13 and 14 in Figure 5.13c).

As far as the behavior of the lower layer elements is concerned (Figure 5.13d), the main phenomenon in the internal force redistribution is the change in force direction (from tension to compression) in elements on the boundary of the lower layer, and the relatively rapid increase in the compression forces of these elements following the buckling of some of the upper layer elements. This phenomenon can be illustrated by the redistribution of some web element forces, as follows. The increased compression of the upper layer boundary elements 4,4′,5, and 5′ result in an increase in the tension force of web element 11 (see Figure 5.13c). This would be followed (for satisfying the equilibrium) by an increase in the compression force of the web elements 12 and 12′. These elements (and the ones symmetric to it) will be compressing the boundary elements of the lower layer at an increasing rate. It is worth mentioning that those boundary elements at the bottom layer which are not compressed by web elements 12 and 12′ (elements 19 and 19′

in Figures 5.13a and d) and the ones symmetric to it will not be significantly influenced by the redistribution of the internal forces.

From the above discussion, it may be concluded that a much deeper insight into the actual behavior of structural systems up to and beyond their peak resistance can be achieved by an accurate inelastic analysis of the system. The assessments of the internal force redistribution will provide information for strengthening some elements which might not seem critical in the elastic analysis, but would play a major role following the inelastic internal force redistributions. Such information is needed for improving the post-peak resistance and the overall ductility of the system. For example, in the structure shown in Figure 5.13, strengthening of some boundary elements in the top and bottom layers (elements 5,6,20 and 21) will positively influence the ductility of the structural failure (noting that in the elastic range, prior to the inelastic force redistribution, the forces in these elements are not insignificant)

5.6.2 Isolated X-Braced System : A popular lateral load resisting system is space trusses (e.g., lattice transmission towers) is the X-braced system. This system is also used extensively in steel frames for resisting the lateral earthquake and wind loads. It is thus important to assess the accuracy of the developed element and structural models in predicting the response of X-braced system to lateral loads. For this purpose, a single X-braced system tested in Reference 46 was chosen. This system (Figure 5.14a) consists of four relatively rigid boundary elements with pinned end connections and two hinged-hinged diagonal bracing elements, which are independent from each other (i.e., they are not bolted at their intersection). The load was applied monotonically at the top corner of the system. The bolted connections of the bracing

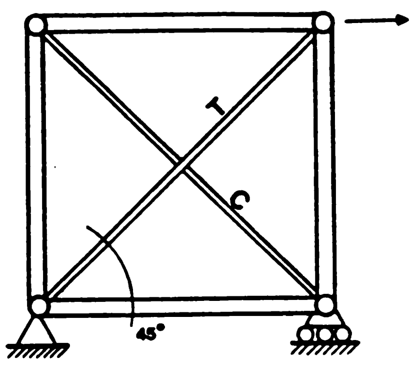

a)

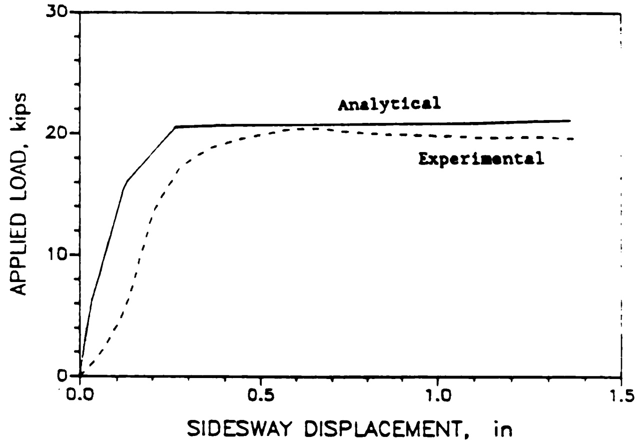

b) Overal Analytical and Experimental Comparison

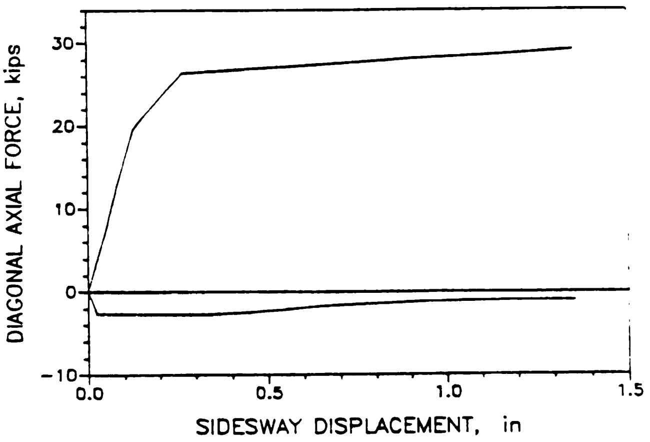

c) Analytical Behavior of the Diagonal Braces

Figure 5.14 Detailed Behavior of an Isolated X-Braced System[46]

elements generated eccentricities equal to 0.03 in (0.76 mm) and 0.6 in (15.24 mm) around the major axes of the angular bracing diagonals.

In modeling the braced system, the reduction in the tension bracing element area at the end regions was taken into account. For this purpose, at the end segments of the tensile bracing element (where the net cross-sectional area is smaller than the gross area), a reduced cross-sectional area was used in the model.

Figure 5.14b shows the analytical and experimental lateral load-deformation relationships (at the load application point) for the braced system. Except for the initial stiffness (which seems to be strongly influenced by the initial slippage at the bolted connections), the developed analytical procedures can satisfactorily predict the experimental behavior of the system. The analytical relationships between the axial force in the two bracing diagonals and the lateral displacement of the structure at the load application point are presented in Figure 5.14c. The drop in structural stiffness at a displacement of 0.04 in (1 mm) can be attributed to the buckling of the compression diagonal. The overall behavior, however, is governed by the tension diagonal performance. This is a result of the relatively high tensile strength of the bracing elements when compared with their compressive one. At a displacement of about 0.12 in (3 mm), the yielding in the end (bolted) regions of the tensile bracing diagonal further reduces the stiffness. The yielding of the tension element at a lateral displacement of about 0.27 in (7 mm) marks the initiation of major inelasticities and yielding of the complete system.

In this specific X-braced system, there is no possibility of buckling of the vertical framing element subjected to compression (since the cross-sectional area of this element is much larger than that of the diagonal elements). This secures a ductile post-yield behavior of the

structure with no significant drop in the load carrying capacity, reflecting the dominance of the tensile diagonal behavior in the response of this X-braced system.

5.6.3 Lattice Transmission Tower : Lattice steel towers are common space truss structural configurations for supporting wires transmitting electrical power. The specific transmission tower analyzed in this study is generally classified as a 230 K.W. single circuit transmission tower of rotated base type.[58] A sketch of the tower is given in Figure 5.15, and Figure 5.16 is a perspective of the tower which identifies the major joints by numbers. The tower members were all angles, generally single and sometimes double, and their sizes are listed in Table 5.1. Test results on this tower , subjected to equal longitudinal loads in the positive X-direction at joints 15 and 16 in addition to the dead weight, have been reported in Reference 58. This simple load case is not exactly a design condition, but it does approach the longitudinal case simulating failed conductors. The lateral loads were applied from zero and increased up to designated holding values at a rate of 1 Kips/min. The lateral loads were then completely removed and applied again starting from zero to a holding value greater than the previous one. This load repetition was done four times and then the structure was loaded to failure in the fifth repetition. The test data reported in Reference 58 included the collapse load as well as the axial loads in various segments versus the total lateral loads.

In analysis, the transmission tower was modeled as a space truss with pinned joints and element models which followed the efficient formulation developed in this study. The connection detailing effects on the element behavior were accounted for by adopting end eccentricities and effective length factors which approximately corresponded to the

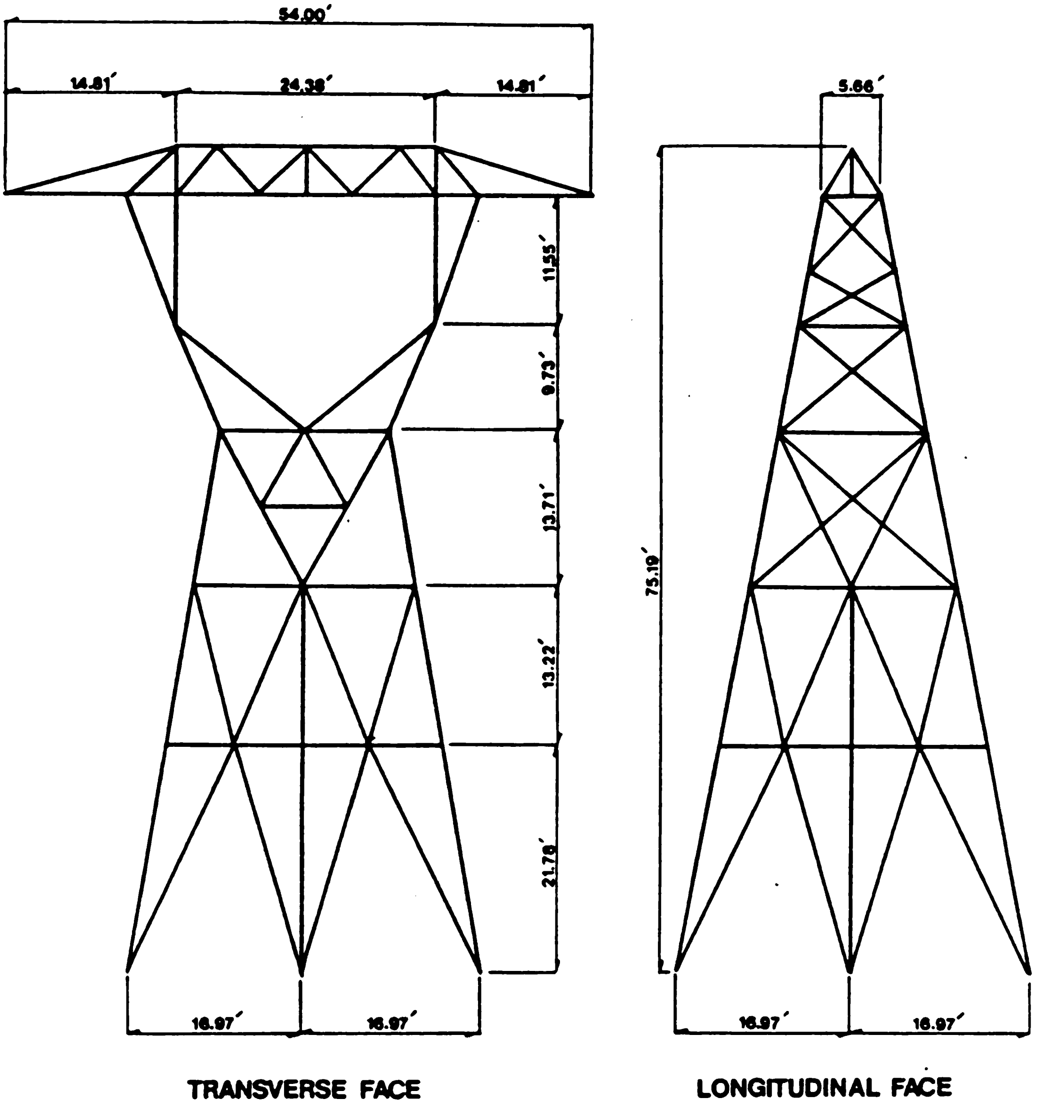
54.00'
14.81'
24.38'
14.81'
5.66'
11.55'
9.73'
13.71'
13.22'
21.78'
75.19'
16.97'
16.97'
16.97'
16.97'
TRANSVERSE FACE
LONGITUDINAL FACE

Figure 5.15 Tower Geometry[58]

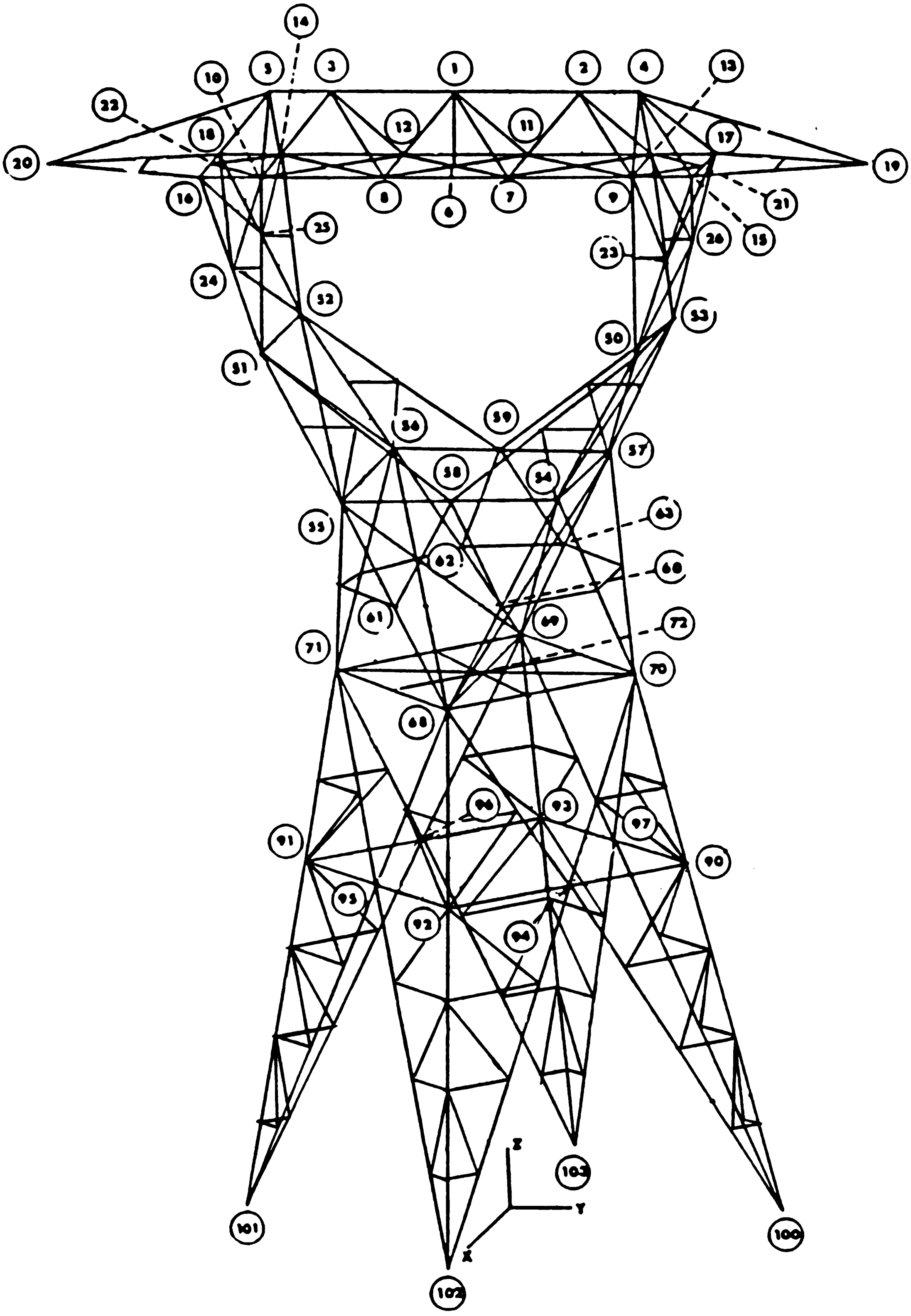
14
10
5
3
1
2
4
13
22
18
12
11
17
20
19
16
8
6
7
9
21
25
26
15
23
24
52
53
50
51
56
59
57
58
54
55
63
62
60
61
69
72
71
70
68
96
93
97
91
90
95
92
94
Z
103
Y
101
100
X
102

Figure 5.16 Tower Perspective

Table 5.1 Properties of Tower Members[58]

Member end joints	Cross-Section	Yield Strength ksi	Critical Buckling Axis
1-6	2L 1.75 X 1.75 X .1875	33	Z
1-2	L 3.5 X 3.5 X .25	33	Z
1-7	L 2.5 X 2.5 X .1875	33	Z
2-4	L 3.5 X 3.5 X .25	33	Z
2-7	L 2.5 X 2 X .1875	33	Z
2-9	L 2.5 X 2.5 X .1875	33	Z
4-9	L 3 X 2.5 X .25	33	Z
4-15	L 4 X 4 X .25	33	Z
4-19	2L 2.5 X 2 X .1875	33	Z
6-7	L 2.5 X 2 X .1875	33	Z
7-8	L 3.5 X 3.5 X .25	45	Z
7-9	L 3.5 X 3.5 X .25	45	Z
7-11	L 1.75 X 1.75 X .1875	33	Z
7-13	L 2 X 2 X .1875	33	Z
9-11	L 2 X 2 X .1875	33	Z
9-13	L 1.75 X 1.75 X .1875	33	Z
9-15	L 3.5 X 3.5 X .25	45	Z
9-21	L 1.75 X 1.75 X .1875	33	Z
9-23	L 1.75 X 1.75 X .1875	33	Z
9-50	L 3 X 2.5 X .25	33	X
15-17	L 2.5 X 2.5 X .25	33	X
15-19	L 5 X 3.5 X .375	33	X
15-23	L 4 X 4 X .25	45	Z
17-23	L 2.5 X 2.5 X .1875	33	Z
23-50	L 4 X 4 X .25	45	Z
26-50	L 2.5 X 2.5 X .1875	33	Z
50-53	L 2.5 X 2.5 X .1875	33	Z
50-54	L 4 X 4 X .3125	45	X
50-57	L 1.75 X 1.75 X .25	33	Z
50-58	L 4 X 3 X .3125	33	X
54-57	L 4 X 3 X .25	33	Z
54-58	L 4 X 3 X .25	33	Z
54-60	L 4 X 4 X .3125	45	Z
54-69	L 1.75 X 1.75 X .1875	33	Z
54-70	L 4 X 4 X .25	33	Z
58-60	L 2.5 X 2.5 X .1875	33	Z
60-68	L 4 X 4 X .3125	45	Z
62-63	L 2.5 X 2.5 X .1875	33	Z
68-69	L 2 X 2 X .1875	33	Z
68-70	L 4 X 3 X .25	33	X
68-92	L 4 X 4 X .375	45	Z
68-94	L 3 X 3 X .25	33	X
92-94	L 2.5 X 2.5 X .1875	33	Z
92-102	L 4 X 4 X .375	45	Z
94-102	L 3 X 2.5 X .25	33	X

Note : not all members are presented due to tower symmetry.

specific element and connection types. In the simple approach to the determination of end eccentricities used in this study, the angles with bolts on both legs were assumed to have zero eccentricities, while the ones with bolts on one leg only were given a uniaxial eccentricity about the major axis (or about the buckling axis if different from the minor axis). The approximate effective length factors were decided based on the degree of rotational fixity provided by the bolted connections at the element ends and also the presence of in-plane redundants. The in-plane redundants and X-braced systems were simulated as discussed earlier in section 5.4 of this chapter. The joints at which the connected elements were all in one plane, were stabilized in analysis by using dummy elements which were connected to such joints to provide out-of-plane stiffness. These elements were dummy in the sense that their axial forces, as predicted in analysis, were negligible.

The failure mechanism in analysis, which was similar to the one in the test, was initiated by the buckling of elements 18-24 and 17-23 (see Figure 5.16) at a total lateral load of 38.6 kips (172 KN) in analysis vs. 39 kips (174 KN) in test. Buckling of these elements resulted in a slight and temporary drop in the lateral load resistance, which was followed by a shift in the critical paths transferring the lateral load effects down the tower (from paths 18-24-51 and 17-23-50 to paths 16-25-51 and 15-26-50, respectively). The shift in load transfer paths was accompanied by a rise in the lateral load resistance following the temporary drop mentioned earlier. The second drop in the lateral load resistance, after which both analysis and test indicated a continuing drop in the lateral load capacity, occurred when the element 68-92 buckled at a total lateral load of 41 kips (183 KN) in analysis (the corresponding test value was not reported in Reference 58 which does not deal with the tower behavior after the first set of elements buckled.

This reference, however, did hint at the force redistributions that led to the buckling of element 68-92. Following the buckling of this element, after a sudden drop in the analytical lateral load resistance, the shift of the internal force transfer from path 68-92-102 to paths 68-95-102 and 68-94-102 led to the buckling of elements 94-102 and 95-102.

The failure mechanism described above is strongly influenced by the load-deformation behavior and buckling of elements 18-24 (and 16-25), 68-92, and 95-102 (and 94-102). The analytical element axial load vs. total lateral load on the structure as well as the element axial load vs. its axial displacement relationships for these critical elements are shown in Figures 5.17a,b, and c. Figure 5.17a indicates that element 18-24 buckled at a total lateral loads of 38.6 kips (172 KN) in analysis vs. 39 kips (174 KN) in test. Following a post-buckling region, it was unloaded due to the shift in the load-transfer paths. Figure 5.17b shows that elements 68-92 buckled at a total lateral load of 41 kips (183 KN) in analysis and continued to be loaded in the post-buckling region thereafter. It is interesting to note that the unloading of element 18-24 (and 16-25) started when element 68-92 buckled. Finally, Figure 5.17c indicates that following a sudden reduction of the total lateral load resistance, which occurred when element 68-92 buckled, the axial load in element 95-102 (and 94-102) continued to increase to the buckling level.

The above discussion on the inelastic force redistribution in lattice transmission towers, following the buckling of certain critical elements, is indicative of the advantages of a reliable nonlinear structural analysis algorithm (capable of considering the inelastic-buckling behavior of the truss elements) in determining the failure mechanism and the secondary force transfer paths which tend to dominate the structural

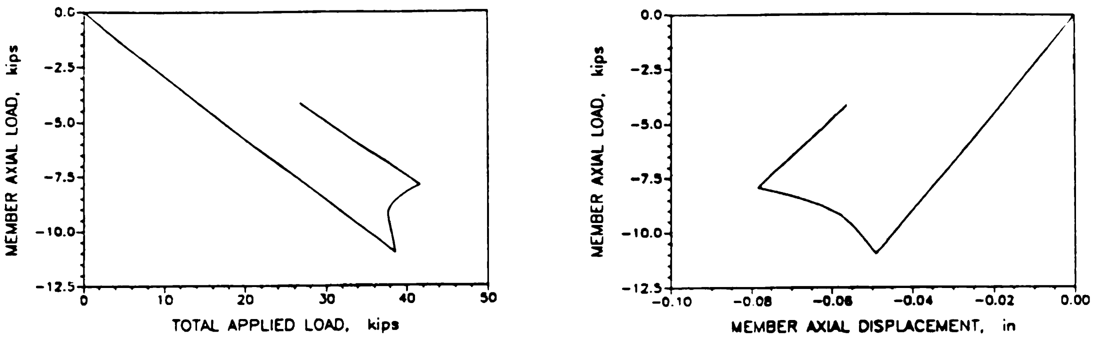

a) Member 18-24

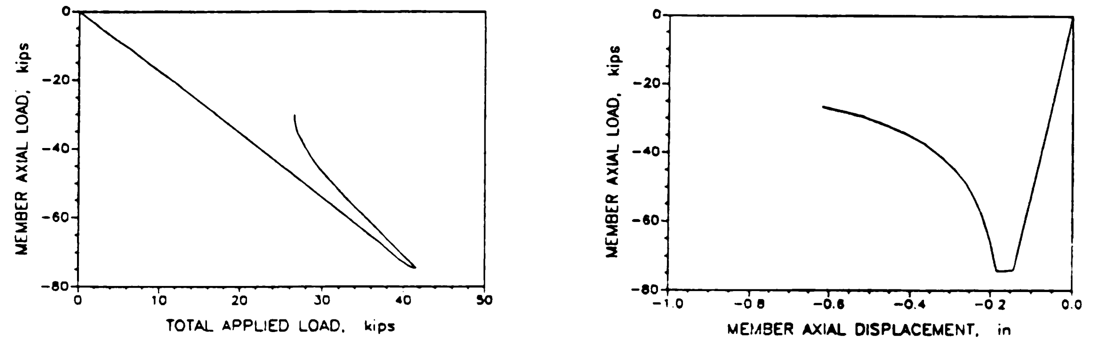

b) Member 68-92

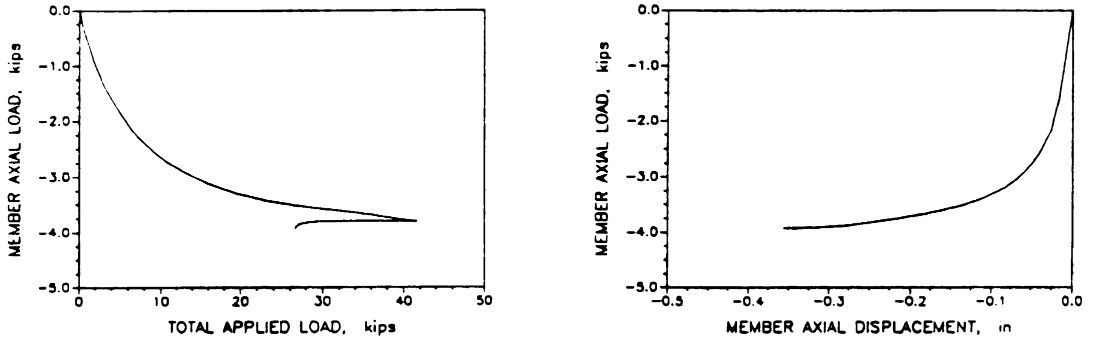

c) Member 94-102

Figure 5.17 Analytical Behavior of Some Key Members in the Tower

behavior after the buckling of some critical elements and the consequent loss of the primary force transfer paths within the structure. Such information can lead to the strengthening of certain critical elements in the secondary paths for enhancing the ductility of failure. A reliable nonlinear structural analysis program is also a strong tool in nonlinear analysis of complete transmission line systems, especially when the inelastic force redistributions and the failure mechanisms within the line following the failure of one or more components (structures) are of interest.

5.7 SUMMARY AND CONCLUSIONS

This chapter dealt with the nonlinear analysis and analytical assessment of the inelastic force redistributions and failure mechanisms of the truss structural systems. The analytical modeling of some special structural subassemblages, namely the X-braced systems and the in-plane redundants, have also been studied in some details. A brief literature review is presented on the nonlinear modeling and numerical techniques used in nonlinear structural analysis, with due consideration to the structural behavior beyond yielding and buckling of some critical elements.

The development of computer program for nonlinear analysis of space trusses, which incorporate the inelastic-buckling element model presented in Chapter 3, has been illustrated. Special attention has been given to the proposed approximate techniques used for simulating the X-braced systems, in-plane redundants, and eccentricities and rotational fixities at the element end joints in space truss systems. A Detailed treatment of the inelastic behavior and failure mode of connections has been outside the scope of this study.

The developed computer program for nonlinear analysis of space trusses was used for predicting the test results reported in the literature on the nonlinear behavior and failure mechanisms of three typical truss systems : a double layer space truss, an isolated X-braced system, and a lattice transmission tower. The results are indicative of the accuracy of the proposed program in predicting the experimental nonlinear behavior, failure mechanisms, inelastic force redistributions and residual strengths in different truss structural systems. The advantages of nonlinear structural analysis in predicting the critical load transfer paths within the structural systems following the buckling and loss of the primary paths have been demonstrated. Strengthening of these secondary paths can provide economical means for improving the ductility of failure in the structural systems. The developed nonlinear analysis program, with its ability to predict the "post-failure" residual strength of structures, is an effective tool in nonlinear analysis of complex systems, like complete transmission lines in which a structure acts as a component interacting with other components (structures) of the system.

CHAPTER 6

SUMMARY AND CONCLUSIONS

The inelastic-buckling behavior of steel struts plays a detrimental role in the analysis of space steel trusses and structural braced systems to static and dynamic loads. This study has been concerned with the development of a reliable and computationally efficient model for predicting the performance of steel struts under generalized loadings, and the application of this element model towards improving the efficiency and accuracy of nonlinear structural analysis programs.

EXPERIMENTAL BEHAVIOR AND ANALYTICAL MODELING OF STEEL STRUTS AND THEIR CONNECTIONS : The results of experimental studies on the inelastic behavior of steel struts and their connections under monotonic and cyclic loads have been briefly reviewed, and the suggested analytical techniques for predicting the response characteristics of the strut elements and connections under generalized loading conditions have been critically discussed. The experimental results on steel struts have indicated that the element behavior under cyclic loads is strongly influenced by : a) concentration of inelastic deformations in the critical regions (plastic hinges); b) slenderness ratio of the struts; c) local plate buckling; and d) initial imperfections and residual stresses. Inelastic cyclic test data have also indicated that the effective length concept, commonly applied to struts under monotonic loads, is also applicable under cyclic loads.

Connections of the steel struts can significantly modify the strut behavior under generalized loads. They influence the element behavior through : a) their ability to transfer moment and shear between adjacent elements; b) rotational restraint of the element ends; c) weakening the element by the fastening action (drilling holes and welding); d) yielding and failure of the connections under axial-flexural forces; and e) slippage at the bolted connections.

The more recently developed analytical models for predicting the steel strut load-deformation behavior under generalized loads can be categorized as the finite element, phenomenological, and physical theory models. Among these, the physical theory simulation techniques seem to combine the realism and generality of the finite element approach with the computational simplicity of the phenomenological modeling technique, and to provide a promising method for simulating the inelastic-buckling behavior of steel struts in large structures. The physical theory models incorporate simplified theoretical formulations based on some assumptions on the physical behavior of struts. From a comprehensive review of the available physical theory models of steel struts, it may be concluded that improvements are needed in : a) their computational efficiency in analysis of large structures; b) consideration of the gradual plastification of the element; c) accounting for the initial imperfections and residual stresses which cause nonlinearities prior to buckling of the virgin element loaded in compression; and d) eccentricities of the axial load at element ends. There are also other aspects of the available physical theory strut models which require improvements, but have been outside the scope of this investigation. These include : a) simulation of local plate buckling, b) the end rotational restraint provided at connections, and c) the possibility of torsional-flexural buckling.

Limited analytical studies have been reported on steel strut connections, especially under cyclic loads. The suggested simplistic simulations of the connection physical performance do not seem to provide realistic means of reproducing the actual behavior, especially in the case of bolted connections. The current practice in design of steel strut connections, based on simple connection models and loading conditions, also fails to account for the combined effects of the transferred axial-flexural forces and the complex stress distribution existing inside connections.

THE DEVELOPED ELEMENT MODEL, EXPERIMENTAL VERIFICATION, AND NUMERICAL STUDIES : the developed physical theory model of steel struts incorporates simplified theoretical formulations based on some assumptions on the physical behavior of steel struts. This model involves a limited number of degrees of freedom and requires limited computer storage for specifying the geometric and material characteristics of the element.

A computationally efficient formulation has been developed for predicting the inelastic-buckling behavior of steel struts under generalized cyclic loading conditions. This formulation expresses the element incremental forces in terms of the incremental axial displacement. It can thus be efficiently incorporated into a conventional nonlinear structural analysis program which follows the incremental stiffness method of analysis. The basic formulation developed in this investigation is also capable of accounting for the effects of the initial imperfection and end eccentricities.

The basic physical theory strut models assume a rigid-perfectly plastic behavior of the plastic hinge and a pure elastic behavior along the element length outside the hinge. This basic model has been refined in this study to consider, in a practical manner, the effects of partial plastification and degradation of the plastic hinge under cyclic loads and the softening, partial plastification and axial yielding along the element length outside the plastic hinge. These refinements were based on semi-empirical procedures, with due consideration to the physics of the strut inelastic-buckling behavior observed in tests. The final model was positively verified using monotonic and cyclic test results on steel struts with wide ranges of material and geometric properties and cross-sectional shapes.

The fully developed and verified element model was used for a numerical study on the effects of the material yield strength, end support rotational fixity (effective length factor), cross-sectional shape, initial imperfection, and end eccentricity of steel struts on their monotonic and cyclic axial load-deformation relationships. From the results of the numerical study it may be concluded that :

a) For the less slender steel struts with an effective slenderness ratio of 60, the ultimate compressive and tensile strengths, the post-buckling compressive resistance, and the hysteretic energy absorption capacity of the strut all substantially increase with increasing yield strength. The more slender struts, with an effective slenderness ratio of 200, are less sensitive to the yield strength variations when loaded in compression. Under tension, however, the effects of variations in yield strength on the performance of the more slender strut are still significant.

b) End rotational restraints are highly effective in enhancing the monotonic and cyclic axial load-deformation characteristics of steel struts with higher slenderness ratios under compression. The behavior of the more slender struts under tension and that of the shorter strut under tension or compression (except for their post-buckling resistance) are not much influenced by providing end rotational restraints.

c) The cross-sectional shape effects on the strut performance are more pronounced for the longer struts. At the same cross-sectional areas, among the four cross-sectional shapes considered (Square Tube, Circular Pipe, WT, and Angle), the Square Tube followed closely by the Pipe-section were the superior ones under monotonic and cyclic loads. The WT came next, followed by the Angle.

d) The increase in initial imperfection significantly reduces the ultimate compressive strength as well as the pre-peak stiffness of the steel struts. The post-buckling behavior, however, is not much influenced by the increase in initial imperfection.

e) The increase in end eccentricity around the minor axis significantly reduces the ultimate compressive strength, the pre-peak tangent stiffness, and the post-peak compressive strength of the more slender struts with effective slenderness ratios of about 200. The effects of minor axis eccentricity on the less slender struts are also significant, except that the pre-peak tangent stiffness is not much sensitive to the minor axis eccentricity. The major axis eccentricity effects on the less slender struts are comparable to those of the minor axis eccentricity. The more slender struts with slenderness ratios of about 200, however, are far less sensitive to the variations in eccentricities around the major axis, when compared with those around the minor axis. The comparisons between the effects of major and minor axis eccentricities were made for an angular strut which eventually buckled around the minor axis, in spite of minor or major axis eccentricities.

The results of the numerical study presented above can be helpful to designers in coming up with balanced designs resulting in steel struts with desirable performance characteristics and minimum material and connection costs.

INELASTIC ANALYSIS OF SPACE TRUSSES : The study concluded with the nonlinear analysis and analytical assessment of the inelastic force redistributions and failure mechanisms of the truss structural systems. The analytical modeling of some special structural subassemblages, namely the X-braced systems and the in-plane redundants, have also been studied in some details. A brief literature review is presented on the nonlinear modeling and numerical techniques used in nonlinear structural analysis, with due consideration to the structural behavior beyond yielding and buckling of some critical elements.

The development of computer program for nonlinear analysis of space trusses, which incorporate the inelastic-buckling element model presented in Chapter 3, has been illustrated. Special attention has been given to the proposed approximate techniques used for simulating the X-braced systems, in-plane redundants, and eccentricities and rotational fixities at the element end joints in space truss systems. A Detailed treatment of the inelastic behavior and failure mode of connections has been outside the scope of this study.

The developed computer program for nonlinear analysis of space trusses was used for predicting the test results reported in the literature on the nonlinear behavior and failure mechanisms of three typical truss systems : a double layer space truss, an isolated X-braced system, and a lattice transmission tower. The results are indicative of the accuracy of the proposed program in predicting the experimental nonlinear behavior, failure mechanisms, inelastic force redistributions and residual strengths in different truss structural systems. The advantages of nonlinear structural analysis in predicting the critical load transfer paths within the structural systems following the buckling and loss of the primary paths have been demonstrated. Strengthening of these secondary paths can provide economical means for improving the

ductility of failure in the structural systems. The developed nonlinear analysis program, with its ability to predict the "post-failure" residual strength of structures, is an effective tool in nonlinear analysis of complex systems, like complete transmission lines in which a structure acts as a component interacting with other components (structures) of the system.

LIST OF REFERENCES

1. Ikeda, K., and Mahin, S.A., "A Refined Physical Theory Model for Predicting the Seismic Behavior of Braced Steel Frames," Report No. UCB/EERC-84/12, Eathquake Engineering Research Center, University of California, Berkeley, July 1984.

2. Zayas, V.A., Shiny, P.B., Mahin, S.A., and Popov, E.P., "Inelastic Structural Modeling of Braced Offshore Platforms for Seismic Loading," Report No. UCB/EERC-81/04, Earthquake Engineering Research Center, University of California, Berkeley, Jan. 1981.

3. Black, R.G., Wenger, W.A., and Popov, E.P., "Inelastic Buckling of Steel Struts under Cyclic Load Reversals," Report No. UCB/EERC-80/40, Earthquake Engineering Research Center, University of California, Berkeley, Oct. 1980.

4. Maison, B.P., and Popov, E.P., "Cyclic Response Prediction for Braced Steel Frames," Journal of the Structural Division, American Society of Civil Engineers, Vol. 106, No. ST7, July 1980, pp. 1401-1416.

5. Structural Stability Research Council, "Guide to Stability Design Criteria for Metal Structures - 3rd Edition," John Wiley & Sons, 1976.

6. Chen, W.F., and Atsuta, T., "Theory of Beam-Columns, Vol. 1: In-Plane Behavior and Design," McGraw-Hill Book Company, 1976.

7. Chen, W.F., and Atsuta, T., "Theory of Beam-Columns, Vol. 2: Space Behavior and Design," McGraw-Hill Book Company, 1977.

8. Dhavajjai, P., Geol, S.G., and Hanson, R.D., "Axial Hysteretic Behavior with End Restraints," Journal of the Structural Division, American Society of Civil Engineers, Vol. 104, No. ST6, June 1978, pp. 883-890.

9. Toma, S., and Chen, W.F., "Cyclic Analysis of Fixed-Ended Steel Beam-Columns," Journal of the Structural Division, American Society of Civil Engineers, Vol. 106, No. ST3, June 1982, pp. 1385-1399.

10. Jain, A.K., Goel, S.C., and Hanson, R.D., "Hysteretic Cycles of Axially Loaded Steel Members," Journal of the Structural Division, American Society of Civil Engineers, Vol. 106, No. ST3, Aug. 1980, pp. 1777-1795.

11. Razzak, Z., "End Restraint Effect on Steel Column Strength," Journal of the Structural Division, American Society of Civil Engineers, Vol. 109, No. 2, Feb. 1983, pp. 314-334.

12. Bjorhorde, R., "Effect of End Restraint on Column Strength-Practical Applications," Engineering Journal, American Institute of Steel Construction, Vol. 21, No. 1, 1st Quarter, 1984, pp. 1-13.

13. Chapris, J., and Galambo, T.V., "Restrained Crooked Aluminum Columns," Journal of the Structural Division, American Society of Civil Engineers, Vol. 103, No. ST3, March 1982, pp. 511-524.

14. Wakabayshi, M., and Nonaka, T., "On the Buckling Strength of Angles In Transmission Towers," Bulletin of the Disaster Prevention Research Institute, Vol. 15, Part 2, No. 91, Nov. 1965.

15. Kennedy, J.B., "Buckling of Angles: State of the Art," Journal of the Structural Division, American Society of Civil Engineers, Vol. 108, No. ST9, Sept. 1982, pp.1967-1980.

16. Smith, E.A., "Buckling of Four Equal -Leg Angle Cruciform Columns," Journal of the Structural Division, American Society of Civil Engineers, Vol. 109, No.ST2, Feb. 1983, pp. 439-450.

17. American Institute of Steel Construction, "Manual of Steel Construction, 8th ed.," AISC, Chicago, Ill., 1980.

18. Nonaka, T., "Approximation of the Yield Condition for the Hysteretic Behavior of a Bar Under Repeated Axial Loading," International Journal of Solids and Structures, Vol. 13, 1977, pp. 637-643.

19. Nilforoushan, R., "Seismic Behavior of Multi-Story K-Braced Frame Structures," University of Michigan Research Report UMEE 73R9, Ann Arbor, MI, Nov. 1973.

20. Singh, P., "Seismic Behavior of Braces and Braced Steel Frames," Dissertation, University of Michigan, Ann Arbor, MI, July 1977.

21. Ikeda, K., Mahin, S.A., and Dermitzakis, S.N., "Phenomenological Modeling of Steel Braces Under Cyclic Loading," Report No. UCB/EERC-84/09, Earthquake Engineering Research Center, University of California, Berkely, CA, May 1984.

22. Sugimate, H., and Chen, W.F., "Inelastic Post-Buckling Behavior of Tubular Members," Journal of the Structural Division, American Society of Civil Engineers, Vol. 111, No. 9, Sept. 1984, pp. 1965-1978.

23. Papandrakakis, M., "Inelastic Post-Buckling Analysis of Trusses," Journal of the Structural Division, American Society of Civil Engineers, Vol. 109, No. ST10, Oct. 1983, pp. 2129-2147.

24. Kalyanaraman, V., Pekoz, T., and Winter, G., "Unstiffened Compression Elements," Journal of the Structural Division, American Society of Civil Engineers, Vol. 103, No. ST9, Sept. 1977, pp. 1833-1848.

25. Rhode, J., and Harvey, J.M., "Examination of Plate Post-Buckling Behavior," Journal of the Engineering Mechanics Division, American Society of Civil Engineers, Vol. 123, No. EM3, June 1977, pp. 481-498.

26. Usami, T., "Post-Buckling of Plates in Compression and Bending," Journal of the Structural Division, American Society of Civil Engineers, Vol. 108, No. ST3, March 1982, pp. 591-609.

27. DeWolf, J.T., and Gladding, C.J., "Post-Buckling Behavior of Beam Webs in Flexure," Journal of the Structural Division, American Society of Civil Engineers, Vol. 104, No. ST7, July 1978, pp. 1109-1122.

28. Jambock, J.K., and Clark, J.W., "Post-Buckling Behavior of Flat Plates," Journal of the Structural Division, American Society of Civil Engineers, Vol. 87, No. ST6, June 1961, pp. 17-33.

29. Sharp, M.L., "Strength of Beams or Columns with Buckled Elements," Journal of the Structural Division, American Society of Civil Engineers, Vol. 96, No. ST5, May 1970, pp. 1011-1013.

30. Rhodes, J. and Harvey, J.M., "Effects of Eccentricity of Load in Compression on the Buckling and Post-Buckling Behavior of Flat Plates," International Journal of Mechanical Science, Vol. 13, No. 10, Oct. 1971, pp. 867-879.

31. Golafshani, A.A., "DRAIN-2D2 - A Computer Program for Inelastic Seismic Response of Structures," Ph.D. Dissertation, Dept. of Civil Engineering, University of California, Berkeley, 1982.

32. Gilani, A.S., and Mahin, S.A., "Earthquake Response of a Tubular Steel Offshore Plateform," Report No. UCB/EERC-84/13, Earthquake Engineering Research Center, University of California, Berkeley, 1984.

33. Fouth, D.A., Yamanovchi, H., Midorikaua, M., and Nishiyama, I., "Construction of Full-Scale Six Story Steel Test Structure," Fourth JTCC Meeting, Part of US-Japan Joint Earthquake Research Project Utilizing Large Scale Testing Facilities, June 1983.

34. Kaba, S.A., and Mahin, S.A., "Interactive Computer Analysis Methods for Predicting the Inelastic Cyclic Behavior of Structural Sections," Report NO. UCB/EERC-83/18, Earthquake Engineering Research Center, University of California, Berkeley, July 1983.

35. Zayas, V.A., Popov, E.P., and Mahin, S.A., "Cyclic Inelastic Buckling of Tubular Steel Braces," Report No. UCB/EERC-80/16, Earthquake Engineering Research Center, University of California, Berkeley, 1980.

36. Zayas, V.A., Mahin, S.A., and Popov, E.P., "Cyclic Inelastic Behavior of Steel Offshore Structures", Report No. UCB/EERC-80/27, Earthquake Engineering Research Center, University of California, Berkeley, 1980.

37. Ghanaat, Y., and Clough, R.W., "Shaking Table Tests of A Tubular Steel Frame Model," Report No. UCB/EERC-82/2, Earthquake Engineering Research Center, University of California, Berkely, Jan. 1982.

38. Gugerli, H., and Geol, S.C., "Inelastic Cyclic Behavior of Steel Bracing Members," Report No. UMCE-82R1, Department of Civil Engineering, University of Michigan, Jan. 1982.

39. Drucker, D.C., "Plasticity," Structural Mechanics, Pergamon Press, London, 1960, pp. 407-488.

40. Hardin, B.O., "Experimental Investigataion of the Primary Stress Distribution in The Gusset Plate of a Double Plane Pratt Truss-Joint with Chord Splice at the Joint," University of Kentucky Engineering Experimental Station Bulletin, No. 49, Sept. 1958.

41. Irvan, W.G., Jr., "Experimental Study of Primary Stersses in Gussest Plates of a Double Plane Pratt Truss," University of Kentucky Engineering Experimental Station Bulletin, No. 46, December, 1957.

42. Whitemore, R.E., "Experimental Investigation of Stresses in Gussest Plates," University of Tennessee Engineering Experiment Station Bulletin, No. 16, May 1952.

43. Astaneh-Asl, A., "Cyclic Behavior of Double Angle Bracing Members with End Gusset Plates," Ph.D. Dissertation, Dept. of Civil Engineering, University of Michigan, Ann Arbor, MI, 1982.

44. Electric Power Research Institute, "Structural Development Studies at the EPRI Transmission Line Mechanical Research Facility," EPRI EL-4756, Project 2016-3, Interim Report, Aug. 1986.

45. Wakabayashi, M., and Nonaka, T., "On the Buckling Strength of Angles in Transmission Towers," Bulletin of the Disaster Prevention Research Institute, Vol. 15, Part2, No. 91, Nov. 1965.

46. Mueller, W.H., and Erzurumlu, H., "Limit State Behavior of Steel Angle Columns," Research Report, Division of Engineering and Applied Science, Portland State University, 1981.

47. Mueller, W.H., and Wanger, A.L., "Plastic Behavior of Steel Angle Columns," Research Report, Division of Engineering and Applied Science, Portland State University, 1983.

48. Papadrakakis, M., "Inelastic Post-Buckling Behavior of Trusses," Journal of the Structural Division, American Society of Civil Engineers, Vol. 109, No. 9, Sept. 1983, pp. 2129-2147

49. Goel, S.C., and El-Tayem, A.A., "Cyclic Load Behavior of Angle X-Bracing," Journal of the Structural Division, American Society of Civil Engineers, Vol. 112, No.11, Nov. 1986, pp. 2528-2539.

50. El-Tayem, A.A., and Goel, S.C., "Effective Length Factor for the Design of X-Bracing Systems," Engineering Journal, American Institute of Steel Construction, 1st Quarter, 1986, pp. 41-45.

51. Bathe, K.J., and Cimento, A.P., "Some Practical Procedures for the Solution of Nonlinear Finite Element Equations," Computer Methods in Applied Mechanics and Engineering, 22, 1980, pp. 59-85.

52. Crisfield, M.A., "Faster Modified Newton-Raphson Iteration," Computer Methods in Applied Mechanics and Engineering, 20, 1979, pp. 267-278.

53. Papadrakakis, M., "Inelastic Post-Buckling Behavior of Trusses," Journal of the Structural Division, American Society of Civil Engineers, Vol. 109, No. 9, Sept. 1983, pp. 2129-2147

54. Papadrakakis, M., "A Family of Methods with Three-Term Recursion Formulae," International Journal For Numerical Methods in Engineering, Vol. 18, 1982, pp. 1785-1799.

55. Papadrakakis, M., "A Method for the Automatic Evaluation of the Dynamic Relaxation Parameters," Computer Methods in Applied Mechanics and Engineering , 25, 1981, pp. 35-48.

56. Salmon, C.G., and Johnson, J.E., "Steel Structures : Design and Behavior, 2nd ed.," Harper & Row, Publishers, New York, 1980.

57. Schmidt, L.C., Morgen, P.R., and Clarkson, J.A., "Space Trusses With Brittle-Type Strut Buckling," Journal of the Structural Division, American Society of Civil Engineers, Vol. 102, No. ST7, July 1976, pp. 1479-1492.

58. Mueller, W.H., Prickett, S.L., and Kempner, L., "Nonlinear Analysis and Full Scale Test of a Transmission Tower," Research Report, Division of Engineering and Applied Science, Portland State University.

MICHIGAN STATE UNIV. LIBRARIES
31293005387455